AMELIORATION DE LA PRECISION ET COMPENSATION DES INCERTITUDES DES METAMODELES POUR L'APPROXIMATION DE SIMULATEURS NUMERIQUES

Victor Picheny

Ecole Nationale Supérieure des Mines
SAINT-ETIENNE

N° d'ordre : 537MA

THÈSE

présentée par

Victor PICHENY

pour obtenir le grade de
Docteur de l'École Nationale Supérieure des Mines de Saint-Étienne

Spécialité : Mathématiques Appliquées

IMPROVING ACCURACY AND COMPENSATING FOR UNCERTAINTY IN SURROGATE MODELING

soutenue à Gainesville (USA), le 15 décembre 2009

Membres du jury

Président :	Bertrand IOOSS	Ingénieur-chercheur, Centre à l'Energie Atomique, Cadarache
Rapporteurs :	Tony SCHMITZ	Associate Professor, University of Florida, Gainesville, FL
	Bertrand IOOSS	
Examinateur(s) :	Grigori PANASENKO	Professeur, Université Jean Monnet, St Etienne
	Nam-Ho KIM	Associate Professor, University of Florida, Gainesville, FL
	Jorg PETERS	Professor, University of Florida, Gainesville, FL
	Olivier ROUSTANT	Maitre-assistant, Ecole des Mines de St Etienne, St Etienne
Directeurs de thèse :	Raphael HAFTKA	Professor, University of Florida, Gainesville, FL
	Alain VAUTRIN	Professeur, Ecole des Mines de St Etienne, St Etienne

Spécialités doctorales :	**Responsables :**
SCIENCES ET GENIE DES MATERIAUX	J. DRIVER Directeur de recherche – Centre SMS
MECANIQUE ET INGENIERIE	A. VAUTRIN Professeur – Centre SMS
GENIE DES PROCEDES	G. THOMAS Professeur – Centre SPIN
SCIENCES DE LA TERRE	B. GUY Maître de recherche – Centre SPIN
SCIENCES ET GENIE DE L'ENVIRONNEMENT	J. BOURGOIS Professeur – Centre SITE
MATHEMATIQUES APPLIQUEES	E. TOUBOUL Ingénieur – Centre G2I
INFORMATIQUE	O. BOISSIER Professeur – Centre G2I
IMAGE, VISION, SIGNAL	JC. PINOLI Professeur – Centre CIS
GENIE INDUSTRIEL	P. BURLAT Professeur – Centre G2I
MICROELECTRONIQUE	Ph. COLLOT Professeur – Centre CMP

Enseignants-chercheurs et chercheurs autorisés à diriger des thèses de doctorat (titulaires d'un doctorat d'État ou d'une HDR)

AVRIL	Stéphane	MA	Mécanique & Ingénierie	CIS
BATTON-HUBERT	Mireille	MA	Sciences & Génie de l'Environnement	SITE
BENABEN	Patrick	PR 2	Sciences & Génie des Matériaux	CMP
BERNACHE-ASSOLANT	Didier	PR 0	Génie des Procédés	CIS
BIGOT	Jean-Pierre	MR	Génie des Procédés	SPIN
BILAL	Essaïd	DR	Sciences de la Terre	SPIN
BOISSIER	Olivier	PR 2	Informatique	G2I
BOUCHER	Xavier	MA	Génie Industriel	G2I
BOUDAREL	Marie-Reine	MA	Génie Industriel	DF
BOURGOIS	Jacques	PR 0	Sciences & Génie de l'Environnement	SITE
BRODHAG	Christian	DR	Sciences & Génie de l'Environnement	SITE
BURLAT	Patrick	PR 2	Génie industriel	G2I
COLLOT	Philippe	PR 1	Microélectronique	CMP
COURNIL	Michel	PR 0	Génie des Procédés	DF
DAUZERE-PERES	Stéphane	PR 1	Génie industriel	CMP
DARRIEULAT	Michel	IGM	Sciences & Génie des Matériaux	SMS
DECHOMETS	Roland	PR 1	Sciences & Génie de l'Environnement	SITE
DESRAYAUD	Christophe	MA	Mécanique & Ingénierie	SMS
DELAFOSSE	David	PR 1	Sciences & Génie des Matériaux	SMS
DOLGUI	Alexandre	PR 1	Génie Industriel	G2I
DRAPIER	Sylvain	PR 2	Mécanique & Ingénierie	SMS
DRIVER	Julian	DR	Sciences & Génie des Matériaux	SMS
FEILLET	Dominique	PR 2	Génie Industriel	CMP
FOREST	Bernard	PR 1	Sciences & Génie des Matériaux	CIS
FORMISYN	Pascal	PR 1	Sciences & Génie de l'Environnement	SITE
FORTUNIER	Roland	PR 1	Sciences & Génie des Matériaux	SMS
FRACZKIEWICZ	Anna	DR	Sciences & Génie des Matériaux	SMS
GARCIA	Daniel	CR	Génie des Procédés	SPIN
GIRARDOT	Jean-Jacques	MR	Informatique	G2I
GOEURIOT	Dominique	MR	Sciences & Génie des Matériaux	SMS
GOEURIOT	Patrice	MR	Sciences & Génie des Matériaux	SMS
GRAILLOT	Didier	DR	Sciences & Génie de l'Environnement	SITE
GROSSEAU	Philippe	MR	Génie des Procédés	SPIN
GRUY	Frédéric	MR	Génie des Procédés	SPIN
GUILHOT	Bernard	DR	Génie des Procédés	CIS
GUY	Bernard	MR	Sciences de la Terre	SPIN
GUYONNET	René	DR	Génie des Procédés	SPIN
HERRI	Jean-Michel	PR 2	Génie des Procédés	SPIN
INAL	Karim	MR	Microélectronique	CMP
KLÖCKER	Helmut	MR	Sciences & Génie des Matériaux	SMS
LAFOREST	Valérie	CR	Sciences & Génie de l'Environnement	SITE
LERICHE	Rodolphe	CR	Mécanique et Ingénierie	SMS
LI	Jean-Michel	EC (CCI MP)	Microélectronique	CMP
LONDICHE	Henry	MR	Sciences & Génie de l'Environnement	SITE
MOLIMARD	Jérôme	MA	Mécanique et Ingénierie	SMS
MONTHEILLET	Frank	DR 1 CNRS	Sciences & Génie des Matériaux	SMS
PERIER-CAMBY	Laurent	PR1	Génie des Procédés	SPIN
PIJOLAT	Christophe	PR 1	Génie des Procédés	SPIN
PIJOLAT	Michèle	PR 1	Génie des Procédés	SPIN
PINOLI	Jean-Charles	PR 1	Image, Vision, Signal	CIS
STOLARZ	Jacques	CR	Sciences & Génie des Matériaux	SMS
SZAFNICKI	Konrad	CR	Sciences & Génie de l'Environnement	DF
THOMAS	Gérard	PR 0	Génie des Procédés	SPIN
VALDIVIESO	François	MA	Sciences & Génie des Matériaux	SMS
VAUTRIN	Alain	PR 0	Mécanique & Ingénierie	SMS
VIRICELLE	Jean-Paul	MR	Génie des procédés	SPIN
WOLSKI	Krzysztof	MR	Sciences & Génie des Matériaux	SMS
XIE	Xiaolan	PR 1	Génie industriel	CIS

Glossaire :

PR 0	Professeur classe exceptionnelle
PR 1	Professeur 1ère catégorie
PR 2	Professeur 2ème catégorie
MA(MDC)	Maître assistant
DR (DR1)	Directeur de recherche
Ing.	Ingénieur
MR(DR2)	Maître de recherche
CR	Chargé de recherche
EC	Enseignant-chercheur
IGM	Ingénieur général des mines

Centres :

SMS	Sciences des Matériaux et des Structures
SPIN	Sciences des Processus Industriels et Naturels
SITE	Sciences Information et Technologies pour l'Environnement
G2I	Génie Industriel et Informatique
CMP	Centre de Microélectronique de Provence
CIS	Centre Ingénierie et Santé

Dernière mise à jour le : 22 juin 2009

ACKNOWLEDGMENTS

First of all, I would like to thank my advisors Dr. Raphael Haftka, Dr. Nam-Ho Kim and Dr. Olivier Roustant. They taught me how to conduct research, gave me priceless advices and support, and provided me with excellent guidance while giving me the freedom to develop my own ideas. I feel very fortunate to have worked under their guidance.

I would also like to thank the members of my advisory committee, Dr. Bertrand Iooss, Dr. Grigori Panasenko, Dr. Jorg Peters, Dr. Alain Vautrin and Dr. Tony Schmitz. I am grateful for their willingness to serve on my committee, for reviewing my dissertation and for providing constructive criticism that helped me to enhance and complete this work. I particularly thank Dr. Iooss and Dr. Schmitz for their work as *rapporteurs* of my dissertation.

I am grateful for many people that contributed scientifically to this dissertation: Dr. Nestor Queipo, who welcomed me for my internship at the University of Zulia (Venezuela) and provided me with thoughtful ideas and advices; Dr. Rodolphe Le Riche, with whom I developed a fruitful collaboration on the study of gear box problems; Dr. Xavier Bay, whose encyclopedic knowledge of mathematics allowed us to find promising results on design optimality; Dr. Felipe Viana, for his efficient contribution to the conservative surrogate problem; and Dr. David Ginsbourger, for his critical input on the targeted designs work... and his contagious motivation.

I wish to thank to all my colleagues for their friendship and support, from the Structural and Multidisciplinary Optimization Group of the University of Florida, the Applied Computing Institute of the University of Zulia, and the 3MI department from the Ecole des Mines: Tushar, Amit, Palani, Erdem, Jaco, Ben, Christian, Felipe, Alex, Camila; Eric, Delphine, Celine, Bertrand, David, Nicolas, Olga, Natacha, Khouloud, Ksenia, and many others... I also thank all the staff of the University of Florida and Ecole des Mines

that made possible my joint PhD program, and in particular Pam and Karen, who helped me many times.

Financial supports, provided partly by National Science Fondation (Grant # 0423280) for my time in Florida and by the CETIM foundation for my time in France, are gratefully acknowledged.

My final thoughts go to my friends, family, and Natacha.

TABLE OF CONTENTS

LIST OF TABLES

LIST OF FIGURES

LIST OF ABBREVIATIONS

BS	Bootstrap
CDF	Cumulative Distribution Function
CEC	Conservative to the Empirical Curve
CSM	Constant Safety Margin
CSP	Conservative at Sample Points
DoE	Design of Experiments
ED	Error Distribution
e_{RMS}	Root Mean Square Error
l_α	Loss in accuracy
LHS	Latin Hypercube Sampling
$MaxUE$	Maximum Unconservative Error
$MaxUE_{\%}$	Reduction of the Maximum Unconservative Error
MCS	Monte-Carlo Simulations
MSE	Mean Square Error
PDF	Probability Density Function
P_f	Probability of failure
PRS	Polynomial Response Surface
RBDO	Reliability-Based Design Optimization
$\%c$	Percentage of conservative results

Abstract of Dissertation Presented to the Graduate School
of the University of Florida in Partial Fulfillment of the
Requirements for the Degree of Doctor of Philosophy

IMPROVING ACCURACY AND COMPENSATING FOR UNCERTAINTY IN SURROGATE MODELING

By

Victor Picheny

December 2009

Chair: Raphael T. Haftka
Major: Aerospace Engineering

In most engineering fields, numerical simulators are used to model complex phenomena and obtain high-fidelity analysis. Despite the growth of computer capabilities, such simulators are limited by their computational cost. Surrogate modeling is a popular method to limit the computational expense. It consists of replacing the expensive model by a simpler model (surrogate) fitted to a few chosen simulations at a set of points called a design of experiments (DoE).

By definition, a surrogate model contains uncertainties, since it is an approximation to an unknown function. A surrogate inherits uncertainties from two main sources: uncertainty in the observations (when they are noisy), and uncertainty due to finite sample. One of the major challenges in surrogate modeling consists of controlling and compensating for these uncertainties. Two classical frameworks of surrogate application are used as a discussion thread for this research: constrained optimization and reliability analysis.

In this work, we propose alternatives to compensate for the surrogate model errors in order to obtain safe predictions with minimal impact on the accuracy. The methods are based on different error estimation techniques, some based on statistical assumptions and some that are non-parametric. Their efficiency are analyzed for general prediction and for the approximation of reliability measures.

We also propose two contributions to the field of design of experiments in order to minimize the uncertainty of surrogate models. Firstly, we address the issue of choosing the experiments when surrogates are used for reliability assessment and constrained optimization. Secondly, we propose global sampling strategies to answer the issue of allocating limited computational resource in the context of RBDO.

All methods are supported by quantitative results on simple numerical examples and engineering applications.

CHAPTER 1
INTRODUCTION

In the past decades, scientists have benefited from the development of numerical tools for the help of learning, prediction and design. The growth of computational capabilities has allowed the consideration of phenomena of constantly increasing level of complexity, which results in better understanding and more efficient solutions of real-life problems.

Complex numerical simulators can be encountered in a wide range of engineering fields. The automotive industry has developed numerical models for the behavior of cars during crash-tests, which involve highly non-linear mechanical modes, in order to integrate it to the design of car structures. In geophysics, flow simulators are used for the prediction of the behavior of CO_2 sequestration into natural reservoirs, or the prediction of oil recovery enhancement, based on a complex mapping of ground characteristics.

The increasing computational power has also allowed the incorporation of uncertainty information into system analysis. In particular, reliability analysis aims at quantifying the chance that a system behaves as it is required, when a set of the problem parameters are uncertain [Rackwitz (2000), Haldar & Mahadevan (2000)]. In structural analysis, uncertainty typically comes from material properties (due to manufacturing) and actual working conditions. For obvious reasons, reliability assessment has been intensively explored in aerospace and nuclear engineering.

However, the gain in realism makes the use of numerical models extremely challenging. Indeed, the complexity of the simulators makes them highly expensive computationally, limiting systematic learning or design process. Also, the number of parameters (or input variables) that explain the phenomenon of interest can potentially be very large, making difficult the quantification of their influence on the simulator response.

To overcome computational cost limitations, surrogate models, or metamodels, have been frequently used on many applications. The idea of surrogate models consists of replacing the expensive model by a simpler mathematical model (or surrogate) fitted to a

few chosen simulations at a set of points called a design of experiments (DoE). Surrogate models are then used to predict the simulator response with very limited computational cost [Box & Draper (1986), Myers & Montgomery (1995), Santner et al. (2003), Sacks et al. (1989a)].

By definition, a surrogate model contains uncertainties, since it is an approximation to an unknown function. A surrogate inherits uncertainties from two main sources: uncertainty in the observations (when they are noisy), and uncertainty due to the lack of data. Indeed, a simulator is an approximation to a real phenomenon, and the confidence one can put in its responses depends on the quality of the numerical model. The properties of the surrogate strongly depend on the accuracy of the observations. Secondly, in most applications, the number of simulations runs is severely limited by the computational capabilities. The information on which the surrogate is fitted is insufficient to obtain an accurate approximation of the simulator behavior. One of the major challenges in surrogate modeling consists of controlling and compensating for these uncertainties.

The present work considers as a discussion thread the classical framework of reliability-based design optimization (RBDO), for which the issues associated with uncertainty in surrogate modeling are particularly crucial. RBDO is a popular way to address uncertainty in the design process of a system. It consists of optimizing a performance function while ensuring a prescribed reliability level. RBDO problems are computationally challenging, since they require numerous calls to reliability measures that are most of the time expensive to estimate, hence being a natural candidate for surrogate application [Rajashekhar & Ellingwood (1993), Venter et al. (1998), Kurtaran et al. (2002)]. Surrogate modeling can be used at two levels of the RBDO: (1) during the optimization process, by approximating the reliability constraint, and (2) during the reliability estimation itself.

The challenges in using surrogate modeling in RBDO are various. Indeed, a poor approximation of the reliability level can severely harm the optimization process: overestimation leads to non-optimal designs, and underestimation to weak designs. Reliability assessment methods are generally based on sampling methods (such as Monte-Carlo simulations) that only provide estimates of the actual reliability levels. Quantification of the uncertainty on both reliability estimates and a surrogate based on such data is needed to limit the risk of poor designs. Ramu et al. (2007) show that the use of surrogates for reliability assessment is particularly challenging, since small errors in the model could result in large errors in the reliability measure. In addition, for computational reasons, the number of reliability estimates is limited to a small value, and efficient sampling strategies must be used to ensure an acceptable accuracy of the surrogate.

It is possible to compensate for the lack of accuracy with extra safety margins. Such approach is often referred as conservative, and a conservativeness level quantify the chance that an approximation is on the safe side for the analysis. For example, Starnes Jr & Haftka (1979) replaced the linear Taylor series approximation with a tangent approximation biased to be conservative in order to reduce the chance of unconservative approximations to buckling loads. Many engineering applications have adopted conservative estimation. For instance, Federal Aviation Administration (FAA) defines conservative material property (A-basis and B-basis) as the value of a material property exceeded by 99% (for A-basis, 90% for B-basis) of the population with 95% confidence. FAA recommends the use of A-basis for material properties and a safety factor of 1.5 on the loads. Traditionally, safety factors have been extensively used to account for uncertainties, even though their effectiveness is questionable [Elishakoff (2004), Acar et al. (2007)].

Estimating the uncertainty in data or the metamodel is crucial for the effectiveness of most surrogate-based approaches. Uncertainty and error quantification is a classical theme of surrogate modeling. Most metamodels contain by construction error estimates [Cressie

(1993), Isaaks & Srivastava (1989), Box & Draper (1986)]. These estimates are based on statistical assumptions; for instance, linear regression assumes normality and independance of the errors. In practice, such assumptions can be violated, making those error measures questionable. Alternatively, numerical techniques are available to quantify the error [Stine (1985), Efron (1982), Goel et al. (2006)].

Uncertainty quantification allows compensating mechanisms, for instance in order to set the conservativeness to a prescribed level. However, little information is available on the effect of error compensation on the surrogate application. Furthermore, conservative estimates are biased to be on the safe side, so the conservativeness comes at a price of accuracy. One goal of present work is to propose alternatives to compensate for the surrogate model errors, based on different error estimation techniques, and demonstrate their efficiency for safe prediction and design of engineering systems.

In many applications, sampling strategies can be chosen by the user. Then, experiments can be designed such that the uncertainty of surrogate models are minimized. When safe prediction is desired, reduced uncertainty allows to obtain conservativeness with a minimal impact on accuracy. The choice and effectiveness of the sampling strategies has been widely explored and discussed in the surrogate literature [Steinberg & Hunter (1984), Sacks et al. (1989b), Fedorov & Hackl (1997)]. This work proposes two contributions to this field. Firstly, we address the issue of choosing the experiments when surrogates are used for reliability assessment and constrained optimization. Secondly, we propose global sampling strategies to answer the issue of allocating limited computational resource in the context of RBDO.

Outline of the dissertation:.

Chapter 2 reviews several aspects of surrogate modeling.

Chapter 3 addresses the issue of generating conservative predictions using surrogate models. Two alternatives are proposed: (1) using statistical information provided by the surrogate model and (2) using model-independent techniques (bootstrap, cross-validation)

to obtain statistical information. Different metrics are defined to measure the trade-off between accuracy and safety. The analysis of the different techniques is supported with the help of an analytical and a structural problem that uses finite elements analysis.

Chapter 4 considers the application of surrogate modeling to reliability-based design, where surrogates are used to fit probability distributions. We focus on the case when low probabilities are estimated from a small number of observations obtained by Monte-Carlo simulations (MCS). By using biased-fitting techniques and resampling methods (bootstrap), we compensate for the uncertainty in the analysis by being on the conservative side, with reasonable impact on the accuracy of the response. An application to the optimization of a laminate composite with reliability constraints is used for demonstration, the constraint being approximated conservatively using bootstrap.

In Chapter 5, we propose an objective-based approach to surrogate modeling, based on the idea that the uncertainty may be reduced where it is most useful, instead of globally. An original criterion is proposed to choose sequentially the design of experiments, when the surrogate needs to be accurate for certain levels of the simulator response. The criterion is a trade-off between the reduction of overall uncertainty in the surrogate, and the uncertainty reduction in target regions. The effectiveness of the method is illustrated on a simple reliability analysis application.

Chapter 6 considers the framework of simulators whose fidelity depends on tunable factors that control the complexity of the model (such as MCS-based simulators, or RBDO framework). For each simulation run, the user has to set a trade-off between computational cost and response precision. When a global computational budget for the DoE is given, one may have to answer the following questions: (1) is it better to run a few accurate simulations or a large number of inaccurate ones, (2) is it possible to improve the surrogate by tuning different fidelities for each run. Answers are proposed for these two questions. For polynomial regression, it joins the well-explored theory of design optimality.

For kriging, both numerical and analytical results are proposed; in particular, asymptotic results are given when the number of simulation runs tends to infinity.

Chapter 7 recapitulates major conclusions and results, and draw perspectives from this work.

CHAPTER 2
ELEMENTS OF SURROGATE MODELING

In this chapter, we introduce the important notions relative to surrogate modeling. We detail two types of models: linear regression models, and Kriging models. We also describe the problematic of design of experiments, and present several popular sampling strategies.

2.1 Surrogate Models

Strategies involving surrogate modeling are recognized in a wide range of engineering fields to efficiently address computationally expensive problems. The aim of this section is to briefly present the notation and main steps in surrogate modeling. Among the numerous types of surrogate models available in the literature, we emphasize two of the most popular ones: linear regression and Kriging. Linear regression, also referred as polynomial response surface in the engineering literature, has been initially developed for statistical inference based on physical experiments. Kriging was developed by geostatisticians to model spatial correlations of the physical characteristics of ground. Both models are now used in many applications, even though the hypotheses on which the models are based are not necessarily guaranteed.

A major notion in surrogate modeling is the design of experiments, or sampling strategy, since it is crucial to the quality of the surrogate analysis. In this chapter, we briefly describe three classical sampling strategies: space-filling, model-based designs and adaptive designs. More advanced notions are addressed in Chapter 5 for adaptive designs and Chapter 6 for model-oriented optimal designs.

2.1.1 Notation And Concepts

Let us first introduce some notation. We denote by y the response of a numerical simulator or function that is to be studied:

$$\begin{aligned} y : D \subset \mathbb{R}^d &\longrightarrow \mathbb{R} \\ \mathbf{x} &\longmapsto y(\mathbf{x}) \end{aligned} \tag{2–1}$$

where $\mathbf{x} = \{x_1, ..., x_d\}^T$ is a d-dimensional vector of input variables, and D is the design space. In order to build a metamodel, the response y is observed at n distinct locations $\mathbf{X}$:

$$\begin{aligned} \mathbf{X} &= [\mathbf{x}_1, ..., \mathbf{x}_n] \\ \mathbf{Y}_{obs} &= [y(\mathbf{x}_1), ..., y(\mathbf{x}_n)]^T = y(\mathbf{X}) \end{aligned} \tag{2–2}$$

$\mathbf{X}$ is called the design of experiments (DoE), and $\mathbf{Y}_{obs}$ is the observations. Since the response y is expensive to evaluate, we approximate it by a simple model, called the metamodel or surrogate model, based on assumptions on the nature of y and on its observations $\mathbf{Y}_{obs}$ at the points of the DoE.

The metamodel can interpolate the data (splines, Kriging) or approximate it (linear regression, Kriging with nugget effect). In the latter case, it is assumed that the function of interest is observed through a noisy process, so the observation differs from the true function by an additive error term:

$$y_{obs,i} = y(\mathbf{x}_i) + \varepsilon_i \tag{2–3}$$

with ε_i the error. In most of the metamodel hypotheses, the error is considered as a white noise normally distributed with zero mean. In this section, we will always consider this hypothesis true.

2.1.2 The Linear Regression Model

In linear regression, the response is modeled as a linear combination of basis functions observed with an additive error term:

$$y(\mathbf{x}) = \sum_{j=1}^{p} \beta_j f_j(\mathbf{x}) \tag{2–4}$$

$$y_{obs,i} = \sum_{j=1}^{p} \beta_j f_j(\mathbf{x}) + \varepsilon_i \tag{2–5}$$

where $f_j(\mathbf{x})$ are the basis functions (for instance polynomial), β_j the weights, and ε_i the error at $\mathbf{x}_i$.

Given a set of design points, the linear regression model, in matrix notation, is defined as follow:

$$\mathbf{Y}_{obs} = \mathbf{f}^T(\mathbf{X})\boldsymbol{\beta} + \boldsymbol{\varepsilon} \tag{2–6}$$

where: $\mathbf{F} = \begin{bmatrix} \mathbf{f}(\mathbf{x}_1)^T \\ \mathbf{f}(\mathbf{x}_2)^T \\ \vdots \\ \mathbf{f}(\mathbf{x}_n)^T \end{bmatrix}$ $\boldsymbol{\beta} = \begin{bmatrix} \beta_1 \\ \beta_2 \\ \vdots \\ \beta_p \end{bmatrix}$ $\boldsymbol{\varepsilon} = \begin{bmatrix} \varepsilon_1 \\ \varepsilon_2 \\ \vdots \\ \varepsilon_p \end{bmatrix}$ and: $\mathbf{f}(\mathbf{x})^T = \begin{bmatrix} f_1(\mathbf{x}) & f_2(\mathbf{x}) & \dots & f_p(\mathbf{x}) \end{bmatrix}$.

Typically, the f_i can be chosen as polynomial functions; in that case the model is often called polynomial response surface (PRS).

Since in practice the error is unknown, we estimate the response by:

$$\hat{y}(\mathbf{x}) = \mathbf{f}(\mathbf{x})^T\hat{\boldsymbol{\beta}} \tag{2–7}$$

where $\hat{\boldsymbol{\beta}}$ is an estimate of $\boldsymbol{\beta}$ and is chosen by minimizing the mean square error (MSE) between the estimates and the actual responses at all design points:

$$MSE = \frac{1}{n}\sum_{i=1}^{n}\left[\hat{y}((\mathbf{x}_i)) - y(\mathbf{x}_i)\right]^2 \tag{2–8}$$

Using the standard linear regression, the value of $\hat{\boldsymbol{\beta}}$ that minimizes the MSE is given by:

$$\hat{\boldsymbol{\beta}} = \left(\mathbf{F}^T\mathbf{F}\right)^{-1}\mathbf{F}^T\mathbf{Y}_{obs} \tag{2–9}$$

$$\hat{\boldsymbol{\beta}} = \mathbf{M}^{-1}\mathbf{F}^T\mathbf{Y}_{obs} \tag{2–10}$$

The quantity $\mathbf{M} = \mathbf{F}^T\mathbf{F}$ is called the Fisher information matrix.

In addition to the best predictor $\hat{y}$, the linear regression model provides a prediction variance, given by:

$$var\left[\hat{y}(\mathbf{x})\right] = \mathbf{f}(\mathbf{x})^T\mathbf{M}^{-1}\mathbf{f}(\mathbf{x}) \tag{2–11}$$

When the error is heteroskedastic, that is, when the error distribution differ from one point to another, the ordinary least square estimator of $\boldsymbol{\beta}$ is not appropriate. Instead, we

estimate the coefficients by the generalized least square estimator $\boldsymbol{\beta}^*$:

$$\boldsymbol{\beta}^* = \left(\mathbf{F}^T\boldsymbol{\Gamma}^{-1}\mathbf{F}\right)^{-1}\mathbf{F}^T\boldsymbol{\Gamma}^{-1}\mathbf{Y}_{obs} \tag{2–12}$$

with: $\boldsymbol{\Gamma} = [cov\left(y(\mathbf{x}_i), y(\mathbf{x}_j)\right)]_{1\leq i,j\leq n}$. In that case, the Fisher information matrix is:

$$\mathbf{M} = \mathbf{F}^T\boldsymbol{\Gamma}^{-1}\mathbf{F} \tag{2–13}$$

Note that if the errors are uncorrelated, $\boldsymbol{\Gamma}$ reduces to $\mathrm{diag}\left[\mathrm{var}(\varepsilon_1), \mathrm{var}(\varepsilon_2), ..., \mathrm{var}(\varepsilon_n)\right]$.

For calculation details, see for instance Box & Draper (1986), Khuri & Cornell (1996) or Myers & Montgomery (1995).

2.1.3 The Kriging Model

The Kriging metamodel was initially developed in the geostatistic framework [Matheron (1969), Cressie (1993)] to predict values based on spatial correlation considerations. Kriging can also be found on the literature under the name of Gaussian Process regression [Rasmussen & Williams (2006)], or regression with spatially correlated errors [Fedorov & Hackl (1997)]. The main hypothesis behind the Kriging model is to assume that the true function y is one realization of a Gaussian stochastic process Y:

$$y(\mathbf{x}) = Y(\mathbf{x}, \omega) \tag{2–14}$$

where ω belongs to the underlying probability space Ω. In the following we use the notation $Y(\mathbf{x})$ for the process and $y(\mathbf{x})$ for one realization. For Universal Kriging, Y is of the form:

$$Y(\mathbf{x}) = \sum_{j=1}^{p} \beta_j f_j(\mathbf{x}) + Z(\mathbf{x}) \tag{2–15}$$

where f_j are linearly independent known functions, and Z is a Gaussian process with zero mean and covariance $k(\mathbf{u}, \mathbf{v})$.

The covariance function (or kernel) k contains all the information of spatial dependency, and depends on parameters Θ. There exists many types of covariance functions; two of the most popular ones are the isotropic gaussian and exponential

covariances:

$$\text{Isotropic Gaussian covariance:} \qquad k(\mathbf{u},\mathbf{v}) = \sigma^2 \exp\left[-\left(\frac{\|\mathbf{u}-\mathbf{v}\|}{\theta}\right)^2\right] \tag{2–16}$$

$$\text{Isotropic Exponential covariance:} \qquad k(\mathbf{u},\mathbf{v}) = \sigma^2 \exp\left[-\left(\frac{\|\mathbf{u}-\mathbf{v}\|}{\theta}\right)\right] \tag{2–17}$$

For these covariances, the parameters Θ are the *process variance* σ^2 and *range* θ. Anisotropic covariance functions can also be defined by attributing a different θ in each direction:

$$\text{Anisotropic Gaussian covariance:} \qquad k(\mathbf{u},\mathbf{v}) = \sigma^2 \exp\left[-\sum_{j=1}^{d}\left(\frac{|\mathbf{u}_j-\mathbf{v}_j|}{\theta_j}\right)^2\right] \tag{2–18}$$

In Chapter 3, we also use the rational quadratic covariance function[Rasmussen & Williams (2006)]:

$$k(\mathbf{u},\mathbf{v}) = \left(1+\frac{\|\mathbf{u}-\mathbf{v}\|^2}{2\alpha l^2}\right)^{-\alpha} \tag{2–19}$$

with $\Theta = \{\alpha, l\}$.

In the geostatistic literature, three terminologies are used, depending on the linear part considered:

- simple Kriging (SK): the linear part reduces to a known constant β_1
- ordinary Kriging (OK): the constant β_1 is unknown
- universal Kriging (UK) is the general case.

The parameters Θ are usually unknown and must be estimated based on the observations, using maximum likelihood, cross-validation or variogram techniques for instance [see Rasmussen & Williams (2006), Stein (1999) or Cressie (1993)]. However, in the Kriging model they are considered as known. To account for additional variability due to the parameter estimation, one may use *Bayesian Kriging* models [see Martin & Simpson (2004) and Oakley & O'Hagan (2004)], which will not be detailed here.

2.1.3.1 Kriging with noise-free observations

First, we consider the most classical framework, where the function is observed without noise:

$$y_{obs,i} = y(\mathbf{x}_i) \tag{2–20}$$

Under such hypothesis, the best linear unbiased predictor (BLUP) for y, knowing the observations $\mathbf{Y}_{obs}$, is given by the following equation:

$$\begin{aligned} m_K(\mathbf{x}) &= E\left[Y(\mathbf{x}) | Y(\mathbf{X}) = \mathbf{Y}_{obs}\right] \\ &= \mathbf{f}(\mathbf{x})^T \hat{\boldsymbol{\beta}} + \mathbf{c}(\mathbf{x})^T \mathbf{C}^{-1} \left(\mathbf{Y}_{obs} - \mathbf{F}\hat{\boldsymbol{\beta}}\right) \end{aligned} \tag{2–21}$$

where:

- $\mathbf{f}(\mathbf{x}) = \begin{bmatrix} f_1(\mathbf{x}) & \dots & f_p(\mathbf{x}) \end{bmatrix}^T$ is $p \times 1$ vector of bases,
- $\hat{\boldsymbol{\beta}} = \begin{bmatrix} \hat{\beta}_1 & \dots & \hat{\beta}_p \end{bmatrix}^T$ is $p \times 1$ vector of estimates of $\boldsymbol{\beta}$,
- $\mathbf{c}(\mathbf{x}) = \begin{bmatrix} cov(\mathbf{x}, \mathbf{x}_1) & \dots & cov(\mathbf{x}, \mathbf{x}_n) \end{bmatrix}^T$ is $n \times 1$ vector of covariance,
- $\mathbf{C} = \left[cov\left(\mathbf{x}_i, \mathbf{x}_j\right)\right]_{1 \leq i,j \leq n}$ is $n \times n$ covariance matrix, and
- $\mathbf{F} = \begin{bmatrix} \mathbf{f}(\mathbf{x}_1) & \dots & \mathbf{f}(\mathbf{x}_n) \end{bmatrix}^T$ is $p \times n$ matrix of bases.

$\hat{\boldsymbol{\beta}}$ is the vector of generalized least square estimates of $\boldsymbol{\beta}$:

$$\hat{\boldsymbol{\beta}} = \left(\mathbf{F}^T \mathbf{C}^{-1} \mathbf{F}\right)^{-1} \mathbf{F}^T \mathbf{C}^{-1} \mathbf{Y}_{obs} \tag{2–22}$$

In addition, the Kriging model provides an estimate of the accuracy of the mean predictor, the Kriging prediction variance:

$$s_K^2(\mathbf{x}) = k(\mathbf{x}, \mathbf{x}) - \mathbf{c}(\mathbf{x})^T \mathbf{C}^{-1} \mathbf{c}(\mathbf{x}) + \left(\mathbf{f}(\mathbf{x})^T - \mathbf{c}(\mathbf{x})^T \mathbf{C}^{-1} \mathbf{F}\right) \left(\mathbf{F}^T \mathbf{C}^{-1} \mathbf{F}\right)^{-1} \left(\mathbf{f}(\mathbf{x})^T - \mathbf{c}(\mathbf{x})^T \mathbf{C}^{-1} \mathbf{F}\right)^T \tag{2–23}$$

Note that the Kriging variance does not depend on the observations $\mathbf{Y}_{obs}$, but only on the design of experiments. Derivation details can be found in Matheron (1969), Cressie (1993), or Rasmussen & Williams (2006). We denote by $M(\mathbf{x})$ the Gaussian process conditional on

the observations $\mathbf{Y}_{obs}$:

$$(M(\mathbf{x}))_{\mathbf{x}\in D} = (Y(\mathbf{x})|Y(\mathbf{X}) = \mathbf{Y}_{obs})_{\mathbf{x}\in D} = (Y(\mathbf{x})|obs)_{\mathbf{x}\in D} \tag{2–24}$$

The Kriging model provides the distribution of M at a prediction point $\mathbf{x}$:

$$M(\mathbf{x}) \sim \mathcal{N}\left(m_K(\mathbf{x}), s_K^2(\mathbf{x})\right) \tag{2–25}$$

Figure 2-1 shows a Kriging model with a first-order trend ($\boldsymbol{\beta} = \beta_1$, simple Kriging) and five equally-spaced observations along with the 95% confidence intervals, which are calculated from $m_K \pm 1.96 s_K$. On this example, the confidence interval contains the actual response.

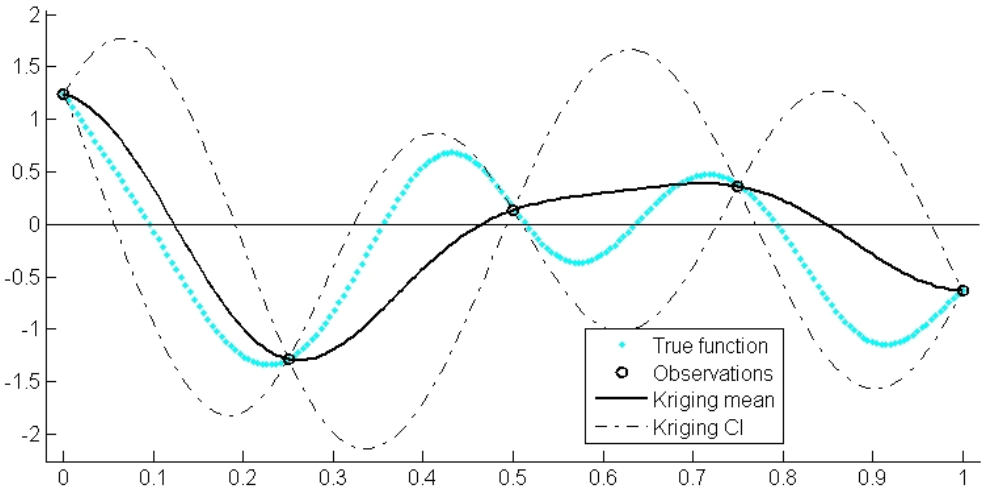

Figure 2-1. Example of Simple Kriging model. The 95% confidence intervals (CI) are equal to $m_K \pm 1.96 \times s_K$. The DoE consists of five points equally spaced in [0, 1].

The Kriging mean m_K interpolates the function $y(\mathbf{x})$ at the design of experiment points:

$$m_K(\mathbf{x}_i) = y(\mathbf{x}_i), \quad 1 \leq i \leq n \tag{2–26}$$

The Kriging variance is null at the observation points $\mathbf{x}_i$, and greater than zero elsewhere:

$$s_K^2(\mathbf{x}_i) = 0, \quad 1 \leq i \leq n \quad and \quad s_K^2(\mathbf{x}) \geq 0, \quad \mathbf{x} \neq \mathbf{x}_i \tag{2–27}$$

Besides, the Kriging variance function increases with the distance of $\mathbf{x}$ to the observations.

2.1.3.2 Kriging with nugget effect

When noisy observations are considered, a diagonal matrix must be added to the covariance matrix:

$$\mathbf{C}_\Delta = \mathbf{C} + \mathbf{\Delta} \tag{2–28}$$

with: $\mathbf{\Delta} = \text{diag}\left([var(\varepsilon_1), var(\varepsilon_2), \ldots, var(\varepsilon_n)]\right)$ the variances of the observations.

Equations for m_K and s_K^2 are the same as in Eqs. 2–21 and 2–23 but using $\mathbf{C}_\Delta$ instead of $\mathbf{C}$. For theoretical details and bibliography, see for instance Ginsbourger (2009) (Chap. 7). The main difference with the classical Kriging is that best predictor is not an interpolator anymore; also, the Kriging variance is non-null at the observation points. Figure 2-2 shows a Kriging model based on noisy observations. Each observation has a different noise variance.

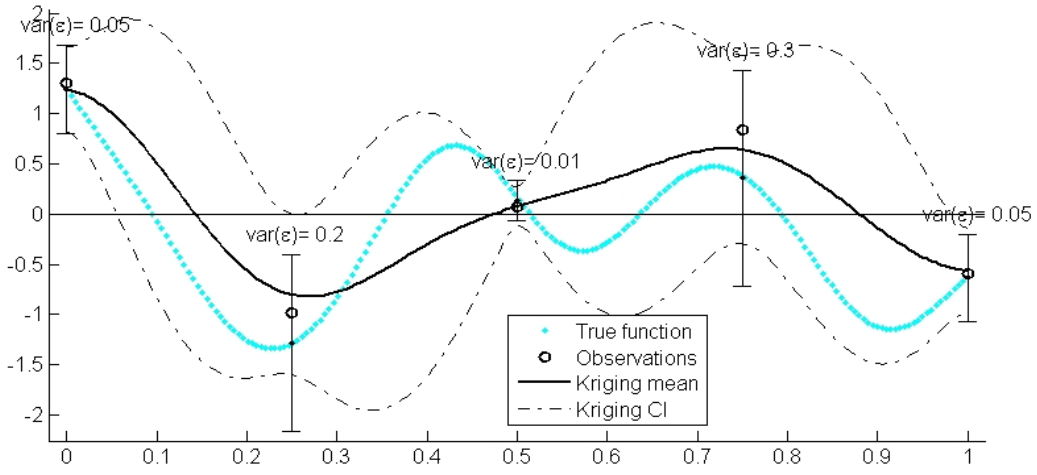

Figure 2-2. Example of Simple Kriging model with noisy observations. The bars represent $\pm$ two times the standard deviation of the noise. The Kriging mean does not interpolate the data and the Kriging variance is non-null at the observation points.

2.2 Design Of Experiment Strategies

Choosing the set of experiments $\mathbf{X}$ plays a critical role in the accuracy of the metamodel and the subsequent use of the metamodel for prediction, learning or optimization. In this section, we detail three families of design of experiments: classical and space-filling designs, model-oriented (or optimal) designs, and adaptive designs.

2.2.1 Classical And Space-Filling Designs

The first family of DoE consists of designs based on geometric considerations. In a full-factorial (FF) design, the variables are discretized into a finite number of levels, and the design consists of all the possible combinations of the discrete variables. Two-level FF designs, where the input variables are taken only at their minimum and maximum values, are typically used for screening in order to identify the most significant variables and remove the others. Although extensively used historically, such type of DoEs suffer from several drawbacks among the following:

- it requires a large number of observations in high dimensions (a FF design with q levels in d dimensions is made of q^d observations), making them impractical for computationally expensive problems
- they do not ensure space-filling in high dimensions
- the number of observation points collapses when projecting on the subspaces (when some variables are removed for instance).

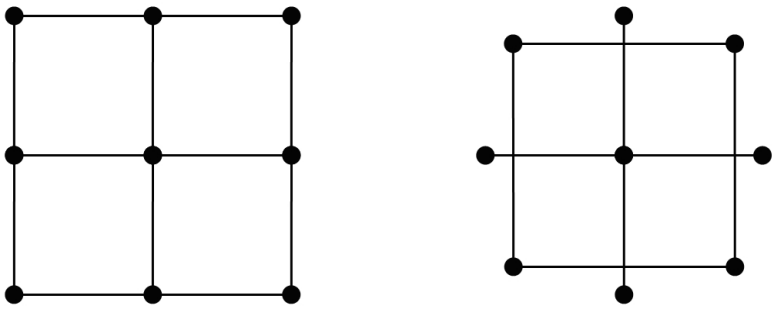

Figure 2-3. Examples of full-factorial and central composite designs.

There exists classical alternatives to FF designs, such as central-composite designs (that consist of 2^d vertices, $2d$ axial points and p repetitions of central point), or fractional

designs (that are subsets of FF designs). See for instance Myers & Montgomery (1995) for details. Figure 2-3 shows a three-level FF design and a central composite design for a two-dimensional domain.

A popular alternative to the geometrical designs is Latin Hypercube sampling (LHS) [McKay et al. (2000)]. LHS is a random DoE that insures uniformity of the marginal distributions of the input variables.

To generate a DoE of n points, each variable range is divided into n equal intervals, for instance for the range $[0, 1]$: $\left\{[0, \frac{1}{n}], [\frac{1}{n}, \frac{2}{n}], ..., [\frac{n-1}{n}, 1]\right\}$. Then, the DoE is constructed by picking n points so that all the intervals for each variable is represented once. Figure 2-4 shows a nine-point LHS design for a two-dimensional domain. In a d-dimensional space, the total number of combinations is n^{d-1}, which increases very rapidly with both sample size and dimension. The variable values can be chosen deterministically as the centre of the interval for instance, or randomly inside the interval.

LHS can also be optimized to ensure better space-filling. Space-filling criteria include:

- maximum minimum distance between sampling points (*maximin* designs),
- maximum-entropy designs [Shewry & Wynn (1987)],
- minimum discrepancy measures, etc.

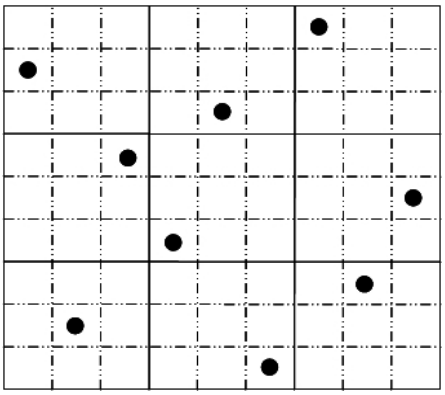

Figure 2-4. A nine-point LHS design. The projections on the margins are non redudant and equally-spaced if the design points are centered in each cell.

Finally, low-discrepancy sequences are also often used for space-filling strategies, such as Sobol, Halton, Harmmersley, Niederreitter or Faure sequences. See Niederreiter (1992) or Sobol (1976) for details.

2.2.2 Model-Oriented Designs

The previous sampling strategies were built independently of the metamodel to be fitted to the observations. Alternatively, when the choice of the metamodel is made *a priori*, it is possible to choose the observation points in order to maximize the quality of statistical inference. The theory of optimal designs has originally been developed in the framework of linear regression, and was extended later to other models such as Kriging since the 80's.

Let ϕ be a functional of interest to minimize that depends on the design of experiments $\mathbf{X}$. A design $\mathbf{X}^*$ is called ϕ-optimal if it achieves:

$$\mathbf{X}^* = argmin\,[\phi(\mathbf{X})] \tag{2–29}$$

A- and D-optimality aim at minimizing the uncertainty in the parameters of the metamodel when uncertainty is due to noisy observations. In the framework of linear regression, D-optimal designs minimize the volume of the confidence ellipsoid of the coefficients, while A-optimal designs minimize its perimeter (or surface for $d > 2$). Formally, the A- and D-optimality criteria are, respectively, the trace and determinant of Fisher's information matrix [Khuri & Cornell (1996)]:

$$A(\mathbf{X}) = trace(M(\mathbf{X})) \tag{2–30}$$

$$D(\mathbf{X}) = det(M(\mathbf{X})) \tag{2–31}$$

In linear regression, these criteria are particularly relevant since minimizing the uncertainty in the coefficients also minimizes the uncertainty in the prediction (according to the D-G equivalence theorem, which is developed further in Chapter 6).

For Kriging, uncertainties in covariance parameters and prediction are not simply related. A natural alternative is to take advantage of the prediction variance associated with the metamodel. The prediction variance allows us to build measures that reflect the overall accuracy of the Kriging. Two different criteria are available: the integrated mean square error (IMSE) and maximum mean square error (MMSE) [Santner et al. (2003), Sacks et al. (1989a)]:

$$IMSE = \int_D MSE(\mathbf{x}) d\mu(\mathbf{x}) \tag{2–32}$$

$$MMSE = max_{\mathbf{x}\in D} \left[MSE(\mathbf{x})\right] \tag{2–33}$$

$\mu(x)$ is an integration measure (usually uniform) and

$$MSE(\mathbf{x}) = E\left[\left(y(\mathbf{x}) - M(\mathbf{x})\right)^2 \middle| obs\right] \tag{2–34}$$

When the function to approximate is a realization of a gaussian process with covariance structure and parameters equal to the ones chosen for Kriging, the MSE coincides with the prediction variance s_K^2. Note that the above criteria are often called I-criterion and G-criterion, respectively, in the regression framework. The IMSE is a measure of the average accuracy of the metamodel, while the MMSE measures the risk of large error in prediction. In practice, the IMSE criterion essentially reflects the spatial distribution of the observations. For dimensions higher than two, the MMSE is not very relevant since the regions of maximum uncertainty are always situated on the boundaries, and MMSE-optimal designs consist of observations taken on the edges of the domain only, which is not efficient for Kriging.

Optimal designs are model-dependent, in the sense that the optimality criterion is determined by the choice of the metamodel. In regression, A- and D-criteria depend on the choice of the basis functions, while in Kriging the prediction variance depends on the linear trend, the covariance structure, and parameter values. A fundamental result, however, is that assuming a particular model structure (and covariance parameters for

Kriging), none of the criteria depends on the *response values* at the design points. The consequence is that the DoEs can be designed *offline* before generating the observations. However, in practice this statement has to been moderated, since the Kriging covariance parameters are most of the time estimated from the observations.

2.2.3 Adaptive Designs

The previous DoE strategies choose all the points of the design before computing any observation. It is also possible to build the DoE sequentially, by choosing a new point as a function of the other points and their corresponding response values. Such approach has received considerable attention from the engineering and mathematical statistic communities, for its advantages of flexibility and adaptability over other methods [Lin et al. (2008), Scheidt (2006), Turner et al. (2003)].

Typically, the new point achieves a maximum on some criterion. For instance, a sequential DoE can be built by making at each step a new observation where the prediction variance is maximal. The algorithmic procedure is detailed in Table 2-1.

Table 2-1. Sequential DoE minimizing the maximum prediction variance at each step.

$\mathbf{X} = \{\mathbf{x}_1, \ldots, \mathbf{x}_n\}$
for i = 1 to k
  $\mathbf{x}_{new} = \arg\max_{\mathbf{x} \in D} s_K^2(\mathbf{x})$
  $\mathbf{X} = \{\mathbf{X}, \mathbf{x}_{new}\}$
end

Sacks et al. (1989b) uses this strategy as a heuristic to build IMSE-optimal designs for Kriging. Theoretically, this sequential strategy is less efficient that the direct minimization of the $IMSE$ criterion. The advantage of sequential strategy here is twofold. Firstly, it is computational, since it transforms an optimization problem of dimension $n \times d$ (for the IMSE minimization) into k optimizations of dimension d. Secondly, it allows us to reevaluate the covariance parameters after each observation. In the same fashion, Williams et al. (2000), Currin et al. (1991), Santner et al. (2003) use a Bayesian approach to derive sequential IMSE designs. Osio & Amon (1996) proposed a multistage approach to enhance

first space-filling in order to accurately estimate the Kriging covariance parameters and then refine the DoE by reducing the model uncertainty. Some reviews of adaptive sampling in engineering design can be found in Jin et al. (2002).

In general, a particular advantage of sequential strategies over other DoEs is that they can integrate the information given by the first k observation values to choose the $(k+1)^{th}$ training point, for instance by reevaluating the Kriging covariance parameters. It is also possible to define response-dependent criteria, with naturally leads to surrogate-based optimization. One of the most famous adaptive strategy is the EGO algorithm (Jones et al. (1998)), used to derive sequential designs for the optimization of deterministic simulation models. At each step, the new observation is chosen to maximize the expected improvement, a functional that represents a compromise between exploration of unknown regions and local search:

$$EI\left(\mathbf{x}\right) = E\left(\max\left[0, \min\left(\mathbf{Y}_{obs}\right) - M\left(\mathbf{x}\right)\right]\right) \tag{2–35}$$

where $M(\mathbf{x})$ is the Kriging model as described in Eq. 2–25.

Kleijnen & Van Beers (2004) proposed an application-driven adaptive strategy using criteria based on response values. Tu & Barton (1997) used a modified D-optimal strategy for boundary-focused polynomial regression. In Chapter 5, we detail an original adaptive design strategy for target region approximation.

CHAPTER 3
CONSERVATIVE PREDICTIONS USING SURROGATE MODELING

3.1 Motivation

In analyzing engineering systems, multiple sources of error - such as modeling error or insufficient data - prevent us from taking the analysis results at face value. Conservative prediction is a simple way to account for uncertainties and errors in a system analysis, by using calculations or approximations that tend to safely estimate the response of a system. Traditionally, safety factors have been extensively used for that purpose, even though their effectiveness is questionable [Elishakoff (2004), Acar et al. (2007)].

When surrogate models are used for predicting critical quantities, very little is known in practice to provide conservative estimates, and how conservative strategies impact the design process. Most surrogates are designed so that there is a 50% chance that the prediction will be higher than the real value. The objective of this work is to propose alternatives to modify the traditional surrogates so that this percentage is pushed to the conservative side with the least impact on accuracy.

Since conservative surrogates tend to overestimate the actual response, there is a trade-off between accuracy and conservativeness. The choice of such trade-off determines the balance between the risk of overdesign and the risk of weak design. The design of conservative surrogates can be considered as a bi-objective optimization problem, and results are presented in the form of Pareto fronts: accuracy versus conservativeness.

The most classical conservative strategy is to bias the prediction response by a multiplicative or additive constant. Such approaches are called empirical because the choice of the constant is somehow arbitrary and based on previous knowledge of the engineering problem considered. However, it is difficult to predict how efficient its application is to surrogates, and how it is possible to design those quantities. Alternatively, it is possible to use the statistical knowledge from the surrogate fitting (prediction variance) to build one-sided confidence intervals on the prediction.

For this study, we consider two types of surrogate models: polynomial response surfaces (PRS) and Kriging. We propose three alternatives to provide conservative estimates: using cross-validation to define constant margins, using confidence intervals given by the surrogate model, and using the bootstrap method. The methods differ in the sense that one assumes a particular distribution of the error, while the others (cross-validation and bootstrap) does not. Different metrics are defined to analyze the trade-off between accuracy and conservativeness. The methods are applied to two test problems: one analytical and one based on Finite Element Analysis.

3.2 Design Of Conservative Predictors

3.2.1 Definition Of Conservative Predictors

Without any loss of generality, we assume here that a conservative estimator is an estimator that does not underestimate the actual value. Hence, a conservative estimators can be obtained by simply adding a positive safety margin to the unbiased estimator:

$$\hat{y}_{SM}(\mathbf{x}) = \hat{y}(\mathbf{x}) + S_m \tag{3–1}$$

Alternatively, it is possible to define a conservative estimator using safety factors, which are more commonly used in engineering:

$$\hat{y}_{SF}(\mathbf{x}) = \hat{y}(\mathbf{x}) \times S_f \tag{3–2}$$

In the context of surrogate modeling, safety margins are more convenient. Indeed, when using a safety factor, the level of safety depends on the response value, while most surrogates model assume that the error is independent of the mean of the response. Hence, in this work we use only safety margins to define a conservative estimator.

The value of the margin directly impacts the level of safety and the error in the estimation. Hence, there is a great incentive to find the margin that ensure a targeted level of safety with least impact on the accuracy of the estimates. The safety margin can be constant, or depend on the location, hence written $S_m(\mathbf{x})$ (pointwise margin). In the

following sections, we provide several ways to design the margin, using parametric and non-parametric methods, for pointwise and constant margins.

3.2.2 Metrics For Conservativeness And Accuracy

As discussed in introduction, conservative estimates are biased, and a high level of conservativeness can only be achieved at a price in accuracy. Thus, the quality of a method can only be measured as a trade-off between conservativeness and accuracy. In order to assess a global performance of the methods, we propose to define accuracy and conservativeness indexes.

The most widely used measure to check the accuracy of a surrogate is the root mean square error (e_{RMS}), defined as:

$$e_{RMS} = \left(\int_D \left(\hat{y}\left(x\right) - y\left(x\right) \right)^2 dx \right)^{\frac{1}{2}} \tag{3–3}$$

The e_{RMS} can be computed by Monte-Carlo integration at a large number of p_{test} test points:

$$e_{RMS} \approx \sqrt{\frac{1}{p_{test}} \sum_{i=1}^{p_{test}} e_i^2} \tag{3–4}$$

where $e_i = (\hat{y}_i - y_i)$, $\hat{y}_i$ and y_i being the values of the conservative prediction and actual simulation at the i-th test point, respectively.

We also define the relative loss in accuracy, in order to measure simply by how much the accuracy is degraded when high levels of conservativeness are targeted:

$$l_\alpha = \frac{e_{RMS}}{e_{RMS}|_{ref}} - 1 \tag{3–5}$$

where e_{RMS} is taken at a given target conservativeness; and $e_{RMS}|_{ref}$ is the e_{RMS} value of reference. In most of the study, which we take equal to the value of e_{RMS} when the target conservativeness is 50%.

There are different measures of the conservativeness of an approximation. Here we use the percentage of conservative errors (i.e. positive):

$$\%c = 100 \int_D I\left[\hat{y}\left(x\right) - y\left(x\right)\right] dx \tag{3–6}$$

where $I(e)$ is the indicator function, which equals 1 if $e > 0$ and 0 otherwise. $\%c$ can be estimated by Monte-Carlo integration:

$$\%c \approx \frac{100}{p_{test}} \sum_{i=1}^{p_{test}} I\left(e_i\right) \tag{3–7}$$

Ideally, for most surrogate models, $\%c = 50\%$ when the approximation is unbiased.

The percentage of conservative errors provides the probability to be conservative. However, it fails to inform by how much it is unconservative when predictions are unconservative. Thus, an alternate measure of conservativeness is proposed; that is, the maximum unconservative error (largest negative error) :

$$\text{MaxUE} = \max\left(\max\left(-e_i\right), 0\right) \tag{3–8}$$

This index can also be normalized by the index of the unbiased estimator:

$$\text{MaxUE}_{\%} = \frac{\text{MaxUE}}{\text{MaxUE}|_{\text{ref}}} - 1 \tag{3–9}$$

where $\text{MaxUE}|_{ref}$ is the value of reference, which we take equal to the value for the unbiased estimator.

A value of $\text{MaxUE}_{\%}$ of 50% means that the maximum unconservative error is reduced by 50% compared to the BLUE estimator.

Alternative measures of conservativeness can be defined, including the mean or the median of the unconservative errors. However, the maximum error decreases monotonically when target conservativeness is increased, while mean and median can increase when we increase conservativeness, for instance when we have initially very small and very large errors.

3.2.3 Constant Safety Margin Using Cross-Validation Techniques

Here, we consider the design of conservative surrogates, when the same safety margin is applied everywhere on the design domain. In the following, we call such estimators CSM estimators (for Constant Safety Margin), and denote it $\hat{y}_{CSM}$.

In terms of the cumulative distribution function (CDF) of the errors, F_e, the safety margin S_m for a given conservativeness, $\%c$, is given as:

$$S_m = F_e^{-1}\left(\frac{\%c}{100}\right) \tag{3–10}$$

The objective is to design the safety margin such that the above equation is ensured. The actual error distribution is, in practice, unknown. We propose here to estimate it empirically using cross-validation techniques in order to choose the margin.

Cross-validation (XV) is a process of estimating errors by constructing the surrogate without some of the points and calculating the errors at these left out points. The process is repeated with different sets of left-out points in order to get statistically significant estimates of errors. The process proceeds by dividing the set of n data points into subsets. The surrogate is fitted to all subsets except one, and error is checked in the subset that was left out. This process is repeated for all subsets to produce a vector of cross-validation errors, $\mathbf{e}_{XV}$. Usually, only one point is removed at a time (leave-one-out cross-validation), so the size of $\mathbf{e}_{XV}$ is equal to n.

The empirical CDF F_{XV}, defined by the n values of $\mathbf{e}_{XV}$, are an approximation of the true distribution F_e. Now, in order to design the margin, we replace F_e in Eq. 3–10 by F_{XV}:

$$S_m = F_{XV}^{-1}\left(\frac{\%c}{100}\right) \tag{3–11}$$

For instance, when $n = 100$ and 75% conservativeness is desired, the safety margin is chosen equal to the 25^{th} highest cross-validation error.

3.2.4 Pointwise Safety Margin Based On Error Distribution

Conservative estimates can also be obtained assuming the error distribution is known as provided by the surrogate analysis. Classical regression provides a confidence interval for the predicted model. A unilateral confidence interval of level α for the response $y(\mathbf{x})$ is given by [see Khuri & Cornell (1996)]:

$$CI = \left]-\infty, \quad \mathbf{f}^T(\mathbf{x})\,\hat{\beta} + t^{-1}_{n-p-1}(1-\alpha)\,s\right] \tag{3–12}$$

where t_{n-p-1} is the Student's distribution with $n-p-1$ degrees-of-freedom, and:

$$s = \hat{\sigma}\sqrt{1 + \mathbf{f}^T(\mathbf{x})\,\mathbf{M}^{-1}(\mathbf{X})\,\mathbf{f}(\mathbf{x})}$$

$$\hat{\sigma}^2 = \frac{1}{n-p-1}\sum_{i=1}^{n}(y_i - \hat{y}_i)^2$$

We define the conservative estimator of level $(1-\alpha)$ as the upper bound of the confidence interval:

$$\hat{y}_{\mathrm{ED}}(\mathbf{x}) = \mathbf{f}^T(\mathbf{x}_{new})\,\hat{\beta} + t^{-1}_{n-p-1}(1-\alpha)\,s \tag{3–13}$$

This conservative estimate has the form of a margin added to the unbiased prediction; the margin depends on the prediction location and is equal to:

$$S_m(\mathbf{x}) = t^{-1}_{n-p-1}(1-\alpha)\,\hat{\sigma}\sqrt{1 + \mathbf{f}^T(\mathbf{x})\,\mathbf{M}^{-1}(\mathbf{X})\,\mathbf{f}(\mathbf{x})} \tag{3–14}$$

Kriging also provides confidence intervals for the prediction, assuming that the prediction error is normally distributed with mean m_K and variance s_K^2. Then, we can define the conservative estimator of level $(1-\alpha)$ as:

$$\hat{y}_{\mathrm{ED}}(\mathbf{x}) = \Phi^{-1}_{m_K(\mathbf{x}),m_K^2(\mathbf{x})}(1-\alpha) \tag{3–15}$$

where $\Phi^{-1}_{m_K(\mathbf{x}),s_K^2(\mathbf{x})}$ is the inverse normal cumulative distribution function of mean $m_K(\mathbf{x})$ and variance $s_K^2(\mathbf{x})$.

In the following, these estimators are referred as ED (error distribution) estimate. They are called *parametric* estimates since they assume a particular form of the distribution of the error. Note that confidence intervals given by kriging have a different interpretation than the ones given by regression. Indeed, in regression the interpretation of the CI is that there is a probability that an observation taken at $\mathbf{x}$ falls into the interval. In kriging, it means that $(1-\alpha)\%$ of the realizations of the gaussian processes conditional to the observations will stay within the interval bounds.

3.2.5 Pointwise Safety Margin Using Bootstrap

Error distribution estimators rely on the fact that the hypothesis behind the surrogate model are satisfied in practice. In particular, normality of the error distribution is always assumed. It is obvious that, when such hypothesis is violated, the safety margin designed with error distribution can be very inaccurate. In this section, we propose the use of bootstrap to obtain confidence intervals without assumptions on the error distribution.

3.2.5.1 The Bootstrap principle

The bootstrap method can provide an efficient way of estimating the distribution of a statistical parameter θ based on samples $\{u_1, \ldots, u_n\}$ of the random variable U using the re-sampling technique [Efron (1982), Chernick (1999)]. The idea is to create many sets of bootstrap samples by re-sampling with replacement from the original data.

This method only requires the initial set of samples. Figure 3-1 illustrates the procedure of the bootstrap method. The size of the initial samples is n and the number of bootstrap re-samplings is p. Each re-sampling can be performed by sampling with replacement n data out of the n initial samples (hence, the bootstrap samples contain repeated values from the initial samples and omit some of the initial values). Since the re-sampling process draws samples from the existing set of samples, it does not require additional simulations. The parameter θ (for instance, the mean or standard deviation of U), is estimated for each bootstrap samples. Since the re-sampling procedure allows selecting data with replacement, the statistical properties of the re-sampled data are

different from that of the original data. Then, the set of p bootstrap estimates θ_{boot} defines an empirical distribution of θ. This approach allows us to estimate the distribution of any statistical parameter without requiring additional data, and without any assumption on the distribution of the parameter.

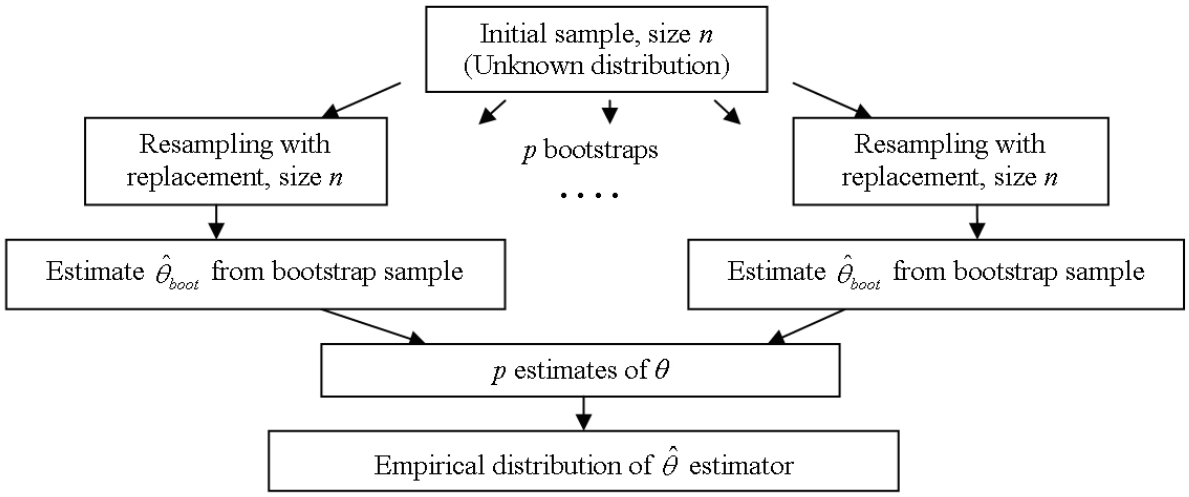

Figure 3-1. Schematic representation of bootstrapping. Bootstrap distribution of θ (histogram or CDF of the p estimates) is obtained by multiple re-sampling (p times) from a single set of data.

3.2.5.2 Generating confidence intervals for regression

In this section, we present the application of bootstrap to regression, as proposed by Stine (1985). Calculations and methodology to obtain confidence intervals come from this paper. The main idea is that resampling with replacement is conducted on the regression residuals.

First, the regression model is estimated using the standard equations. Then, the observations are perturbed by resampling the residuals:

$$\mathbf{Y}^* = \mathbf{X}\hat{\boldsymbol{\beta}} + \boldsymbol{\varepsilon}^* \tag{3–16}$$

$\boldsymbol{\varepsilon}^*$ is the bootstrap vector of residuals, obtained by sampling with replacement from the empirical distribution of the residual vector $\boldsymbol{\varepsilon}$.

Note that the bootstrap model assumes that the mean of the true function is equal to the best predictor of the regression model, that is, the true function is assumed to be of the form:

$$y^*(\mathbf{x}) = \mathbf{f}^T(\mathbf{x})\,\hat{\boldsymbol{\beta}} + \varepsilon^* \tag{3–17}$$

where ε^* follows the empirical distribution of $\boldsymbol{\varepsilon}^*$.

Then, the model is built based on the bootstrap observations:

$$\boldsymbol{\beta}^* = \left(\mathbf{f}^T(\mathbf{X})\,\mathbf{f}^T(\mathbf{X})\right)^{-1}\mathbf{f}^T(\mathbf{X})\,\mathbf{Y}^* \tag{3–18}$$

Using bootstrap, we account for the variability in $\hat{\boldsymbol{\beta}}$ through various bootstrap estimates ${\boldsymbol{\beta}^*}_1, {\boldsymbol{\beta}^*}_2, {\boldsymbol{\beta}^*}_3, ...$, and also for the noise ε at the predicted point.

The structure of the noise leads to valuable computational shortcut. Indeed, the error E^* for the bootstrap model consists of two additive components:

$$E^* = \varepsilon^* + b^* \tag{3–19}$$

with ε^* taken from the initial vector of residuals and b^* is the error due to uncertainty in $\hat{\beta}$:

$$\begin{aligned} b^*(\mathbf{x}) &= \mathbf{f}^T(\mathbf{x})\,\boldsymbol{\beta}^* - \mathbf{f}^T(\mathbf{x})\,\hat{\boldsymbol{\beta}} \\ &= \mathbf{f}^T(\mathbf{x})\,\mathbf{M}^{-1}\mathbf{f}^T(\mathbf{X})\,\boldsymbol{\varepsilon}^* \end{aligned} \tag{3–20}$$

Since b^* and ε^* are independent, the distribution of E^* is their convolution. Then, the distribution F_e^* of the error can be approximated by:

$$F_e^*(u) = \frac{1}{N}\sum_{j=1}^{N} F_n\left(u - b_j^*(\mathbf{x})\right) \tag{3–21}$$

with:

- F_n the empirical distribution of the (initial) residuals ε
- u a scalar

- $b_j^*(\mathbf{x})$ the error of the j^{th} bootstrap model at $\mathbf{x}$
- N the number of bootstrap replicates.

$F_e^*(u)$ is the probability, computed by bootstrap, that the error at $\mathbf{x}$ exceeds u.

Then, the pointwise safety margin $p_{1-\alpha}$ needed to achieve $(1-\alpha)\%$ conservativeness is defined as the inverse of F_e^* taken at $(1-\alpha)\%$:

$$p_{1-\alpha} = (1-\alpha) \tag{3–22}$$

However, F_e^{*-1} cannot be known analytically. In practice, we choose a finite number of values of u for which we compute $F_e^*(u)$ for a given $\mathbf{x}$; then we obtain the inverse of the distribution (as shown in Figure 3-2) by interpolation.

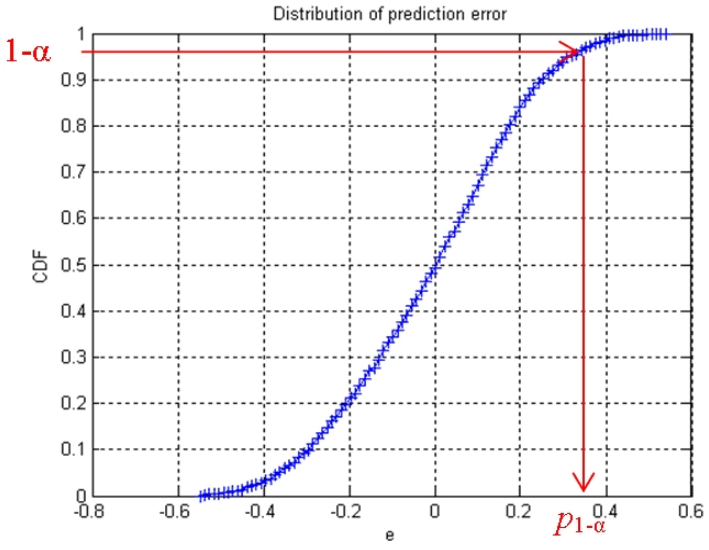

Figure 3-2. Percentile of the error distribution interpolated from 100 values of u.

Finally, the bootstrap conservative predictor is defined as:

$$\hat{y}_{BS} = \mathbf{x}_{pred}\hat{\boldsymbol{\beta}} + p_{1-\alpha} \tag{3–23}$$

In the following, these estimators are called BS (bootstrap) estimators and denoted by $\hat{y}_{BS}$.

3.2.6 Alternative Methods

In the context of conservative predictions, we proposed two other alternatives. The first is called biased fitting: it consists of adding constraints to the least square minimization problem in order to bias the surrogate to be on one side of the observations. The second is Indicator Kriging (IK), which is a non-parametric method that estimates probabilities of exceeding a particular threshold. However, these methods were found to be less efficient than the other methods to produce conservative predictions. Hence, we do not present it here. They can be found in Appendix A.1 and A.2.

3.3 Case Studies

3.3.1 Test Problems

3.3.1.1 The Branin-Hoo function

The first test function is a deterministic two-dimensional function, which is often used to test optimization methods [Dixon & Szego (1978)]. The input variable domains are: $x \in [-5 \;\; 10]$ and $y \in [0 \;\; 15]$. The expression of the Branin-Hoo function is given as:

$$f(x,y) = \left(y - \frac{5.1x^2}{4\pi^2} + \frac{5x}{\pi} - 6\right)^2 + 10\left(1 - \frac{1}{8\pi}\right)\cos(x) + 10 \qquad (3\text{–}24)$$

The range of the function is between zero and 300. Large values are located on the bounds of the domain.

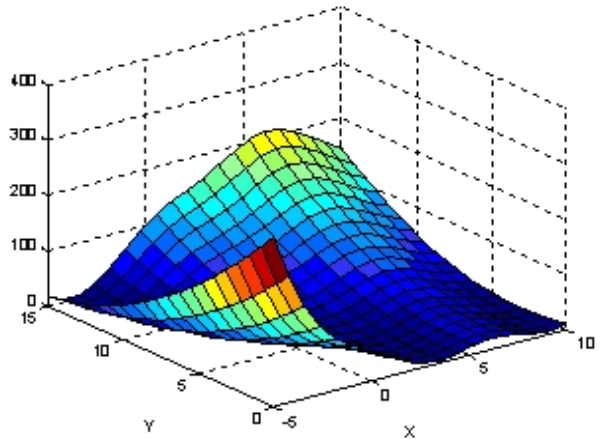

Figure 3-3. Branin-Hoo function.

3.3.1.2 The torque arm model

This second example was originally presented by Bennett & Botkin (1986). It consists of the shape design of a particular piece from automotive industry called a torque arm. The toque arm model, shown in 3-4, is under a horizontal and vertical load, $F_x = -2789$N and $F_y = 5066$N, respectively, transmitted from a shaft at the right hole, while the left hole is fixed. The torque arm consists of a material with Young's modulus, $E = 206.8$GPa and Poisson's ratio, $\nu = 0.29$.

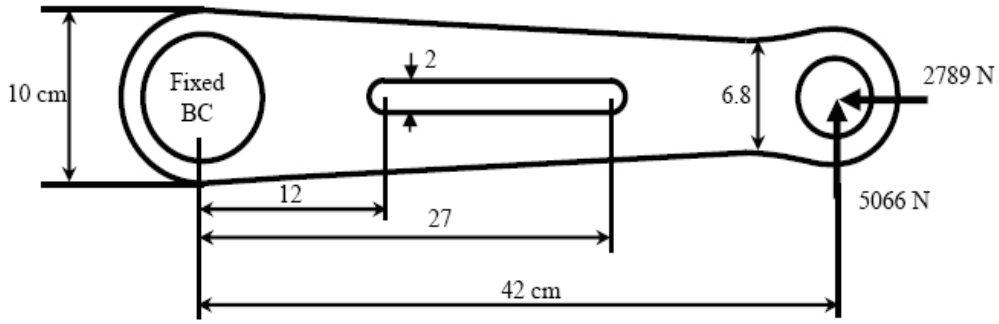

Figure 3-4. Initial design of the Torque arm.

The objective of the analysis is to minimize the weight with a constraint on the maximum stress. Seven design variables are defined to modify the initial shape. Figure 3-5 and Table 3-1 show the design variables and their lower and upper bounds, respectively. The lower and upper bounds are selected such that the topology of the design is unchanged.

Table 3-1. Range of the design variables (cm).

Design variable	Lower bound	Upper bound
1	-2.0	3.5
2	-0.2	2.5
3	-2.0	6.0
4	-0.2	0.5
5	-0.1	2.0
6	-1.5	2.0
7	-0.1	2.0

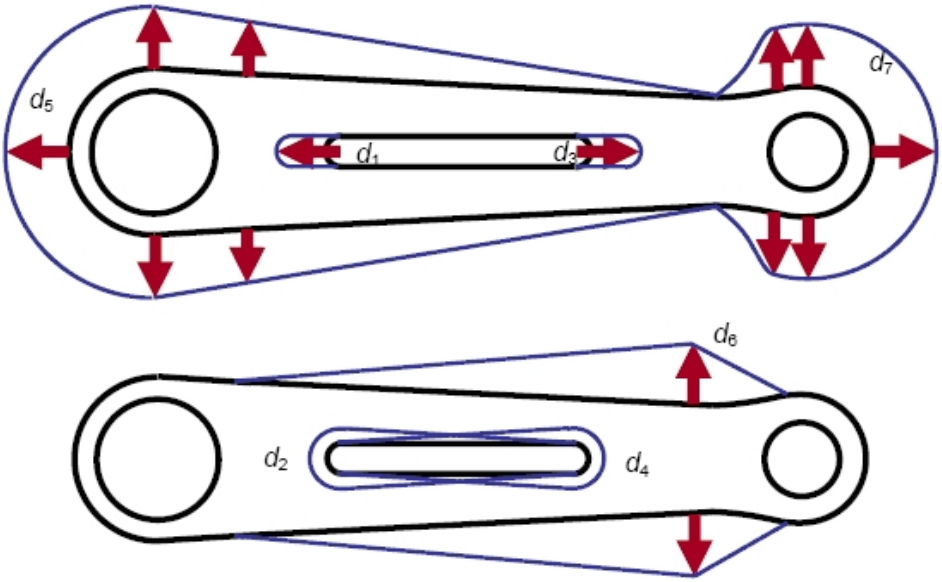

Figure 3-5. Design variables used to modify the shape.

The stress analysis is performed using a commercial finite element analysis (FEA) software, ANSYS. Convergence analysis is performed to find an appropriate mesh size. Smaller mesh size is used for the region that has possibility of having maximum stress.

Figure 3-6 shows a typical stress contour plot from FEA results. The contour lines represent the von Mises stress. For the initial design, the von Mises stress range is between 10 kPa and 196 MPa. The maximum stress occurs at the end of the cutout. However, the location of maximum stress may change for different designs. In fact, the maximum stress is discontinuous function of design variables. However, we assume that it is a continuous function, and the optimum design must be inspected carefully.

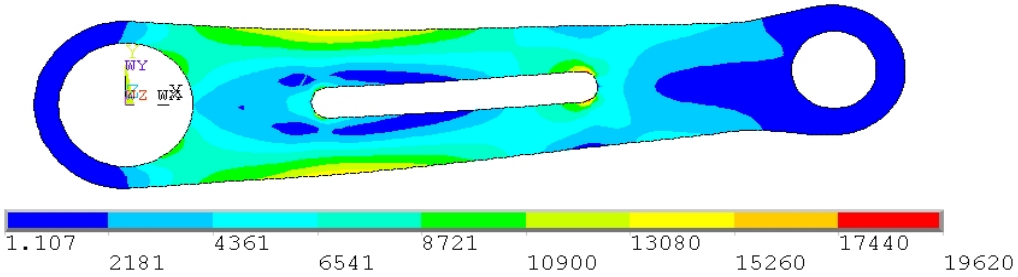

Figure 3-6. Von Mises stress contour plot at the initial design (Color bar indicates stress values in 10^4 Pa).

The FEA is computationally expensive; thus, a surrogate model is used to approximate the maximum stress on the design domain. Here, we do not focus on the optimization but on the quality of the surrogate prediction.

3.3.2 Numerical Procedure

3.3.2.1 Graphs of performance

We dispose of several techniques to increase the conservativeness of surrogate models; our objective is to determine, through the examples, if some of them are better than others. Moreover, it is possible that some techniques are more efficient for low levels of conservativeness, and other for high levels of conservativeness. For each method, the level of bias can be modified by changing the level of the confidence interval $(1-\alpha)$ (from 50% to 100%).

Then, the indices of performance defined in Section 3.2.2 can be calculated for each method at each level. In order to analyze and compare the different methods, we use the following graphs:

- $\%c$ against l_α: the first indicator of performance is the evolution of conservativeness level ($\%c$) against the loss in accuracy (l_α). It can be considered as a Pareto front, and can be used to design trade-offs between these quantities. Also, it allows us to compare the different methods by looking at partial or global dominations.
- $\%c$ against $MaxUE_{\%}$: this curve allows to check the consistency of the two conservativeness indices l_α and $MaxUE_{\%}$ when $\%c$ increases.
- Target conservativeness against $\%c$: for all estimates except biased fitting models, the level of bias is designed using a target level of $\%c$. Then, it is of crucial interest to measure the adequacy to the actual $\%c$ to the expected on. To analyze this performance, we draw the QQ-plot of the target conservativeness $(1-\alpha)$ vs. the actual conservativeness $\%c$.

3.3.2.2 Numerical set-up for the Branin-Hoo function

Two DoEs are used for this function, that consist of the four corners of the design region plus 13 and 30 points, respectively, generated using Latin Hypercube Sampling (LHS) with maximum minimum distance criterion; i.e., a total of 17 and 34 observations, respectively. The test points are generated using a 32×32 uniform grid (total 1024 points).

The e_{RMS} is weighted such that the points inside the domain have a weight 1, the points on the edges a weight 1/2 and the points on the corners 1/4 .

The PRS is a cubic polynomial. For Kriging, an ordinary kriging (OK) with rational quadratic covariance function is used, which is provided by the GPML Toolbox [Rasmussen & Williams (2006)].

LHS are random designs, which allows us to repeat the procedure a large number of times. We present the results as the average over 500 repetitions. In addition, we use error bars to represent 95% confidence intervals on l_α and $MaxUE_{\%}$ for a given level of $\%c$, and on $\%c$ for a given level of target conservativeness.

The unbiased polynomial response surfaces are computed using MatLab function *regress*; the kriging estimates are computed using the GPML toolbox for MatLab.

3.3.2.3 Numerical set-up for the Torque arm model

The DoE consists of 300 points generated from LHS with maximum minimum distance criterion; 1000 test points are generated using LHS. For each point, the ANSYS code is run and returns the maximum stress. The response values are of the order of 10^2 MPa. For the PRS, a third order polynomial is used. For Kriging, several covariance functions were tested, and it was found that a sum of a rational quadratic covariance function (Eq. 2–19) and nugget effect reflected accurately the covariance structure.

Since the finite element analysis is computationally expensive, it is impractical to generate a large number of DoEs for variability analysis, as we do for the Branin-Hoo function. In order to obtain some confidence intervals, we randomly choose 300 points out of the 1300 points generated (300 training + 1000 test points), and use the remaining 1000 as test points. This procedure is repeated 500 times. On the graphs, the average curve correspond to the original DoE and the error bars to the variability estimation procedure.

3.4 Results And Discussion

3.4.1 Branin-Hoo Function

3.4.1.1 Analysis of unbiased surrogate models

First, we look at the performance of the unbiased surrogate models on the Branin-Hoo function. Table 3-2 reports the e_{RMS}, $\%c$ and $MaxUE$ for both PRS and Kriging.

Table 3-2. Mean values of statistics based on 1,024 test points and 500 DoEs for the unbiased surrogates based on 17 observations. Number in parenthesis are standard deviations of the quantities.

Surrogate	e_{RMS}	$\%c$	$MaxUE$
PRS	8.1 (4.6)	53.1 % (8.4)	25.3 (15.7)
Kriging	9.1 (1.2)	55.8 % (5.8)	22.6 (8.1)

On average, PRS and Kriging perform similarly on the Branin-Hoo function. Kriging is less sensitive to the DoE, since the standard deviations of e_{RMS} and $MaxUE$ are smaller than for PRS. The $MaxUE$ is relatively small compared to the range of the function ([0 300]). Both surrogates have an average percentage of conservative errors slightly larger than 50%, which shows that some hypothesis of the model may be violated.

3.4.1.2 Comparing Constant Safety Margin (CSM) and Error Distribution (ED) estimates

Now, we compare, for each metamodel, constant and pointwise safety margins using error distribution. Figure 3-8 shows the results corresponding to PRS, and Figure 3-7 to Kriging. For both graphs, the range of the safety margin is chosen in the interval $[0; 15]$; the target conservativeness is chosen between 50% and 99%.

For PRS, we see in Figure 3-8 A) that the two methods are equivalent in terms of accuracy and variability. 95% conservativeness is obtained for an e_{RMS} twice as large as the e_{RMS} of the unbiased response surface. However, there is a substantial difference for the maximum unconservative error. For the same proportion of conservative results, this error is more reduced with ED than with CSM.

For Kriging, the CSM estimator clearly outperforms the ED estimator in terms of accuracy vs. conservativeness (Figure 3-7 A)). The same level of conservativeness is

obtained with less effect on the error, especially for the 70-90% range. Moreover, the variability is much larger for the statistical estimator.

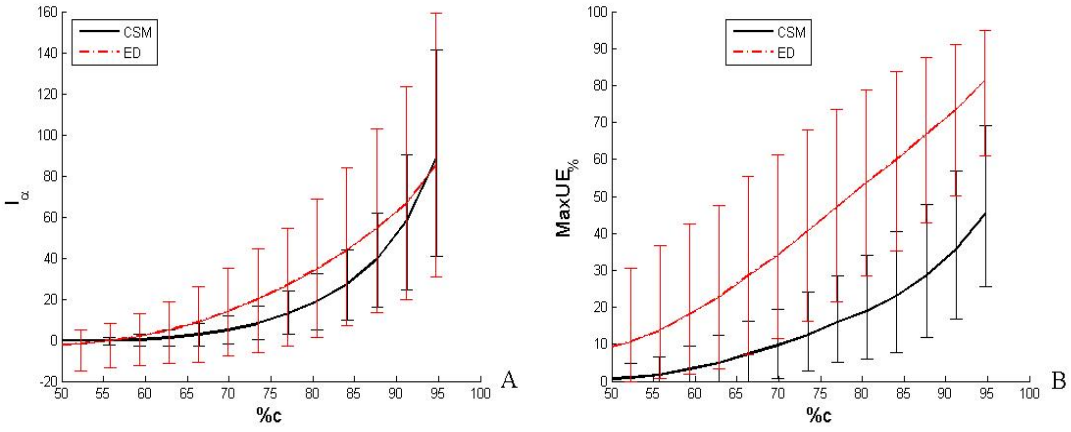

Figure 3-7. Average results for CSM (plain black) and ED (mixed grey) for Kriging based on 17 points. A) $\%c$ vs. l_α; B) $\%c$ vs. $MaxUE_\%$.

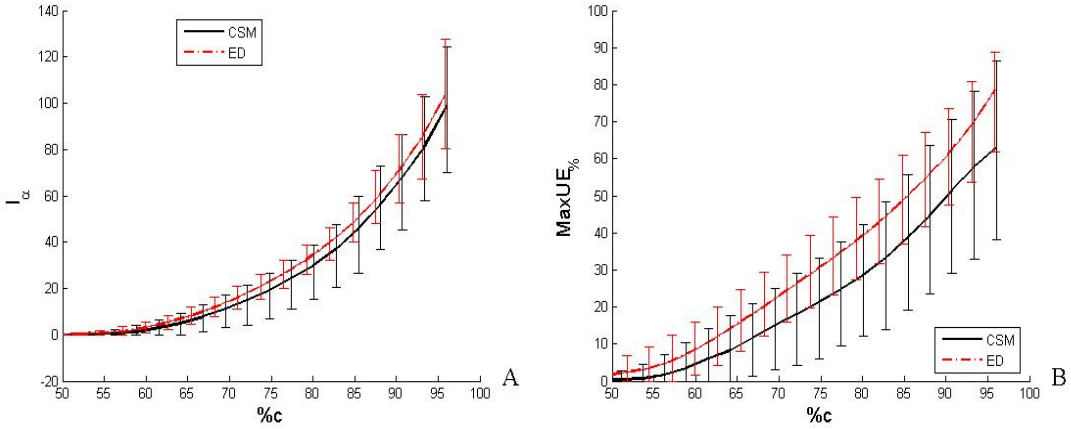

Figure 3-8. Average results for CSM (plain black) and ED (mixed grey) for PRS based on 17 points. A) $\%c$ vs. l_α; B) $\%c$ vs. $MaxUE_\%$.

The loss in accuracy of the CSM estimator increases very slowly with $\%c$ (Figure 3-7 A)). Up to 70% conservativeness is achieved with very little effect on e_{RMS}. This behavior can be imputed to the nature of the Kriging model. Since Kriging is an interpolation, errors are very small at the vicinity of the training points. Thus, adding a small constant is sufficient to be conservative but has little effect on the accuracy.

On the other hand, ED estimator appears to be much better to reduce the maximum unconservative error. As shown in Figure 3-7 B), the ED curve (grey) is always higher than the CSM one (black), which means, for a equivalent proportion of conservative results, the maximum unconservative error is more reduced with ED than with CSM.

This behavior is amplified when Kriging is based on a larger DoE. Figure 3-9 shows the graphs of performance for the Kriging fitted from 34 design points. The CSM estimator curve has a very flat portion up to 75% conservativeness, while the ED estimator curve increases rapidly. A longer flat portion is logical because the region where errors are small, at the vicinity of the DOE points, is larger since there are more points. The variability is much higher for the ED estimator. On the other hand, the CSM estimator does not prevent large unconservative errors: the maximum error remains almost the same even for large proportions of conservative results. The ED estimator performs a lot better according to this indicator.

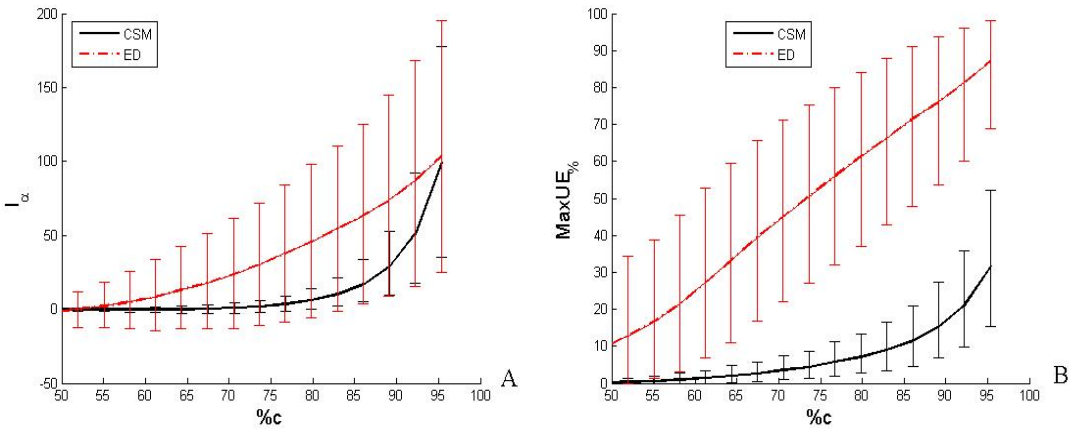

Figure 3-9. Average results for CSM (plain black) and ED (mixed grey) for Kriging based on 34 points. A) $\%c$ vs. l_α; B) $\%c$ vs. $MaxUE_{\%}$.

Now, we compare the fidelity to target conservativeness of both CSM and ED estimators, when the constant margin is designed with the help of cross-validation. Figure 3-10 shows the results for PRS, and Figure 3-11 for Kriging.

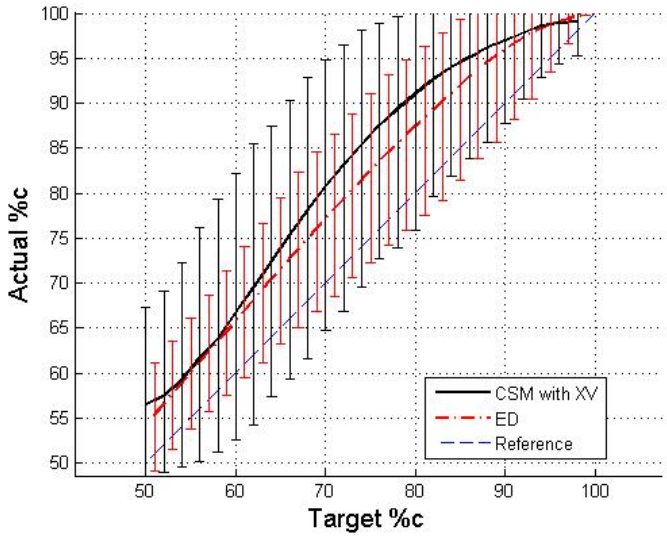

Figure 3-10. Target vs. actual $\%c$ for PRS using CSM with cross-validation (plain black) and ED (mixed gray) based on 17 points.

For PRS, both ED and CSM estimators show poor fidelity to target conservativeness. For the ED estimator, the mean actual $\%c$ is 5% higher than the target, and the errorbars show a variability of the order of $\pm 5\%$. The assumptions of regression may be violated with the Branin-Hoo function; for the unbiased PRS, the actual conservativeness is 55% where 50% is expected.

The CSM designed by cross-validation is inaccurate and has very large variability. The poor performance of cross-validation can be explained by the size of the DoE. Indeed, removing one observation out of 17 can modify substantially the quality of the surrogate, so cross-validation overestimates the error amplitude. Then, the CSM is chosen from 17 values only, which is not enough to ensure a good precision.

For Kriging, in average the ED estimator shows good fidelity since the trend is almost equal to the straight line. For the higher levels, the actual conservativeness is a less than the target. This is due to the fact that Kriging assume normality of errors, while for the Branin-Hoo function this assumption may be at a certain degree violated. When looking at the variability, the confidence interval is about $\pm 20\%$, which is very large. In particular, when 97% conservativeness is expected, the actual conservativeness can be as low as 70%.

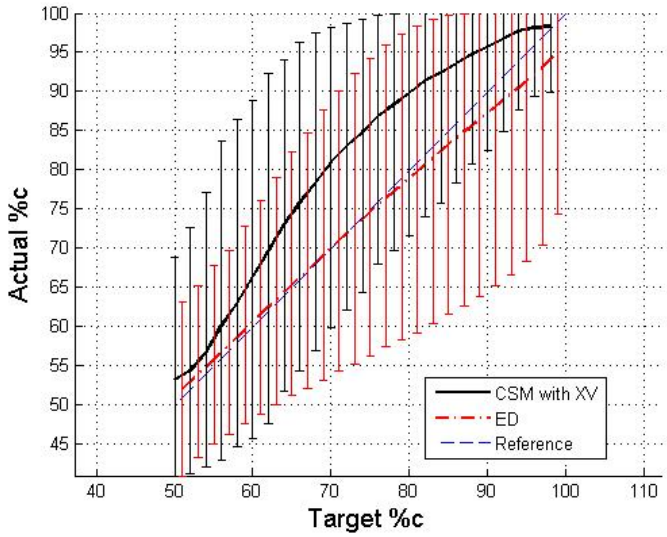

Figure 3-11. Target vs. actual $\%c$ for Kriging using CSM with cross-validation (plain black) and ED (mixed gray) based on 17 points.

As well as for PRS, the CSM estimator shows both inaccuracy and large variability. In addition to the reasons exposed above, cross-validation suffers here from the interpolating nature of Kriging in low dimension. Indeed, there are regions of small errors (in the vicinity of training points) and regions of large errors. Since the observations are chosen according to a space-filling DoE, training points are away from each other, and cross-validation estimates the error in regions of high uncertainty of the model, which explains why here CSM is overconservative.

3.4.1.3 Comparing Bootstrap (BS) and Error Distribution (ED) estimates

We have seen for PRS that ED estimates perform a little bit better than CSM on the Branin-Hoo function, but show poor fidelity to target level of conservativeness, which leads for this example to unnecessarily large margins. Now, we compare this estimator to the estimator based on bootstrap.

Before analyzing the results for the Branin-Hoo function, we propose to illustrate the advantage of bootstrap over classical confidence intervals on a test case where the bootstrap is supposed to show better accuracy. This is the case in particular when the assumption of normality of residuals is violated [Stine (1985)].

The experimental setup is as follow:

- the function to approximate is a second order polynomial $y = x - \frac{x^2}{2}$
- the DoE consists of 100 observations uniformly taken on $[0, 1]$
- the noise follows a lognormal distribution, with $\mu = 0$ and $\sigma = 1$. The distribution is shifted by $-\exp(\mu + \sigma^2/2)$ so the mean is zero, and divided by two to reduce the amplitude.

Figure 3-12 shows the observations, polynomial response surface and 95% confidence intervals (CI) computed using both classical formula and bootstrap.

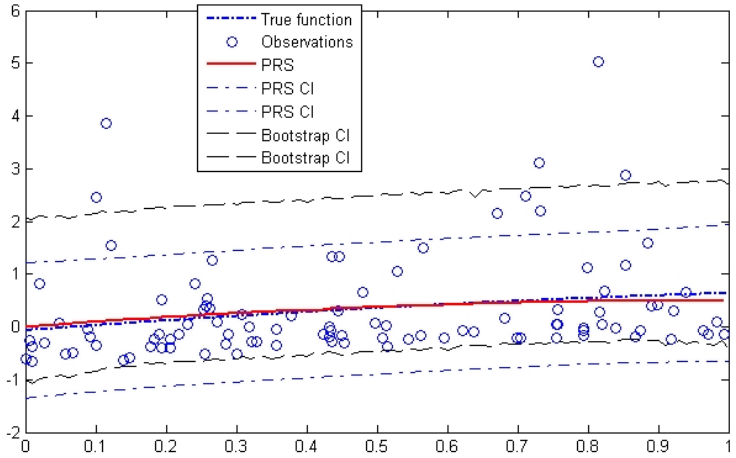

Figure 3-12. Confidence intervals (CI) computed using classical regression and bootstrap when the error follows a lognormal distribution. Bootstrap catches the asymetry of the distribution and provides accurate confidence intervals.

First, we see that the observations are not evenly distributed around the true function (70% are below). The heavy tail shape of the distribution of the noise is clearly apparent with the few large positive noises.

Since it is based on a large number of observations, the regression best predictor is correct even if assumption of normality is violated. However, the confidence intervals are inaccurate: they are symmetric while the noise is not. So, (in absolute values) the lower bound is overestimated, and the upper bound is underestimated. On the other hand, the bootstrap confidence interval is accurate: it is strongly asymmetric and matches the distribution of the residuals.

In this example bootstrap is very accurate since it is based on a lot of observations and the regression model is very simple. Now, we compare BS and CSM estimators on the Branin-Hoo function. The graphs of performance are given in Figure 3-13, and Figure 3-14 shows the fidelity of both estimators to target $\%c$.

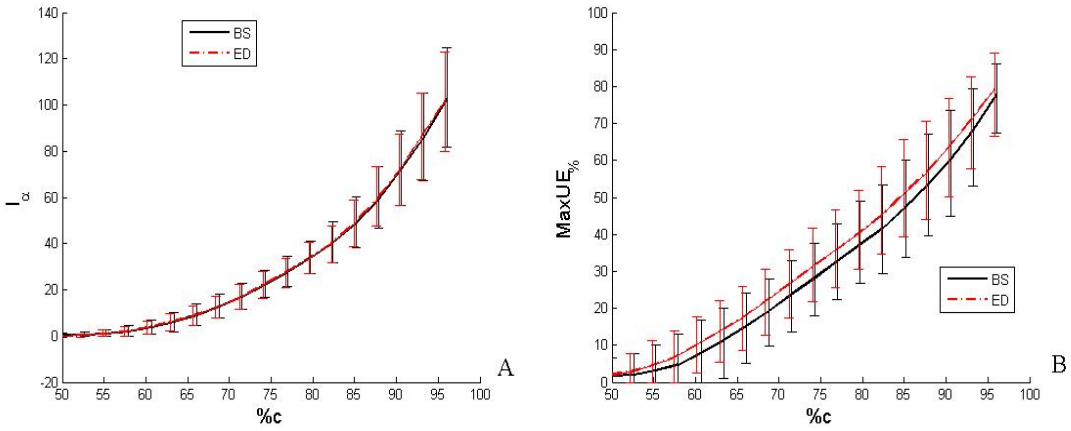

Figure 3-13. Average results for BS (plain black) and ED (mixed grey) for PRS based on 17 points.. A) $\%c$ vs. l_α; B) $\%c$ vs. $MaxUE_\%$.

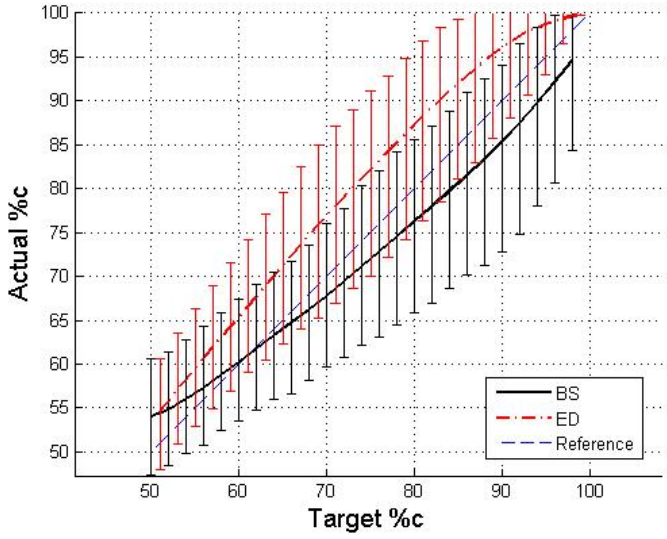

Figure 3-14. Target vs. actual $\%c$ for Kriging using CSM and cross-validation (plain black) and ED (mixed gray) based on 17 points.

First, we see that the evolution of the loss in accuracy with the percentage of conservative results is the same for the two estimators (Figure 3-13 A)). ED is a more

efficient than bootstrap to reduce the maximum unconservative error (Figure 3-13 B)). For the fidelity to target conservativeness, on average, BS performs a little bit better than ED but their variability are similar. On this example, bootstrap does not provide substantially better results than ED.

3.4.2 Torque Arm Model

3.4.2.1 Analysis of unbiased surrogate models

First, we look at the performances of the unbiased surrogate models for the torque arm stress analysis. Table 3-3 reports the e_{RMS}, $\%c$ and $MaxUE$ for both PRS and Kriging.

Table 3-3. Statistics based on 1,000 test points for the unbiased surrogates.

Surrogate	e_{RMS}	$\%c$	$MaxUE$
PRS	16.3	52.0%	77.5
Kriging	14.5	51.6%	60.7

Kriging performs better in terms of error. Both surrogates have approximately 50% negative errors. Their e_{RMS} are reasonable compared to the mean value of the stress (210 MPa). However, we see that the maximum error is very large, especially for PRS. Designing the torque arm based on these surrogates would result in a great risk of poor design.

3.4.2.2 Comparing Constant Safety Margin (CSM) and Error Distribution (ED) estimates

Figure 3-15 shows the results corresponding to PRS, and Figure 3-16 to Kriging.

For PRS, we see the same behavior for the Branin-Hoo function and torque arm analysis: CSM and ED are similar when comparing the loss in accuracy when the percentage of conservative results increases, but ED reduces better the maximum unconservative error. Here, it is important to notice that even when $\%c$ is higher than 95%, the $MaxUE$ is reduced by less than 50% in the best case.

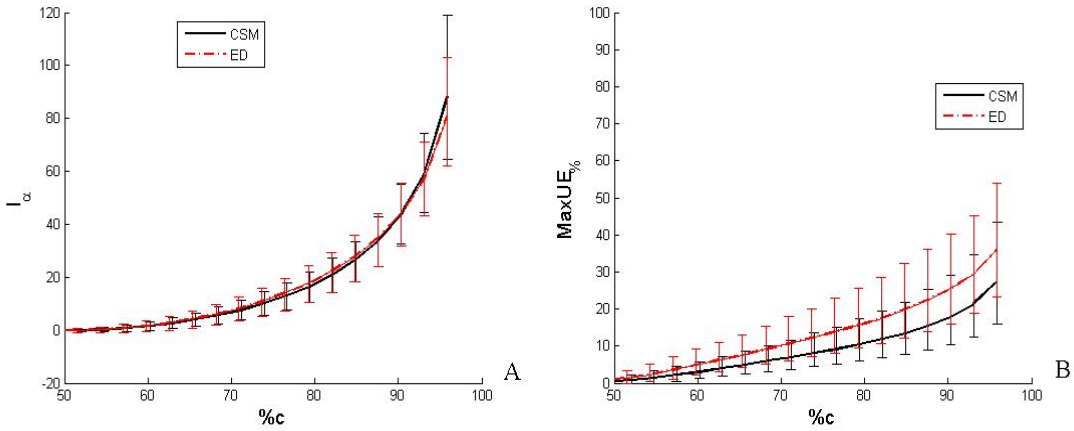

Figure 3-15. Average results for CSM (plain black) and ED (mixed grey) for PRS on the torque arm data. A) $\%c$ vs. l_α; B) $\%c$ vs. $MaxUE_\%$.

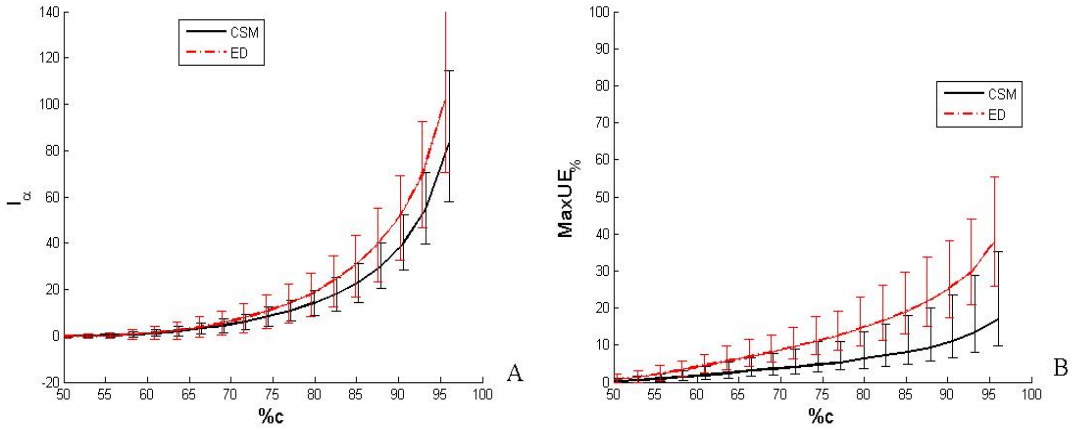

Figure 3-16. Average results for CSM (plain black) and ED (mixed grey) for Kriging on the torque arm data. A) $\%c$ vs. l_α; B) $\%c$ vs. $MaxUE_\%$.

For Kriging, again CSM performs better in terms of loss in accuracy l_α, but reduces very poorly the $MaxUE$. ED performs better regarding this indicator, but as well as for PRS, high levels of $\%c$ only correspond to about 50% reduction of $MaxUE$.

Now, we look at the fidelity to target $\%c$. Figure 3-17 shows the results corresponding to PRS, and Figure 3-18 to Kriging.

On both figures, we see that using constant margin and cross-validation results in a great fidelity to target conservativeness. ED estimators are a little bit biased regarding fidelity: PRS slighlty underestimates $\%c$ for all probability range, and Kriging

overestimates conservativeness for high probabilities. These errors can be imputed to the parametric (gaussian) form of the error model.

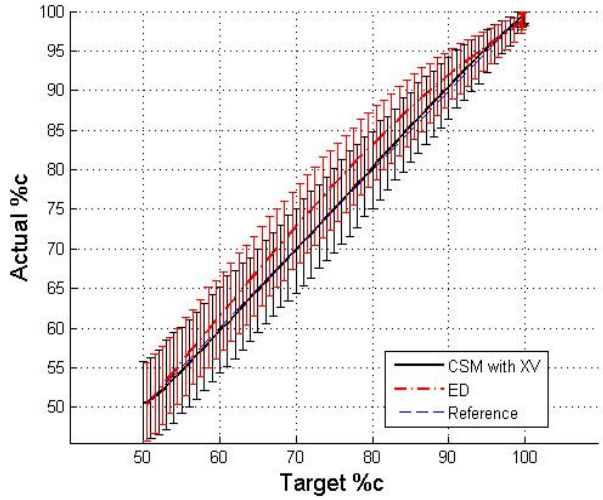

Figure 3-17. Target vs. actual $\%c$ for PRS using CSM and cross-validation (plain black) and ED (mixed gray) on the torque arm data.

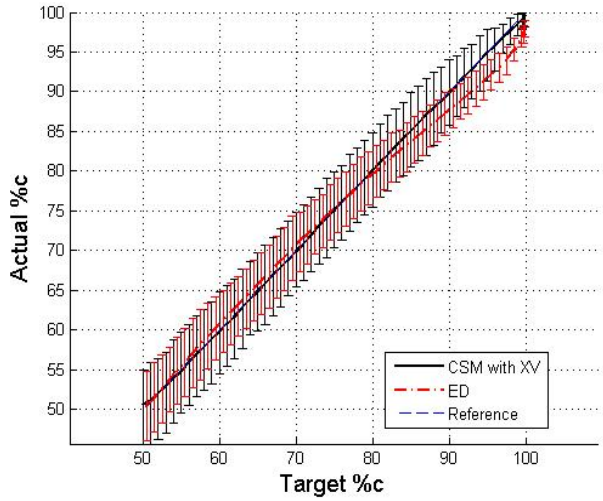

Figure 3-18. Target vs. actual $\%c$ for Kriging using CSM and cross-validation (plain black) and ED (mixed gray) on the torque arm data.

In contrast, cross-validation does not assume any form for the error. The quality of cross-validation margins are a lot better than in the previous test cas, which can be explained by the larger number of observations. Firstly, with 300 observations, leaving one

observation out has very little impact on the accuracy of the surrogate, so the error vector given by cross-validation is more realistic. Secondly, the CSM is based on a large number of values (300 instead of 17 previously), which allows to design it with better accuracy.

3.4.2.3 Comparing Bootstrap (BS) and Error Distribution (ED) estimates

Figure 3-19 shows the results of BS and ED estimates. For those indicators, the two methods are similar.

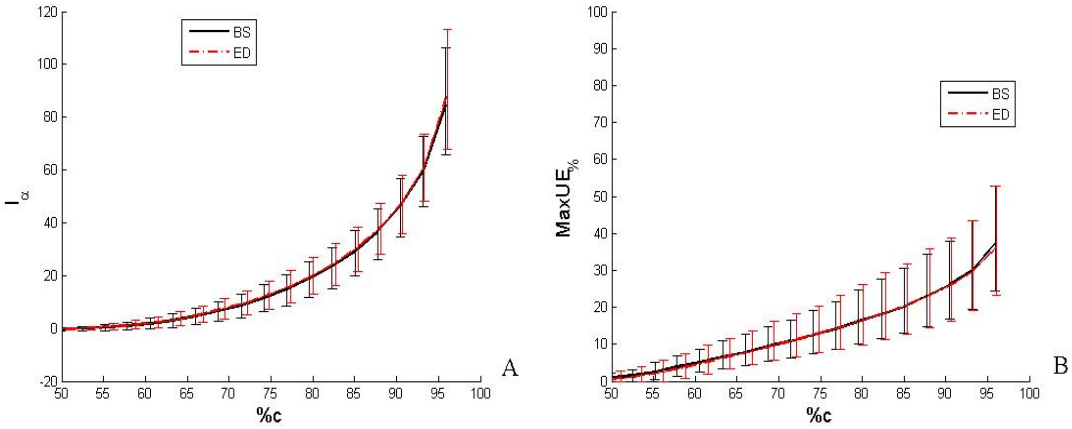

Figure 3-19. Average results for BS (plain black) and ED (mixed grey) for PRS on the torque arm data. A) $\%c$ vs. l_α; B) $\%c$ vs. $MaxUE_\%$.

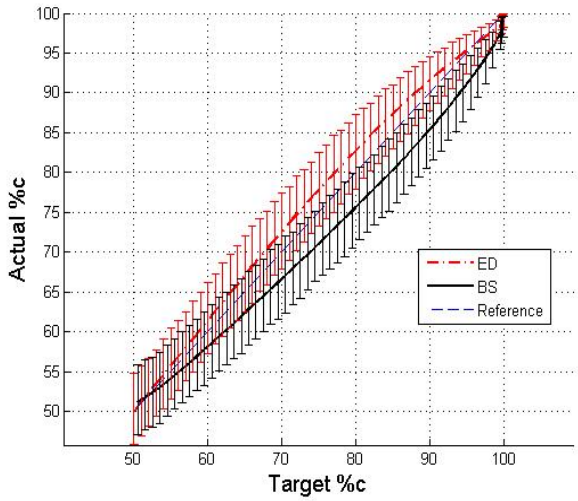

Figure 3-20. Target vs. actual $\%c$ for PRS using BS (plain black) and ED (mixed gray) on the torque arm data.

Figure 3-20 shows the fidelity of both estimators to target $\%c$. Here, bootstrap does not perform as well as ED. It is interesting to notice than they have opposite bias, since ED is overconservative and BS overconfident.

3.5 Concluding Comments

In this chapter, we explored the alternatives to obtain conservative predictions using surrogate modeling. First, we showed that conservativeness could be obtained using parametric methods, by taking advantage of error distribution measures given by the model, or non-parametric, such as bootstrap or cross-validation. Then, a Pareto front methodology was introduced to measure the quality of the different methods. Finally, the methods are implemented for two test problems: one analytical and one based on Finite Element Analysis. Results showed that:

- The use of safety margins and error distribution lead to very comparable results when the trade-off between accuracy and conservativeness are considered
- ED estimators, for an equivalent level of conservativeness and accuracy, prevent better than CSM from the risk of large unconservative errors
- ED estimators are based on assumptions that may not be violated in order to obtain acceptable fidelity of conservativeness level.
- When the model hypothesis are violated, bootstrap offers an efficient alternative to obtain accurate fidelity
- Cross-validation is an efficient technique to design constant margins when the number of observations is high.

More generally, it has been shown that measuring the conservativeness of a method is not easy and can be very problem-dependant. Indeed, the chance of being conservative and the risk of large unconservative errors are two measures of conservativeness that do not behave identically. One may choose a conservative strategy based on the trade-off between these two quantities and the global measure of accuracy.

CHAPTER 4
CONSERVATIVE PREDICTIONS FOR RELIABILITY-BASED DESIGN

4.1 Introduction And Scope

When an engineering system has uncertainty in its input parameters and operating conditions, the safety of the system can be evaluated in terms of reliability. Many methods have been proposed to estimate the reliability of a system, such as Monte Carlo simulation (MCS) method [Haldar & Mahadevan (2000)], First and Second-order Reliability Method [Enevoldsen & Sørensen (1994), Melchers (1987)], importance sampling method [Engelund & Rackwitz (1993)), tail modeling (Kim et al. (2006)], or inverse methods [Qu & Haftka (2004)]. MCS is often used to estimate the reliability of the system that has many random inputs or multiple failure modes, because its accuracy is independent of the complexity of the problem. In this paper, reliability analysis using MCS method is considered. The comparison between different reliability analysis methods is beyond the scope of this chapter and can be found in the literature [Rackwitz (2000), Lee et al. (2002)].

When the cost of simulation is high, engineers can afford to have only a limited number of samples, which is not sufficient to estimate the reliability with acceptable accuracy [Ben-Haim & Elishakoff (1990), Neal et al. (1992)]. In such a case, it is often required to compensate for the lack of accuracy with conservative approaches. For example, anti-optimization [Elishakoff (1991), Du et al. (2005)] and possibility-based design [Du et al. (2006), Choi et al. (2005)] are used to compensate for the lack of knowledge in the input distribution by seeking the worst case scenario for a given design. Such approaches have been found to lead to conservative designs [Nikolaidis et al. (2004)]. Bayesian reliability-based optimization [Youn & Wang (2008)] uses Bayesian theory to ensure to produce reliable designs when only insufficient data is available for the inputs.

In this chapter, we focus on the case when the probability of failure, P_f, of a system is estimated from a limited number of samples. The objective is to find a conservative estimate, $\hat{P}_f$, that is likely to be no lower than the true P_f. P_f is estimated using

particular types of surrogate models, which are distribution function models. To provide such estimation, two alternatives are considered: the first method is based on biasing the process of fitting the distribution used to compute the estimator of P_f. The second is the use of bootstrap method [Efron (1982), Chernick (1999)] for quantifying the uncertainty in probability of failure estimations, and defining conservative estimators based on bootstrapping. As well as in the previous chapter, a trade-off analysis between accuracy and the level of conservativeness is proposed with the help of numerical examples.

In the next section, we discuss how we use sampling techniques to estimate the probability of failure. Section 4.3 shows how to use constraints to obtain conservative estimators. Section 4.4 describes how to use the bootstrap method to define conservative estimator. The accuracy of such estimators is analyzed using a simple numerical example in Section 4.5, and an analysis of the effects of sample sizes and target probability of failure on the quality of the estimates conservative estimators is given in Section 4.6. Finally, the conservative approach is applied to an engineering problem in Section 4.7, followed by concluding remarks in Section 4.8.

4.2 Estimation Of Probability Of Failure From Samples

4.2.1 Limit-State And Probability Of Failure

Failure of a system can usually be determined through a criterion, called a limit-state, G. The limit-state is defined so that the system is considered safe if $G \leq 0$ and fails otherwise. Typically, the limit-state of a structure can be defined as the difference between response, R, (e.g., maximum stress or strain) and capacity, C, (e.g., maximum allowable stress or strain):

$$G(\mathbf{x}) = R(\mathbf{x}) - C(\mathbf{x}) \tag{4–1}$$

Due to uncertainties in input parameters, the limit-state is random. Thus, one can estimate the safety of the system in terms probability of failure, which is defined as

$$P_f = Prob(G \geq 0) \tag{4–2}$$

There are many methods for calculating the failure probability of a system [Haldar & Mahadevan (2000), Enevoldsen & Sørensen (1994), Melchers (1987)]. Some of them use the relation between input random variables and the limit-state (e.g., first and second-order reliability methods) and some consider the limit-state as a black-box output (e.g., MCS). When the number of input random variables is large, and the limit-state is complex and multi-modal, MCS has a particular advantage as its accuracy is independent of the problem dimension or complexity of the limit-state function. MCS generates samples of the limit-state $\{g_1, g_2, , g_n\}$ and counts the number of failed samples [Melchers (1987)]. The ratio between the numbers of failures and the total number of samples approximates the probability of failure of the system:

$$P_f \approx \hat{P}_f = \frac{1}{N} \sum_{i=1}^{n} I\left[g_i \geq 0\right] \tag{4–3}$$

The variance of MCS estimates is inversely proportional to the square root of the number of samples times the probability of failure (for large N):

$$var(\hat{P}_f) \approx \frac{P_f(1 - P_f)}{N} \tag{4–4}$$

Thus, the accuracy is poor when the number of samples is small or when the probability of failure is low. For instance, if a probability of failure of 10^{-4} is estimated (which is a typical value in reliability based design), 10^6 samples are needed for 10% relative error.

In this chapter, we focus on situations where only small samples are available regarding the probability of failure; by small is meant from ten to 500, for probabilities of failure going from 1% to 10^{-6}. In such a case, the direct use of MCS (counting the number of failed samples) is unrealistic, since the probability estimate would most probably be zero.

An alternative is to approximate the cumulative distribution function (CDF) F_G of the limit-state by a continuous function and estimate the probability of failure using:

$$\hat{P}_f = 1 - F_G(0) \tag{4–5}$$

In general, F_G is unknown and is approximated by a parametric distribution F_θ, which is defined by distribution parameters, θ. F_θ can be considered as a one-dimensional surrogate model that must be fitted from the data $\{g_1, g_2, , g_n\}$. F_θ can be a logistic regression model, or the CDF of the normal distribution (hence $\theta = \{\mu, \sigma\}$), defined by:

$$F_\theta(g) = \frac{1}{\sigma\sqrt{2\pi}} \int_{-\infty}^{g} \exp\left[\frac{-(u-\mu)^2}{2\sigma^2}\right] du \tag{4–6}$$

The samples of limit states can be obtained by generating input random variables and propagating through the system. However, the proposed method can be applied to the case when input random variables and uncertainty propagation are unknown. For example, the samples of limit states can be obtained from experiments.

In the following section, two methods of estimating distribution parameters from a set of samples are discussed.

4.2.2 Estimation Of Distribution Parameters

There exists several alternatives to estimate the distribution parameters. The difficulty here is to define a fitting criterion, since the usual assumptions of surrogate models are not met (for instance, normality of the residuals). When possible (for example for the normal distribution), they can be estimated using moment-based methods. Here, we propose to define criteria based on the adequacy of the parametric model to the empirical CDF.

Consider n limit-state samples arranged in increasing order: $\{g_1, g_2, , g_n\}$. The empirical CDF F_n is defined as:

$$F_n(g) = \begin{cases} 0 & \text{for } g \leq g_1 \\ k/n & \text{for } g_k \leq g \leq g_{k+1} \\ 1 & \text{for } g \geq g_n \end{cases} \tag{4–7}$$

It is then possible to estimate the parameters θ of the CDF that approximates F_n best. Two different approximation methods are discussed here:

- minimizing the root-mean-square (RMS) error,
- minimizing the Kolmogorov-Smirnov distance [Kenney & Keeping (1954)].

To minimize the RMS difference between the empirical and the estimated CDF, errors are calculated at the sample points. In order to have an unbiased estimation, the values of the empirical CDF are chosen at the middle of the two discrete data, as (see Figure 4-1 A)):

$$\overline{F}_n(g_k) = \frac{k - \frac{1}{2}}{n}, \quad 1 \leq k \leq n \tag{4–8}$$

Then the estimated parameters $\hat{\theta}$ are chosen to minimize the following error:

$$\hat{\theta} = \arg\min_{\theta} \sqrt{\sum_{k=1}^{n} \left[F_\theta(g_k) - \overline{F}_n(g_k)\right]^2} \tag{4–9}$$

The estimate based on Eq. 4–9 is called an RMS estimate.

The Kolmogorov-Smirnov (K-S) distance is the classical way to test if a set of samples are representative of a distribution. The K-S distance is equal to the maximum distance between two CDFs (see Figure 4-1 B)). The optimal parameters for the K-S distance are:

$$\hat{\theta} = \arg\min_{\theta} \left[\max_{1 \leq k \leq n} \left(\left| F_\theta(g_k) - \frac{k}{n} \right|, \left| F_\theta(g_k) - \frac{k-1}{n} \right| \right)\right] \tag{4–10}$$

Figure 4-1 A) shows the empirical CDF from ten samples and the data points that are used in Eq. 4–8. Figure 4-1 B) shows the K-S distance between a normally distributed CDF and an empirical CDF from 10 samples.

In the cases we consider in this work, it is found that the two criteria give equivalent results. K-S distance links to classical statistical framework, but can be difficult to minimize because it is non-smooth. The RMS error minimization appears to be more robust.

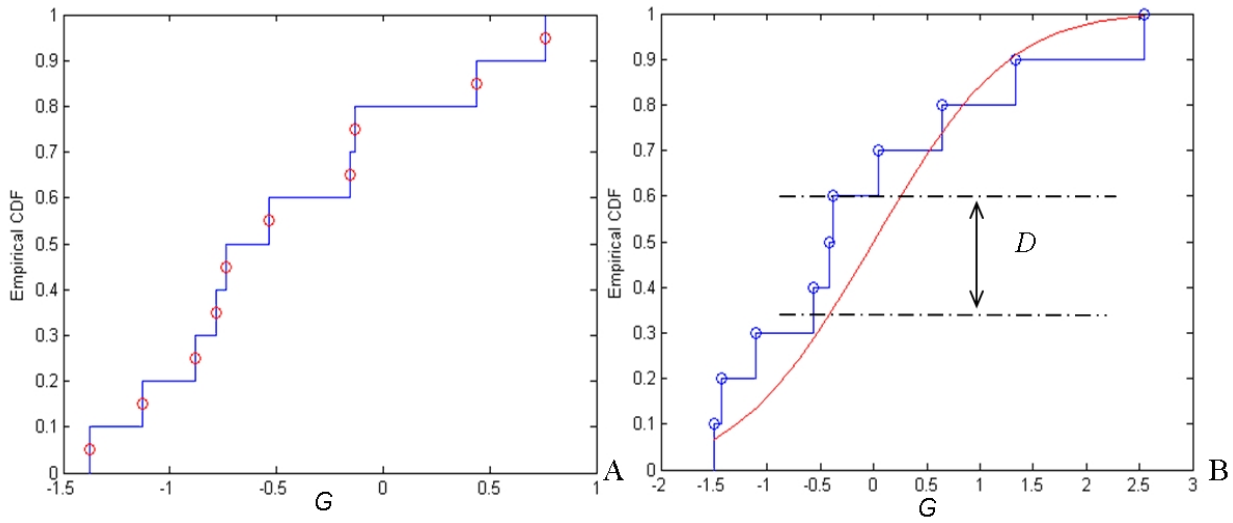

Figure 4-1. Criteria to fit empirical CDFs: A) Points (circles) chosen to fit an empirical CDF (line) with RMS criterion. B) K-S distance between an empirical CDF with ten samples and a normal CDF (continuous line). Data is obtained by sampling ten points from $N(0,1)$

s

The choice of the distribution F_θ is critical for accurate estimation of the probability of failure. Wrong assumption on the form of the distribution can lead to large bias in the estimate, for instance, if the distribution is assumed to be normal while it is heavy-tailed. Statistical techniques are available to test if a sample belongs to a given distribution type (goodness-of fit tests), such as the Kolmogorov-Smirnov (for any distribution), Lilliefors or Anderson-Darling tests (for normal distributions) [Kenney & Keeping (1954)]. Some statistical software also offers automated procedures to choose from a benchmark of distributions which fits best the data.

4.3 Conservative Estimates Using Constraints

In the spirit of the biased fitting estimates proposed in Appendix A.1, we propose to add constraints to the fitting problem in order to make the estimates more conservative.

A conservative estimate of the probability of failure should be equal or higher than the actual one. Hence, a conservative estimate can be obtained by constraining the estimated CDF to be lower than the true CDF when the parameters are found through the optimization problems in Eqs. 4–9 or 4–10. Besides, we consider only small probabilities, so the failure occurs in the upper tail region of the distribution. Hence, the constraints will be applied to only the right half of the data. When the failure occurs in the lower tail region, the constraints should be applied on the left half of the data.

The first conservative estimate of the CDF is obtained by constraining the estimate to pass below the sampling data points. A second can be obtained by constraining the estimated CDF below the entire empirical CDF. They will be called, respectively, CSP (Conservative at Sample Points) and CEC (Conservative to Experimental CDF). The latter is more conservative than the former. Obviously, both methods introduce bias, and the choice between the two constraints is a matter of balance between accuracy and conservativeness.

CSP constraints:

$$F_\theta(g_i) - \frac{i}{n} \leq 0 \qquad \text{for} \qquad \frac{n}{2} \leq i \leq n \tag{4–11}$$

CEC constraints:

$$F_\theta(g_i) - \frac{i-1}{n} \leq 0 \qquad \text{for} \qquad \frac{n}{2} \leq i \leq n \tag{4–12}$$

To illustrate these conservative estimators, ten samples are generated from a random variable G whose distribution is $N(2.33, 1.0^2)$. The mean is chosen in such a way that the probability of failure $P(G \geq 0)$ is equal to 1%. Figure 4-2 shows the empirical CDF along with the three estimates based on minimum RMS error: (1) with no constraint, (2) with CSP constraints, and (3) with CEC constraints. Table 4-1 shows the parameters of the three estimated distributions and the corresponding probabilities of failure.

The effect of the constraints is clear from the graph. The CSP estimator is shifted down to the ninth data point; hence, the CDF at the tail is decreased. The CEC estimator

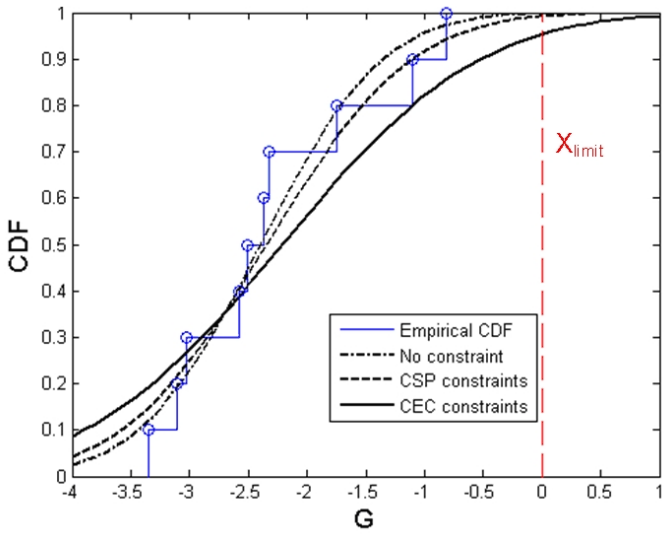

Figure 4-2. Example of CDF estimators based on RMS error for a sample of size 10 generated from $N(-2.33, 1.0^2)$

Table 4-1. Comparison of the mean, standard deviation, and probability of failure of the three different CDF estimators for $N(-2.33, 1.0^2)$. Exact value of P_f is 1% (same sample as Figure 4-2).

	No constraint	CSP	CEC
$\hat{\mu}$	2.29	2.34	2.21
$\hat{\sigma}$	0.84	0.97	1.31
$\hat{P}_f$	0.32%	0.77%	4.65%

is shifted even further down. Since the conservative estimators are unconstrained on the left half of the distribution, their CDF curves cross the empirical curve on that side.

For this illustration, we chose a sample realization that is unfavorable for conservativeness. As a consequence, the estimate with no constraint is strongly unconservative (0.32% compared to 1.0%) even though the estimation is unbiased. The CSP estimate is unconservative, but substantially less than the unbiased estimate. The CEC estimate is conservative. In order to generalize these results and derive reliable conclusions, statistical experiments based on large number of simulations will be performed in Section 4.5.

4.4 Conservative Estimates Using The Bootstrap Method

An alternative to biased fitting is to obtain confidence intervals for the probability of failure estimates in order to determine the margin needed to be conservative. However,

analytical derivation of confidence intervals for the probability of failure is very challenging. To overcome this problem, we propose to obtain confidence intervals using numerical procedures, i.e. bootstrap.

The bootstrap principle is described in section 3.2.5.1. When only limited samples are available, the bootstrap method can provide an efficient way of estimating the distribution of statistical parameter θ. Regardless of its construction, the probability of failure is estimated from samples of the limit-state $\{g_1, \ldots, g_n\}$. Hence, it is possible to resample with replacement from $\{g_1, \ldots, g_n\}$, and for each set of bootstrap re-samples, fit the CDF and compute P_f.

The standard error or confidence intervals of the statistical parameter can be estimated from the bootstrap distribution. However, the bootstrap method provides only an approximation of the true distribution because it depends on the values of the initial samples. In order to obtain reliable results, it is suggested that the size of the samples should be larger than 100 (i.e., n) [Efron (1982)]. The number of bootstrap re-samplings (i.e., p) is chosen large enough so that it does not affect the quality of the results (the major source of uncertainty being the initial sample). The value of p is typically taken from 500 to 5,000.

For illustrating the process, the following case is considered: $n = 100$ and $p = 5,000$. That is, 100 samples of a random variable G are generated from the normal distribution $N(-2.33, 1.0^2)$. The true probability of failure is 1%. Pretending that the statistical parameters (mean μ, standard deviation σ, or probability of failure P_f) are unknown, these parameters as well as their confidence intervals will be estimated using the bootstrap method.

Using the given set of 100 initial samples, 5,000 bootstrap re-samplings are performed. Similar to the conservative estimations in the previous section, the distribution type is first assumed to be normal. Using each set of bootstrap re-samples, the mean μ and standard deviation σ are estimated, from which the estimated probability of failure $\hat{P}_f$ is calculated.

The 5,000 $\hat{P}_f$ values define the empirical bootstrap distribution of the estimator $\hat{P}_f$, represented in Figure 4-3 in a histogram form.

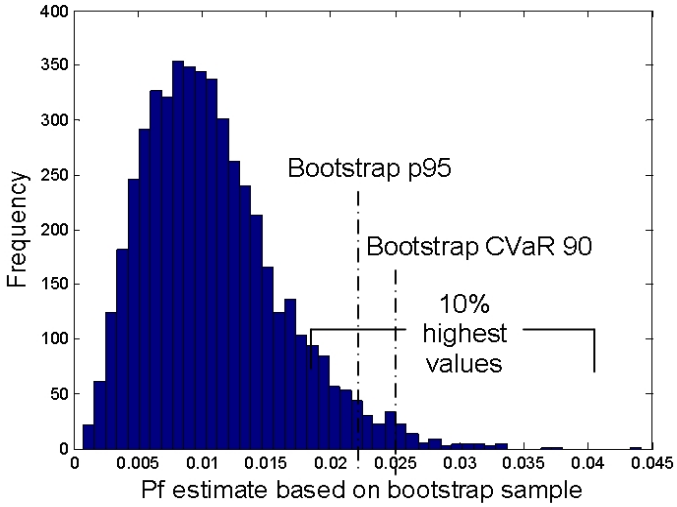

Figure 4-3. Conservative estimators of P_f from bootstrap distribution: 95^{th} percentile (p95) and mean of the 10% highest values (CVaR).

The empirical bootstrap distribution can be used to minimize the risk of yielding unconservative estimate. In other words, we want to find a procedure that calculates the following quantity:

$$\alpha = P\left(\hat{P}_f \geq P_f\right) \tag{4–13}$$

A procedure that satisfies Eq. 4–13 is called an α-conservative estimator of P_f. For example, if $\alpha = 0.95$ is desired, then $\hat{P}_f$ is selected at the 95^{th} percentile of the bootstrap distribution of the estimated probability of failure. This estimator will be referred to 'Bootstrap p95' (see Figure 4-3). Due to the finite sample size, however, Eq. 4–13 will be satisfied only approximately.

Besides this α-conservative estimator, the mean of the δ-highest bootstrap values (conditional value-at-risk CVaR [Holton (2003)]) is also used as a conservative estimate. Here $\delta = 10\%$ is used, so the estimator consists of the mean of the 10% highest bootstrap values. Since CVaR is a mean value, it will be more stable than the α-conservative estimator. However, it is difficult to determine the value of δ that makes Eq. 4–13 satisfied

precisely. This estimator will be referred to 'Bootstrap CVaR 90' (see Figure 4-3). Note that any bootstrap percentile higher than 50% will be a conservative estimator. A very high α or low δ will increase the value of $\hat{P}_f$ and will yield over-conservative estimation.

4.5 Accuracy And Conservativeness Of Estimates For Normal Distribution

The goal of this section is to evaluate the accuracy and the conservativeness of the estimators presented in Sections 4.3 and 4.4, when the actual distribution is known to be normal. Statistical measures of the estimators are evaluated by estimating P_f a large number of times.

We also introduce here the reliability index, which is denoted by β and related to the probability of failure as:

$$\beta = -\Phi^{-1}(P_f) \tag{4–14}$$

where Φ is the CDF of the standard normal distribution.

The reliability index is often used instead of P_f in reliability based design because the range of β values (typically between one and five) is more convenient and its variability is lower than P_f. It is important to note that since $-\Phi^{-1}$ is a monotonically decreasing function: a low probability corresponds to a high reliability index. Thus, a conservative estimation of β should not overestimate the true β (since a conservative estimation should not underestimate the true P_f). In the following, we present the results for both probability of failure and reliability index.

First, 100 samples of G are randomly generated from the normal distribution with mean -2.33 and standard deviation 1.0. The failure is defined for $G \geq 0$, which corresponds to an actual probability of failure of 1.0%. For a given set of samples, different estimators are employed to estimate P_f. Five different estimators are compared: the unbiased fitting, CSP, CEC, Bootstrap p95, and Bootstrap CVaR90 estimators. This procedure was repeated 5,000 times in order to evaluate the accuracy and conservativeness of each estimator. For the unbiased, CSP and CEC estimators, we tested both RMS and Kolmogorov-Smirnov distance criteria and found that their performance was comparable

but using K-S distance slightly increases variability. So, results are presented for RMS criterion only.

Most of the estimated values will exceed the actual probability of failure, but it is desirable to maintain a certain level of accuracy. Thus, the objective is to compare each estimator in terms of accuracy and conservativeness.

Table 4-2 shows the statistical results from 5,000 repetitions. Results are presented in the form of the mean value and the 90% symmetric confidence interval [5% ; 95%]. For the probability of failure estimates, the lower bound of the confidence interval shows the conservativeness of the estimator; the mean and the upper bound show the accuracy and the variability of the estimator. A high lower bound means a high level of conservativeness, but a high mean and upper bound mean poor accuracy and high variability. For the reliability index estimates, the upper bound shows the conservativeness and the mean and lower bound the accuracy.

Table 4-2. Means and confidence intervals of different estimates of $P(G \geq 0)$ and corresponding β values where G is the normal random variable $N(-2.33, 1.02)$. The statistics are obtained over 5,000 simulations.

Estimators	P_f (%)		β		% of cons.
	90% C.I.	Mean	90% C.I.	Mean	results
Unbiased	[0.37 ; 2.1]	1.02	[2.0 ; 2.7]	2.34	48
CSP	[0.63 ; 3.6]	1.86	[1.8 ; 2.5]	2.12	82
CEC	[0.95 ; 5.5]	2.97	[1.6 ; 2.3]	1.96	94
Boot. p95	[0.83 ; 3.7]	2.06	[1.8 ; 2.4]	2.07	92
Boot. CVaR90	[0.88 ; 3.8]	2.15	[1.8 ; 2.4]	2.05	93
Actual	1.00		2.33		

First, the confidence interval of the unbiased estimator illustrates the risk of unconservative prediction: indeed, the lower bound is 0.37%, which means there is a five per cent chance to underestimate P_f by a factor of at least 2.7 ($1.0/0.37 = 2.7$). This result provides an incentive for finding a way to improve the conservativeness of the probability estimate.

The CSP and CEC estimators are biased on the conservative side. As expected, the CEC is more conservative than the CSP. As a consequence, CEC is more biased and the risk of large overestimate is increased. The CEC confidence interval shows that there is a five per cent chance to overestimate P_f by at least a factor of 5.5, while this value is 3.6 for the CSP estimator; on the other hand the CEC leads to 94 percent conservative results, while the CSP estimator leads to only 82 percent conservative results. The choice between the CSP and CEC estimators will be a choice between accuracy and conservativeness.

The Bootstrap p95 estimator achieves 92 percent conservativeness and the Bootstrap CVaR90 93 percent conservativeness. From the upper bounds of both estimations, we find that the risk of overestimating P_f by at least a factor of 3.7 is five percent.

The amplitude of error in the reliability index β is much lower than the amplitude in the probability of failure. For the CEC estimator, the lower bound of the confidence interval corresponds to 31% error ($[2.33 - 1.6]/2.33 = 0.31$). For the bootstrap estimators, this error is reduced to 23%. The mean errors are respectively 16% and 11%.

Bootstrap methods appear to be more efficient than the biased fitting (CSP and CEC) in terms of accuracy and conservativeness. For the equivalent level of conservativeness (92-94 percent), the level of bias is reduced and the risk of overestimations is lower when the bootstrap method is used. However, as mentioned earlier, the bootstrap method needs a minimum sample size to be used. It has been observed that when very small samples are available (10 to 50 data), the accuracy of the bootstrap method drops dramatically. In such a case, the optimization based methods should be used instead.

4.6 Effect Of Sample Sizes And Probability Of Failure On Estimates Quality

In the previous section, we showed that the bias in the conservative estimate can lead to large overestimations of the probability of failure. The magnitude of such an error mainly depends on two factors: the sample size and the value of the true probability. Indeed, increasing the sample size will reduce the variability of CDF fitting and, as a

consequence, the upper bound of the confidence interval. Meanwhile, in order to estimate a lower value of the probability of failure, we need to use the tail of the CDF, which increases the variability of the estimation.

Controlling the level of uncertainty is crucial in optimization in order to avoid over-design. In this section, we quantify a measure of the uncertainty in the conservative estimates as a function of the sample size and the value of the actual P_f. Such a measure can help in deciding on the appropriate sample size to compute the estimate.

Bootstrap p95 performed well based on the previous example. Thus, in this section we consider only this estimator. We study two distribution cases: standard normal distribution and lognormal distribution with parameters $\mu = 0$ and $\sigma = 1$ (mean and standard deviation of the logarithm of the variable). Three sample sizes are considered: 100, 200 and 500 and seven probabilities of failure are estimated: (1×10^5, 3×10^5, 1×10^4, 3×10^4, 1×10^3, 3×10^3 and 1×10^2) [1] .

For a given distribution, sample size and P_f, the mean and 90% confidence intervals are calculated using 5000 repetitions. Results are presented in Figure 4.6 for normal distribution and in Figure 4.6 for lognormal. The accuracy is measured in terms of ratios for the estimate over the true probability of failure.

As expected, the variability of $\hat{P}_f$ increases when the sample size and actual P_f decrease. Here, the most unfavorable case is when the sample size is equal to 100 and the actual P_f is equal to 10^5. In such a case, for both distributions there is a five percent chance to overestimate P_f by more than 25 times its actual value! On the other hand, the case with 500 samples leads to a very reasonable variability. For the three sample sizes and all target probabilities, the lower bound of the ratio is equal to one, which

[1] For the normal distribution, the failures are defined for G greater, respectively, than 4.26, 4.01, 3.72, 3.43, 3.09, 2.75 and 2.33; for the lognormal case, the values are 71.2, 54.6, 41.2, 30.5, 22.0, 15.3 and 10.2.

means that the 95% conservativeness do not depends on these factors. The bootstrap estimates performances are remarkably similar for the two distributions, even though the distribution shapes are very different.

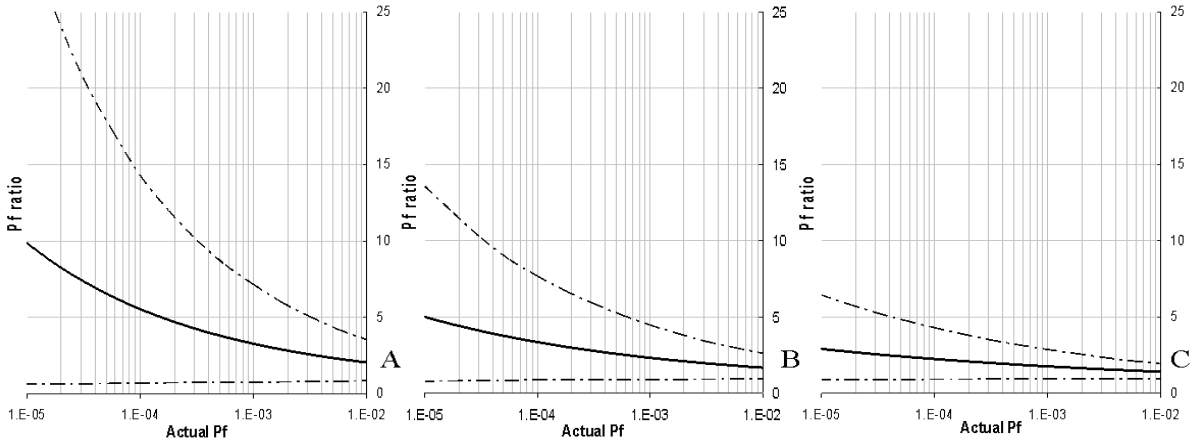

Figure 4-4. Mean and confidence intervals of the bootstrap p95 conservative estimators for Normal distribution based on (a) 100, (b) 200, and (c) 500 samples. x-axis is the true probability (lognormal scale), and y-axis is the ratio between the estimate and the true probability. Variability increases when target probability or sample size are smaller.

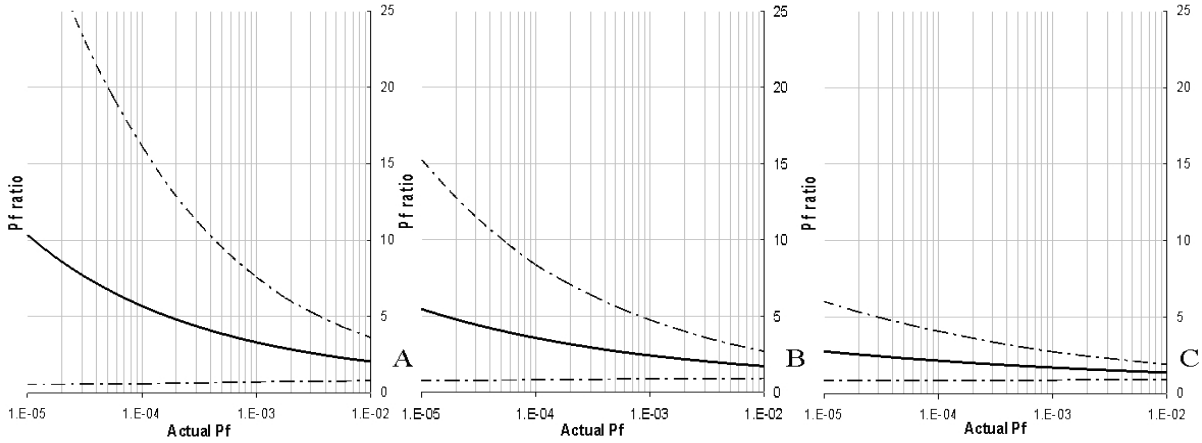

Figure 4-5. Mean and confidence intervals of the bootstrap p95 conservative estimators for lognormal distribution based on (a) 100, (b) 200, and (c) 500 samples. Results are almost identical to the normal distribution case.

For any given reliability analysis problem, careful attention needs to be given to the accuracy of probability of failure estimates. The graphs in Figures 4.6 and 4.6 address

this issue. They show the confidence intervals and therefore define adequate sample sizes needed to compute reliable estimates. In terms of cost-effectiveness, the figures indicate that it may be smart to allocate greater number of simulations to low probability designs than to high probability design in order to get constant level of relative accuracy.

4.7 Application To A Composite Panel Under Thermal Loading

In this section, conservative estimates are obtained for the probability of failure of a composite laminated panel under mechanical and thermal loadings. The panel is used for a liquid hydrogen tank. The cryogenic operating temperatures are responsible for large residual strains due to the different coefficients of thermal expansion of the fiber and the matrix, which is challenging in design.

Qu et al. (2003) performed the deterministic and probabilistic design optimizations of composite laminates under cryogenic temperatures, using response surface approximations for probability of failure calculations. Acar & Haftka (2005) found that using CDF estimations for strains improves the accuracy of probability of failure calculation. In this chapter, the optimization problem addressed by Qu et al. (2003) is considered. The geometry, material parameters and the loading conditions are taken from their paper.

4.7.1 Problem Definition

The composite panel is subject to resultant stress caused by internal pressure ($N_x = 8.4 \times 10^5 N/m$ and $N_y = 4.2 \times 10^5 N/m$) and thermal loading due to the operating temperature in the range of 20K - 300K. The objective is to minimize the weight of the composite panel that is a symmetric balanced laminate with two ply angles $[\pm\theta_1, \pm\theta_2]_s$ (that means an eight-layer composite). The design variables are the ply angles and the ply thicknesses $[t_1, t_2]$. The geometry and loading condition are shown in Figure 4-6. The thermal loading is defined by a stress free temperature of 422K, and working temperature of 300K to 20K. The material used in the laminates composite is IM600/133 graphite-epoxy, defined by the mechanical properties listed in Table 4-3.

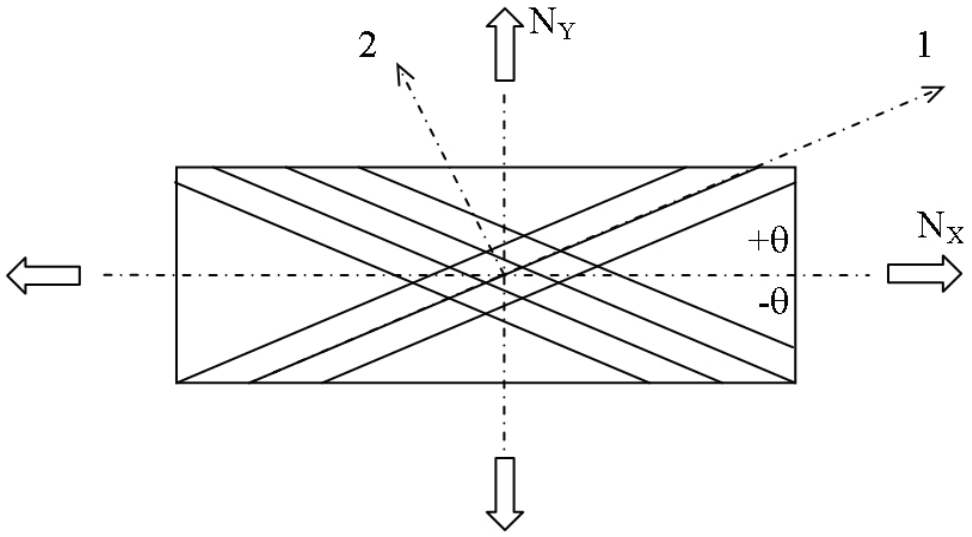

Figure 4-6. Geometry and loading of the cryogenic laminate.

Table 4-3. Mechanical properties of IM600/133 material. Quantities with $*$ are temperature dependent; the numerical values in the bracket are the range for T going from 20 to 300 K.

Elastic properties	E_1 (GPa)	147
	ν_{12}	0.359
	E_2^* (GPa)	[14 8]
	G_{12}^* (GPa)	[8 4]
Coefficients of thermal expansion	α_1^* (K^{-1}	$[-5\times10^{-7}, -1.5\times10^{-7}]$
	α_2^* (K^{-1}	$[1\times10^{-5}, 3\times10^{-5}]$
Stress-free temperature	T_{zero} (K)	422
Failure strains	ε_1^U	0.0103
	ε_2^L	-0.013
	ε_2^U	0.0154
	γ_{12}^U	0.0138

The minimum thickness of each layer is taken as 0.127 mm, which is based on the manufacturing constraints as well as for preventing hydrogen leakage. The failure is defined when the strain values of the first ply exceed failure strains.

The deterministic optimization problem is formulated as:

$$\begin{aligned} \underset{t_1,t_2,\theta_1,\theta_2}{\text{Minimize}} \quad & h = 4\,(t_1 + t_2) \\ & t_1, t_2 \geq 0.127 \\ & \varepsilon_1^L \leq S_F \varepsilon_1 \leq \varepsilon_1^U \\ \text{s.t.} \quad & \varepsilon_2^L \leq S_F \varepsilon_2 \leq \varepsilon_2^U \\ & S_F\,|\gamma_{12}| \leq \gamma_{12}^U \end{aligned} \tag{4–15}$$

where S_F is chosen at 1.4.

The analysis of the structural response is based on classical lamination theory using temperature-dependent material properties. E_2, G_{12}, α_1 and α_2 are function of the temperature. Since the design must be feasible for the entire range of temperature, strain constraints are applied at 21 different temperatures, which are uniformly distributed from 20K to 300K. Details on the analysis and the temperature dependence of the properties are given in Qu et al. (2003). Their solutions for the deterministic optimization problem are summarized in Table 4-4. For those results, t_1 and t_2 were chosen only as multiples of 0.127 mm. Three optima are found with equal total thickness but different ply angles and ply thicknesses.

Table 4-4. Deterministic optima found by Qu et al. (2003).

θ_1 (deg)	θ_2 (deg)	t_1 (mm)	t_2 (mm)	h (mm)
27.04	27.04	0.254	0.381	2.540
0	28.16	0.127	0.508	2.540
25.16	27.31	0.127	0.508	2.540

4.7.2 Reliability-Based Optimization Problem

Given the material properties and the design variables, the ply strains can be calculated using Classical Lamination Theory [Kwon & Berner (1997)]. Due to the manufacturing variability, the material properties and failure strains are considered random variables. All random variables are assumed to follow uncorrelated normal distributions. The coefficients of variation are given in Table 4-5. Since E_2, G_{12}, α_1 and α_2

are function of the temperature, the mean values of the random variables are calculated for a given temperature, and then, a set of random samples are generated according to their distributions.

Table 4-5. Coefficients of variation of the random variables.

$E_1, E_2, G_{12}, \nu_{12}$	α_1, α_2	T_{zero}	ε_1^L,ε_1^U	ε_2^L,ε_2^U,γ_{12}^U
0.035	0.035	0.03	0.06	0.09

The critical strain is the transverse strain on the first ply (direction 2 in Figure 4-6), the effect of other strains on the probability of failure being negligible. Hence, the limit-state is defined as the difference between the critical strain and the failure strain:

$$G = \varepsilon_2 - \varepsilon_2^U \tag{4–16}$$

Then, the probability of failure is defined in Eq. 4–5 using the distribution F_G of the limit-state.

In order to determine which distribution type fits the best the limit-state G, we generated 1,000 samples at each of the three first optimum designs. Using a Lilliefors test [Kenney & Keeping (1954)], we found that all the samples belong to a normal distribution. Hence, we assumed that the limit-state G is normally distributed for any design.

One might prefer not to assume a single distribution type over the design domain and test, every time a new design is considered, several distributions to find the one that fits best the data. Such a procedure is necessary for instance when the limit-state distribution varies from normal to heavy-tail within the design domain; assuming a single distribution can lead to large error in the reliability estimation. More generally, one has to keep in mind that the method proposed here can become hazardous if the determination of the distribution type is uncertain.

In our case, since the three designs considered are quite different from one another and have the same limit-state distribution, it is reasonable to assume that the limit-state distribution is always normal, hence reducing the computational burden.

The reliability-based optimization replaces the constraints on the strains in Eq. 4–15 by a constraint on the probability of failure. The target reliability of the cryogenic tank is chosen as 10^{-4}. Since the probability of failure can have a variation of several orders of magnitude from one design to another, it is preferable to solve the problem based on the reliability index:

$$\begin{aligned} \underset{t_1,t_2,\theta_1,\theta_2}{\text{Minimize}} \quad & h = 4\left(t_1 + t_2\right) \\ \text{s.t.} \quad & t_1, t_2 \geq 0.127 \\ & \beta\left(t_1, t_2, \theta_1, \theta_2\right) \geq -\Phi^{-1}\left(10^{-4}\right) = 3.719 \end{aligned} \tag{4–17}$$

4.7.3 Reliability Based Optimization Using Conservative Estimates

By solving Eq. 4–17 with a sampling-based estimate of reliability, we face the problem of having noise in the constraint evaluation, which can severely harm the optimization process. To address this issue, we chose to fit a polynomial response surface (PRS) to approximate the reliability index everywhere on a region of the design space and solve the optimization with the response surface. We have then two levels of surrogate modeling: one surrogate to approximate the reliability index of a given design, and one surrogate to approximate the reliability index for all the design region.

The PRS is based on the estimation of the reliability index for a selected number of designs: $\{\beta_1, \ldots, \beta_p\}$. All the estimates are done before the optimization process. The range of the response surface is given in Table 4-6. The number of training points is taken as 500; the points are generated using Latin hypercube sampling to ensure a good space-filling property. Each estimate of the reliability index is based on the same $n = 200$ samples, which gives us a total number of 100,000 simulations to fit the response surface.

Table 4-6. Variable range for response surface.

Variables	Range
θ_1, θ_2 (deg)	[20 30]
t_1, t_2 (mm)	[0.127 0.800]

With the 3,000 simulations used to determine the distribution of the limit state, the total number of simulations is 103,000. This number is a reasonable total budget for solving the RBDO problem: indeed there is no further simulation run during the optimization, the reliability being estimated by the PRS. To compare this number to classical MCS estimates, in order to achieve reasonable noise for a probability of failure of 10^4, at least 10^6 samples are needed for a single evaluation, and the reliability is reestimated at each optimization step. It is more difficult to compare to FORM and SORM methods, but due to the large number of random parameters in the problem, they would not be efficient.

The reliability indexes are calculated using two methods: the unbiased fitting and the bootstrap conservative estimation with 95% confidence. The estimates are denoted respectively $\hat{\beta}^{(i)}_{unb}$ and $\hat{\beta}^{(i)}_{cons}$. Figure 4.6 B) shows that with 200 samples, the confidence interval of the conservative estimator for a probability of 10^{-4} is $[10^{-4}; 8 \times 10^{-4}]$, which corresponds to an error in β between 0 and 20%. Since the number of observations is much larger than the number of coefficients (500 compared to 70), the noise is filtered by the PRS.

A different response surface is fitted to each set of data. For both, we found that a fourth order polynomial provided a good approximation for the reliability index. Table 4-7 shows the statistics of each response surface. Both R^2 values (percentage of variance explained) are very close to one, and p-values show that both models are very significant.

In addition, we computed accurate estimates of the reliability index at 22 designs uniformly chosen in the design space using separable Monte-Carlo method (SMC) [Smarslok et al. (2008)] with 40,000 samples for each design. Table 4-8 shows the statistics based on the test points: the root mean square error (e_{RMS}) between the 22 accurate responses and the response surface, error mean and number of unconservative predictions. Based on the test points, we can see that the first PRS is unbiased: the error mean is approximately zero and there are ten unconservative errors for twelve conservative. On

the other hand, the second PRS has large bias since the error mean is 0.34 and all the predictions at test points are conservative.

Table 4-7. Statistics of the PRS for the reliability index based on the unbiased and conservative data sets.

Data sets	R^2	F	p-value
$\left\{\hat{\beta}^{(1)}_{unb}, \ldots, \hat{\beta}^{(p)}_{unb}\right\}$	0.96	138	$< 10^{-6}$
$\left\{\hat{\beta}^{(1)}_{cons}, \ldots, \hat{\beta}^{(p)}_{cons}\right\}$	0.96	136	$< 10^{-6}$

Table 4-8. Statistics of the PRS based on 22 test points

Data sets	e_{RMS}	Error mean	Nb of unconservative predictions
$\left\{\hat{\beta}^{(1)}_{unb}, \ldots, \hat{\beta}^{(p)}_{unb}\right\}$	0.081	-0.01	10
$\left\{\hat{\beta}^{(1)}_{cons}, \ldots, \hat{\beta}^{(p)}_{cons}\right\}$	0.354	-0.34	0

Remark 1. Since we have two levels of surrogate models, it is possible to apply conservative strategy to either one one them, or both of them, by applying to the PRS one of the methods proposed in Chapter 3. Here, we found that using a conservative strategy only on the reliability index estimation was sufficient to guarantee safe design, and more efficient than using unbiased estimation of β and conservative PRS.

Remark 2. The balance between the number of MCS by design n and the number of design points p is an open question. Here, we chose a small number of MCS since we were able to compensate efficiently for it. Chapter 7 deals with this question and provide theoretical answers to choose this balance for PRS and Kriging.

4.7.4 Optimization Results

We present the results for the two probabilistic optimizations based on the response surfaces fitted on unbiased and conservative estimates. To compare deterministic and probabilistic approaches, the deterministic optimization as stated in Eq. 4–15 is also performed for the same range of the ply angles ([20 30] degrees). The optimization is performed using MATLAB's function fmincon repeated 20 times with different initial points to ensure global convergence. The optimal designs (best over the 20 optimizations)

are given in Table 4-9. For these designs, an accurate estimate of the probability of failure is computed using SMC with 40,000 samples.

Table 4-9. Optimal designs of the deterministic and probabilistic problems with unbiased and conservative data sets.

	t1	t2	θ_1	θ_2	h	β from PRS	Actual β	P_f from PRS	Actual P_f (SD)*
Unbiased data set	0.127	0.507	22.2	30.0	2.536	3.72	3.61	10-4	1.51e-4 (2.28e-6)
95% cons. data set	0.127	0.582	21.9	30.0	2.835	3.72	3.98	10-4	3.50e-5 (6.3e-7)
Determ. optima	0.127	0.416	20.0	30.0	2.170	x	2.97	x	15.0e-4 (9.6e-6)

The three optima are similar in terms of ply angles, and for all the first ply thickness t_1 is the lower bound; the significant difference is in the second ply thickness t_2. Both probabilistic designs are heavier than the deterministic optimum. The optimum found using unbiased dataset is substantially lighter than the other ($h = 2.54$ compared to 2.84); however, the accurate estimate of reliability shows that the optimum design using unbiased dataset violates the constraint. On the other hand, the design found using conservative dataset is conservative; the actual probability is 3 times smaller than the target probability of failure. The deterministic design is very unconservative, its probability of failure being 15 times the target.

The fact that an unbiased strategy leads to an unconservative design is not surprising. Indeed, optimization is biased to explore regions where the error is 'favorable'; that is, where the constraint is underestimated. Using the conservative approach, the level of bias is sufficient to overcome this problem, but at the price of overdesign: since the probability of failure is three times the target, the actual optimum is lighter than the one we found.

We have shown that despite a very limited computational budget (103,000 MCS to solve the RBDO problem), it was possible to obtain a reasonable design by compensating the lack of information by taking conservative estimates.

4.8 Concluding Comments

The estimation of the probability of failure of a system is crucial in reliability analysis and design. In the context of expensive numerical experiments, or when a limited number of data samples are available, the direct use of Monte Carlo Simulation is not practical, and estimation of continuous distributions is necessary. However, classical techniques of estimation of distribution do not prevent dangerous underestimates of the probability of failure.

Several methods of estimating safely the probability of failure based on the limited number of samples are tested, when the sample distribution type is known. The first method constrains distribution fitting in order to bias the probability of failure estimate. The second method uses the bootstrap technique to obtain distributions of probability of failure estimators, and these distributions define conservative estimators.

In the case of samples generated from normal distribution, the numerical test case shows that both methods improve the chance of the estimation to be conservative. Bootstrap based estimators outperformed constrained fits to the experimental CDF. That is, for the same confidence in the conservativeness of the probability estimate, the penalty in the accuracy of the estimate was substantially smaller. However, optimization based methods can be used when the sample size is very small, where the bootstrap method cannot be used.

We also explored the influence of sample sizes and target probability of failure on estimates quality. We found that larger sample sizes are required to avoid large variability in probability of failure estimates when that probability is small. The results indicated that when sampling at different points in design space it may be more cost effective to have different number of samples at different points. Such approach is addressed in Chapter 6.

Finally, we have applied the conservative estimation procedures to perform the optimization of a composite laminates at cryogenic temperatures. We compared the

optimization results found where response surfaces are fitted to unbiased and conservative estimates respectively. We found that the unbiased response surfaces led to unsafe designs, while the conservative approach returned an acceptable design.

CHAPTER 5
DESIGN OF EXPERIMENTS FOR TARGET REGION APPROXIMATION

The accuracy of metamodels is crucial for the effectiveness of their use in prediction, design or propagation of uncertainty. In Chapters 3 and 4, we proposed some alternatives to compensate for the error in surrogate models. In this chapter, we aim at minimizing the uncertainty of the models. The design of experiment strategy is one of the most important factors that affect the quality of the metamodel. In many practical problems, the total number of function evaluations is drastically limited by computational cost; hence, it is of crucial interest to develop methods for selecting efficiently the experiments.

Sampling strategies have been extensively studied over the past decades. In Chapter 2, we described some of the most popular strategies that aim at optimizing the global accuracy of the metamodels. The scope of the present research is to propose an objective-based approach to design of experiments, based on the idea that the uncertainty in surrogates may be reduced where it is most useful, instead of globally. In particular, we aim at finding efficient strategies for two applications of metamodeling: reliability estimation and constrained optimization.

5.1 Motivation And Bibliography

Most sampling strategies are developed to achieve the best global performances of the metamodel. Such approach is fully justified when the model is used for prediction over all the domain of interest, inference of global behavior of the phenomenon studied, or when all the design of experiment is generated at the same time without prior information on the response behavior, for instance when series of physical experiments or parallel computation are involved.

However, many metamodel applications focus on the value of the function response. For instance, when a metamodel is used for optimization purpose, it is obvious that the metamodel accuracy is much more important for low values of the response rather than

large values. Hence, global strategies do not appear as the most efficient responses to such application.

The present research focuses on applications where metamodels are used in a way that their accuracy is crucial for certain level(s) of the response function. Such situation appears in particular in two popular frameworks:

In constrained optimization. The constraint function often relies on expensive calculations. For instance, a typical structural optimization formulation is to minimize a weight function such that the maximum stress, computed by finite element analysis, does not exceed a certain value. When using a metamodel to approximate the constraint, it is of utmost importance that the approximation error is minimal on the boundary that separates the feasible designs from infeasible ones. Substantial errors for values far from the boundary, on the other hand, are not detrimental.

In reliability analysis. We consider the case where the metamodel is used to approximate the limit state function of a system, $G(\mathbf{x})$. As well as for constraint approximation, the metamodel discriminates between samples that are below and above a critical value, in this case zero. When the limit state is far from zero, the chance of misclassification is negligible even if the metamodel poorly approximate the true function, while the accuracy is crucial for values close to zero.

The present chapter presents a methodology to construct a design of experiments such that the metamodel accurately approximates the vicinity of a boundary in design space defined by a target value of the function approximated by the surrogate. This problem has been addressed by several authors. Mourelatos et al. (2006) used a combination of global and local metamodels to first detect the critical regions and then obtain a locally accurate approximation. Shan & Wang (2004) proposed a rough set based approach to identify sub-regions of the design space that are expected to have performance values equal to a given level. Oakley (2004) uses Kriging and sequential strategies for uncertainty propagation and estimation of percentiles of the output of computer codes. Ranjan et al.

(2008) proposed a modified version of the EGO algorithm to sequentially explore the domain region along a contour line. Tu & Barton (1997) used a modified D-optimal strategy for boundary-focused polynomial regression. Vazquez & Piera-Martinez (2006) proposed an iterative strategy to minimize the classification error when computing a probability of failure based on Kriging.

5.2 A Targeted IMSE Criterion

In this chapter, we consider only probabilistic metamodels - that associate a distribution to a prediction point instead of a single value. Kriging is explicitly a probabilistic metamodel, but most of the other models can have a probabilistic interpretation, such as regression and splines for instance. However, we limit our investigation to the kriging model here.

We gave the definition in Section 2.2.2 of the IMSE criterion, which sums up the uncertainty associated with the Kriging model over the entire domain D. However, when one is more interested in predicting y accurately in the vicinity of a contour line $\mathbf{u} = \mathbf{y^{-1}}(\mathbf{T})$ (T a constant), such a criterion is not suitable since it weights all points in D according to their Kriging variance, which does not depend on the observations $\mathbf{Y}_{obs}$, and hence does not favor zones with respect to properties concerning their y values but only on the basis of their position with respect to DoE.

We propose to change the integration domain from D to a neighborhood of $y^{-1}(T)$. Two approaches are proposed that differ by the definition of the neighborhood of the contour line. The neighborhood is defined with the help of an indicator function and a gaussian distribution, respectively, which can be encountered in the literature under the denomination of *desirability functions*.

5.2.1 Target Region Defined By An Indicator Function

We define a region of interest $\mathbf{X}_{T,\varepsilon}$ (parameterized by ε) as the subset in D whose image is within the bounds $T-\varepsilon$ and $T+\varepsilon$:

$$\mathbf{X}_{T,\varepsilon} = y^{-1}\left([T-\varepsilon, T+\varepsilon]\right) = \left\{\mathbf{x} \in D \middle| \, y\left(\mathbf{x}\right) \in [T-\varepsilon, T+\varepsilon]\right\} \tag{5–1}$$

Figure 5-1 illustrates a one-dimensional function with the region of interest being at $T = 0.8$ and $\varepsilon = 0.2$. Note that the target region consists of two distinct sets.

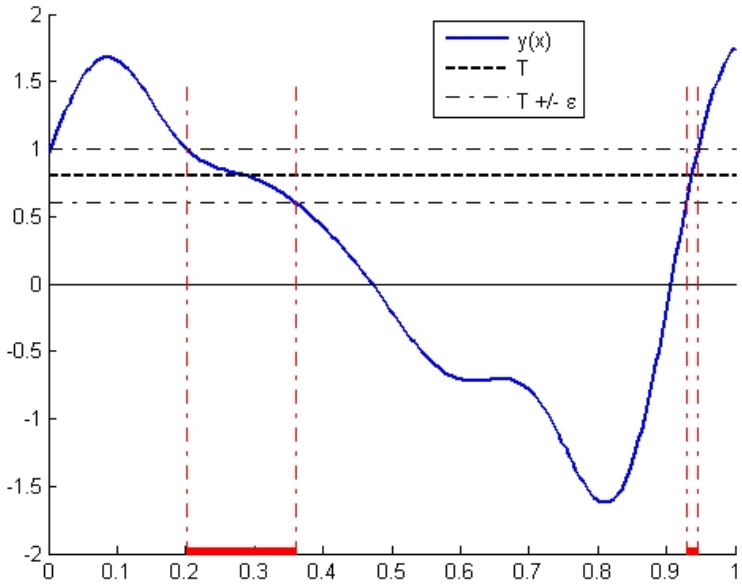

Figure 5-1. One-dimensional illustration of the target region. The level-set T is equal to 0.8, and ε to 0.2. The target region consists of two distinct sets.

With the region of interest, the targeted IMSE criterion is defined as follows:

$$imse_T = \int_{X_{T,\varepsilon}} s_K^2(\mathbf{x})d\mathbf{x} = \int_D s_K^2(\mathbf{x})\mathbf{1}_{[T-\varepsilon,T+\varepsilon]}\left[y\left(\mathbf{x}\right)\right]d\mathbf{x} \tag{5–2}$$

where $\mathbf{1}_{[T-\varepsilon,T+\varepsilon]}\left[y\left(\mathbf{x}\right)\right]$ is the indicator function, equal to 1 when $y\left(\mathbf{x}\right) \in [T-\varepsilon, T+\varepsilon]$ and 0 elsewhere.

Finding a design that minimizes $imse_T$ would make the metamodel accurate in the subset $\mathbf{X}_{T,\varepsilon}$, which is exactly what we want. Weighting the IMSE criterion over a region of interest is classical and proposed for instance by Box & Draper (1986), pp.433-434. However, the notable difference here is that this region is unknown *a priori*.

Now, we can adapt the criterion in the context of Kriging modeling, where y is a realization of a random process Y (see Section 2.1.3).

Thus, $imse_T$ is defined with respect to the event ω:

$$\int_D s_K^2(\mathbf{x})\mathbf{1}_{[T-\varepsilon,T+\varepsilon]}\left[Y\left(\mathbf{x},\omega\right)\right]d\mathbf{x} = I(\omega) \tag{5–3}$$

To come back to a deterministic criterion, we consider the expectation of $I\left(\omega\right)$, conditional on the observations (which is the best approximation in the L^2 sense):

$$IMSE_T = E\left[I(\omega)|obs\right] = E\left[\int_D s_K^2(\mathbf{x})\mathbf{1}_{[T-\varepsilon,T+\varepsilon]}\left[Y\left(\mathbf{x},\omega\right)\right]d\mathbf{x}|obs\right] \tag{5–4}$$

Since the quantity inside the integral is positive, we can commute the expectation and the integral:

$$\begin{aligned} IMSE_T &= \int_D s_K^2(\mathbf{x})E\left[\mathbf{1}_{[T-\varepsilon,T+\varepsilon]}\left[Y\left(\mathbf{x},\omega\right)\right]|obs\right]d\mathbf{x} && (5–5)\\ &= \int_D s_K^2(\mathbf{x})E\left[\mathbf{1}_{[T-\varepsilon,T+\varepsilon]}\left[M\left(\mathbf{x}\right)\right]\right]d\mathbf{x} && (5–6)\\ &= \int_D s_K^2(\mathbf{x})W\left(\mathbf{x}\right)d\mathbf{x} && (5–7) \end{aligned}$$

According to Eq. 5–7, the reduced criterion is the average of the prediction variance weighted by the function $W(\mathbf{x})$. Besides, $W(\mathbf{x})$ is simply the probability that the response is inside the interval $[T-\varepsilon, T+\varepsilon]$. Indeed:

$$\begin{aligned} W(\mathbf{x}) &= E\left[\mathbf{1}_{[T-\varepsilon,T+\varepsilon]}\left[M\left(\mathbf{x}\right)\right]\right] && (5–8)\\ &= P\big(M(\mathbf{x}) \in [T-\varepsilon, T+\varepsilon]\big) && (5–9)\\ &= P\big(Y(\mathbf{x}) \in [T-\varepsilon, T+\varepsilon]\,|obs\big) && (5–10) \end{aligned}$$

The Gaussian process interpretation of Kriging adopted here (see Section 2.1.3) allows us to explicitly derive the conditional distribution of $M(\mathbf{x}) = \left(Y\left(\mathbf{x}\right) \mid obs\right)$ at any prediction point:

$$\text{For any } \mathbf{x} \in D: \qquad M\left(\mathbf{x}\right) \sim N\left(m_K\left(\mathbf{x}\right), s_K^2\left(\mathbf{x}\right)\right) \tag{5–11}$$

We can obtain a simple analytical form for $W(\mathbf{x})$:

$$W(\mathbf{x}) = \int_{T-\varepsilon}^{T+\varepsilon} g_{N\left(m_K(\mathbf{x}),s_K^2(\mathbf{x})\right)}(u)\, du \tag{5–12}$$

where $g_{N(m_K(\mathbf{x}),\sigma_K^2(\mathbf{x}))}(u)$ is the probability density function (PDF) of $M(\mathbf{x})$. By integrating the PDF we obtain:

$$W(\mathbf{x}) = \Phi\left(\frac{T+\varepsilon-m_K(\mathbf{x})}{s_K(\mathbf{x})}\right) - \Phi\left(\frac{T-\varepsilon-m_K(\mathbf{x})}{s_K(\mathbf{x})}\right) \tag{5–13}$$

where Φ is the CDF of the standard normal distribution.

Remark. It is possible to define a weight function with $\varepsilon \to 0$. To do so, we have to divide first $W(\mathbf{x})$ by the constant 2ε. Then, we obtain:

$$\lim_{\varepsilon\to 0} \quad \frac{1}{2\varepsilon}\left[\Phi\left(\frac{T+\varepsilon-m_K(\mathbf{x})}{s_K(\mathbf{x})}\right) - \Phi\left(\frac{T-\varepsilon-m_K(\mathbf{x})}{s_K(\mathbf{x})}\right)\right] = \varphi\left(\frac{T-m_K(\mathbf{x})}{s_K(\mathbf{x})}\right) \tag{5–14}$$

where φ is the probability density function (PDF) of the standard normal distribution.

5.2.2 Target Region Defined By A Gaussian Density

Defining the region of interest as $\mathbf{X}_{T,\epsilon}$ is intuitive and makes it easy to derive the weight function. However, it might not always correspond exactly to our objective. Indeed, if we consider an ideal case where the function is exactly known, the indicator function will yield a weight 1 to a point $\mathbf{x}$ where $M(\mathbf{x}) - T = \varepsilon$, but 0 if $M(\mathbf{x}) - T = \varepsilon + 10^{-9}$. Also, it will not discriminate between a point where the difference is equal to ε and another one where this difference is equal to zero.

Instead, we prefer a criterion that continuously increases the importance of the location when the response approaches the threshold. For instance, we can choose a triangular function (with a maximum at T) or a sigmoid function. Here, we choose to use the probability density function of a normal distribution which leads to a simple analytical form of the weight function. In the spirit of Eq. 5–8, the Gaussian-based weight function

is therefore defined as follows:

$$W(\mathbf{x}) = E\left[g_\varepsilon\left(M(\mathbf{x}) - T\right)\right] \tag{5–15}$$

where $g_\varepsilon(u)$ is the PDF of $N(0, \sigma_\varepsilon^2)$.

When $M(\mathbf{x})$ stands for the Kriging model, we can obtain a simple form for the weight function:

$$W(\mathbf{x}) = \int_{-\infty}^{+\infty} g_\varepsilon(u - T) g_{N\left(m_K(\mathbf{x}), s_K^2(\mathbf{x})\right)}(u)\, du \tag{5–16}$$

Since g_ε is symmetric:

$$W(\mathbf{x}) = \int_{-\infty}^{+\infty} g_\varepsilon(T - u) g_{N\left(m_K(\mathbf{x}), s_K^2(\mathbf{x})\right)}(u)\, du \tag{5–17}$$

This integral is the convolution of the two Gaussian densities, which is well-known to be the density of a sum of independent Gaussian variables. Hence, we obtain:

$$W(\mathbf{x}) = \frac{1}{\sqrt{2\pi\left(\sigma_\varepsilon^2 + s_K^2(\mathbf{x})\right)}} e^{\left(-\frac{1}{2}\frac{\left(m_k(\mathbf{x}) - T\right)^2}{\sigma_\varepsilon^2 + s_K^2(\mathbf{x})}\right)} \tag{5–18}$$

This new weight function depends on a single parameter σ_ϵ that allows us to select the size the domain of interest around the target level of the function. A large value of σ_ϵ would enhance space-filling, since the weight function would tend to a constant and the weighted IMSE to a uniform IMSE criterion. On the contrary, a small value would enhance the accuracy of the surrogate on a narrow region around the contour line of interest.

5.2.3 Illustration

We consider a one-dimensional case, where the function y to approximate is a realization of a Gaussian process with Gaussian covariance structure. y is defined on $[0, 1]$; the design of experiments consists of five observations equally spaced in this interval. The level-set of interest T is chosen as 1.3, and both ε and σ_ε are taken as 0.2. Figure 5-2 represents the true function, the Kriging metamodel and corresponding weights. The

weight function in Eq. 5–13 is shown as "interval", while that in Eq. 5–18 is shown as "Gaussian" in the figure.

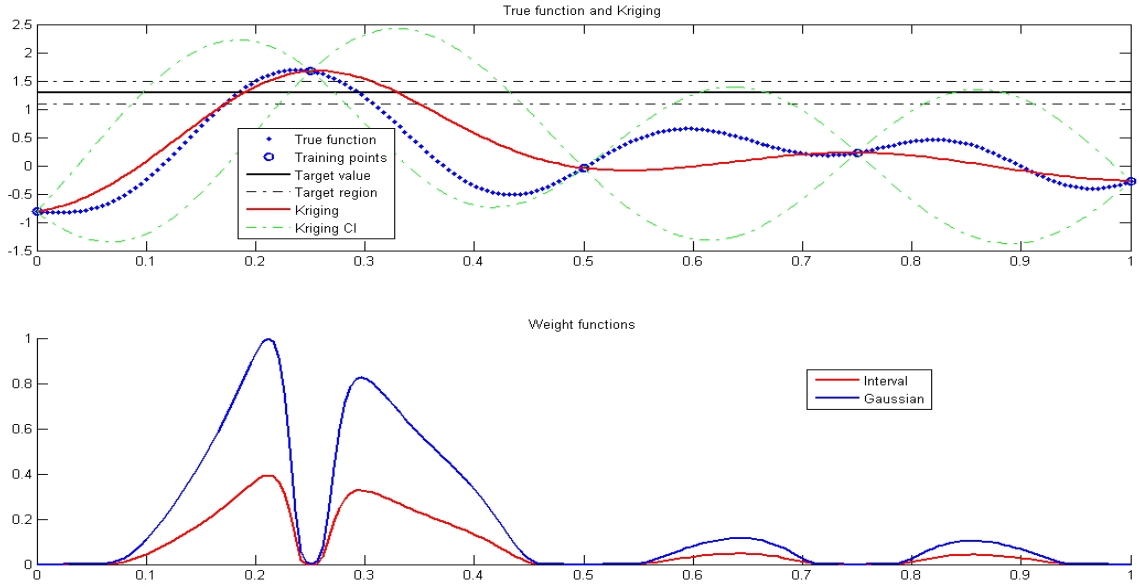

Figure 5-2. Illustration of the weights functions. Upper graph: true function, observations, Kriging mean and confidence intervals, and target region. Lower graph: weight functions. Both weights are large where the true function is inside the target region, but also signaling regions of high uncertainties (around $x = 0.65$ and 0.85).

Among the five observations, one is substantially closer to T than the others. As a consequence, the weight functions are large around this observation point. For the indicator-based weight function, the weights are null at the observation points, since for this example no observation is inside the target value interval. For the Gaussian-based weight, it is also very close to zero. For both functions, high weights are given to regions for which the actual function is inside the target interval. Both weight functions are also non-zero where the uncertainty is high, even if the Kriging mean is far from T (around $x = 0.65$ and 0.85).

5.3 Sequential Strategies For Selecting Experiments

Without any observation, the weight function $W(\mathbf{x})$ is, assuming stationarity, a constant (the probability is the same everywhere). Every time a new observation is performed, the weight function will more precisely discriminate the regions of interest from

the others. Hence, the procedure to build an optimal DoE is necessarily iterative. If we add one observation at a time we can use the procedure shown in Table 5-1.

Table 5-1. Procedure of the $IMSE_T$-based sequential DoE strategy.

Create an initial DoE, $\mathbf{X}_k$, and generate observations $\mathbf{Y}_k = y(\mathbf{X}_k)$
For i going from one to the total number of additional observations n:
Fit the Kriging model to the data $\{\mathbf{X}_{k+i-1}, \mathbf{Y}_{k+i-1}\}$
Find a new training point $\mathbf{x}_{new}$ that minimizes the criterion $\mathrm{IMSE_T}\left(\{\mathbf{X}_{\mathrm{k+i-1}}, \mathbf{x}_{\mathrm{new}}\}\right)$
Compute the new observation $y_{new} = y(\mathbf{x}_{new})$
Update the DoE and observations:
$\mathbf{X}_{k+i} = \{\mathbf{X}_{k+i-1}, \mathbf{x}_{new}\}$
$\mathbf{Y}_{k+i} = \{\mathbf{Y}_{k+i-1}, y_{new}\}$
End of loop

The Kriging parameters can be reevaluated after every new observation, or only from the initial DoE before the iterative procedure. Note that the evaluation of the parameters is critical to obtain a good Kriging model. Besides, the parameters affect the criterion: underestimation of the range makes the weight function flatter and enhances space-filling; on the contrary, overestimation of the range leads to a very discriminating (over-confident) weight function. However, in the numerical examples used in this work, we found that the parameter re-evaluation had a negligible impact on the efficiency of the method.

Finding the new training point requires an inner optimization procedure. When the classical IMSE criterion is considered, the optimization can be expressed as:

$$\min_{\mathbf{x}_{new} \in D} \quad \mathrm{IMSE}\left(\mathbf{X}_{k+1}\right) = \mathrm{IMSE}\left(\{\mathbf{X}_k, \mathbf{x}_{new}\}\right) \tag{5–19}$$

where

$$\mathrm{IMSE}\left(\{\mathbf{X}_k, \mathbf{x}_{new}\}\right) = \int_D s_K^2\left(\mathbf{x} | \{\mathbf{X}_k, \mathbf{x}_{new}\}\right) \mathrm{d}\mathbf{x}$$

$s_K^2\left(\mathbf{x} | \{\mathbf{X}_k, \mathbf{x}_{new}\}\right)$ is the variance at $\mathbf{x}$ of the Kriging based on the design of experiments $\mathbf{X}$ augmented with the training point $\mathbf{x}_{new}$. Since the Kriging variance does not depend on the observation, there is no need to have $y(\mathbf{x}_{new})$ to compute the IMSE.

In contrast, the weighted IMSE depends on the observations through the weight function $W(\mathbf{x})$. The weight function cannot take into account the new observation, since the response is not available. Hence, when expressing the weighted IMSE as a function of $\mathbf{x}_{new}$, we update only the variance part under the integral:

$$\mathrm{IMSE_T}\left(\mathbf{X_k}, \mathbf{Y_k}, \mathbf{x_{new}}\right) = \int_{\mathrm{D}} \mathrm{s_K^2}\left(\mathbf{x}\middle|\left\{\mathbf{X_k}, \mathbf{x_{new}}\right\}\right) \mathrm{W}\left(\mathbf{x}\middle|\,\mathbf{X_k}, \mathbf{Y_k}\right) \mathrm{d}\mathbf{x} \tag{5–20}$$

where $s_K^2\left(\mathbf{x}\middle|\left\{\mathbf{X}_k, \mathbf{x}_{new}\right\}\right)$ is the same as in Eq. 5–19 and $W\left(\mathbf{x}\middle|\,\mathbf{X}_k, \mathbf{Y}_k\right)$ is the weight function based on the existing DoE. Using this expression, we have the simple formulation for the inner optimization problem:

$$\min_{\mathbf{x}_{new} \in D} \mathrm{IMSE}_T\left(\mathbf{X}_k, \mathbf{Y}_k, \mathbf{x}_{new}\right) \tag{5–21}$$

5.4 Practical Issues

5.4.1 Solving The Optimization Problem

Finding the new observation $\mathbf{x}_{new}$ by solving the optimization problem of Eq. 5–21 is, in practice, challenging. Indeed, the $IMSE_T$ criterion in Eq. 5–20 must be evaluated by numerical integration, which is computationally intensive. Besides, for any candidate $\mathbf{x}_{new}$, the Kriging model must be reevaluated with this new observation to obtain $s_K^2\left(\mathbf{x}\middle|\left\{\mathbf{X}_k, \mathbf{x}_{new}\right\}\right)$). Therefore we propose here some alternatives that may be used to reduce the cost.

A popular heuristic to minimize sequentially the IMSE is to find the point where the prediction variance is maximum [Sacks et al. (1989a), Williams et al. (2000)], which can be used here with the weighted prediction variance. This strategy has the advantage of saving both the numerical integration and the inversion of a new covariance matrix. However, the prediction variance is likely to have many (local or global) maximizers, which are not equivalent in terms of the IMSE. In particular, many optima are located on the boundaries, which is very inefficient for the IMSE minimization. To compensate for this issue, one may in a first time get a large number of local optima using adapted

optimization strategies (multi-start, etc.), and in a second time evaluate those optima in terms of the weighted IMSE criterion, and perform a local optimization on the best point.

A valuable computational shortcut can be achieved in the update of the inverse of the covariance matrix when adding an observation. Let us call $\mathbf{C}_k$ the covariance matrix corresponding to a DoE with k observations. Then, the covariance matrix of the DoE augmented with the $k+1$th observation can be written:

$$\mathbf{C}_{k+1} = \begin{bmatrix} \sigma^2 & \mathbf{c}_{new}^T \\ \mathbf{c}_{new} & \mathbf{C}_k \end{bmatrix} \tag{5–22}$$

with:

- $\sigma^2 = k\left(\mathbf{x}_{new}, \mathbf{x}_{new}\right)$ (process variance), and
- $\mathbf{c}_{new}^T = \left[k\left(\mathbf{x}_{new}, \mathbf{x}_1\right), \ldots, k\left(\mathbf{x}_{new}, \mathbf{x}_k\right)\right]$ a $1 \times k$ vector.

Using Schur's complement formula, we get:

$$\mathbf{C}_{k+1}{}^{-1} = \begin{bmatrix} 1 & 0 \\ -\mathbf{C}_k^{-1}\mathbf{c}_{new} & \mathbf{I}_k \end{bmatrix} \begin{bmatrix} \frac{1}{\sigma^2 - \mathbf{c}_{new}^T \mathbf{C}_k^{-1} \mathbf{c}_{new}} & 0 \\ 0 & \mathbf{C}_k^{-1} \end{bmatrix} \begin{bmatrix} 1 & -\mathbf{C}_k^{-1}\mathbf{c}_{new} \\ 0 & \mathbf{I}_k \end{bmatrix} \tag{5–23}$$

This formula allows to compute $\mathbf{C}_{k+1}{}^{-1}$ from $\mathbf{C}_k{}^{-1}$ without doing any matrix inversion, and compute $s_K^2\left(\mathbf{x}\middle|\left\{\mathbf{X}_k, \mathbf{x}_{new}\right\}\right)$ at reasonable cost. More detailed calculations on this topic can be found in Marrel (2008).

In general, the criterion has several local minimizers. Then, it is necessary to use global optimization methods, such as population-based methods, multi-start strategies, etc. In the test problems presented in this chapter, we optimize the criterion on a fine grid for low dimensions, and using the population-based CMA-ES algorithm [Covariance Matrix Adaptation Evolution Strategies, Hansen & Kern (2004)] for higher dimensions. Experimentation showed that due to the numerical integration precision, the targeted IMSE strategy becomes inefficient for dimensions higher than ten.

5.4.2 Parallelization

It is often of interest to produce algorithms that allow to compute several observations at a time, for instance when the numerical simulator can be run in parallel on several computers. The criterion we propose is fully adaptable to parallel strategies. Indeed, the targeted IMSE consists of two parts: the weight function that depends on the response values, and the prediction variance, that only depends on the observation locations. The later quantity can be updated with several observations without the need of calculating the response. The weight function, on the other hand, remains the same.

Let p be the number of observations to be computed in parallel. The criterion to be minimized can be written:

$$\mathrm{IMSE}_T\left(\mathbf{X}_k, \mathbf{Y}_k, \{\mathbf{x}_{new}^{(1)}, \ldots, \mathbf{x}_{new}^{(p)}\}\right) = \int_D s_K^2\left(\mathbf{x} \middle| \left\{\mathbf{X}_k, \{\mathbf{x}_{new}^{(1)}, \ldots, \mathbf{x}_{new}^{(p)}\}\right\}\right) W\left(\mathbf{x} \middle| \mathbf{X}_k, \mathbf{Y}_k\right) \mathrm{d}\mathbf{x} \tag{5–24}$$

This strategy is less accurate than the sequential strategy, since the weight function is updated only every p evaluations. However, we observed that for low values of p (≤ 5), the parallelization has little impact, in particular when the kriging uncertainty is initially high.

The parallel optimization problem is of dimension $d \times p$ (where d is the design space dimension). The dimension of the numerical integration remains the same as in Eq. 5–20. The optimization can be solved directly, or, in order to reduce the problem dimension, by finding one point at a time.

5.5 Application To Probability Of Failure Estimation

As mentioned in the beginning of this chapter, when approximating the limit-state, it is clear that a particular effort must be given to the regions where it is close to zero, since error in that region is likely to affect the probability estimate. Naturally, the critical region is where the value of limit state is close to zero.

The targeted IMSE criterion allows us to sample in target regions. However, substantial improvement can be given, by taking into account the distribution of the

input variables. Indeed, let us consider the case of two distinct failure regions, one of it dominating the other (that is, the probability that the input falls onto the first region is much larger than the probability that it falls onto the other). Instead of exploring equally the two critical regions, it will be more efficient to spend more computational effort on the one that will affect most the probability estimate. In the same sense, when learning a single critical region, it is efficient to explore it only where the samples are more likely to be.

Instead of using the indicator function on the Kriging mean, we use the full Kriging information by computing, at each sampling point, the probability that the response exceeds the threshold:

$$\hat{P}_f = \frac{1}{N} \sum_{i=1}^{N} \Phi_k^{(i)}(0) \tag{5–25}$$

where $\Phi_k^{(i)}$ denotes the cumulative distribution function (CDF) of the Kriging model at $\mathbf{x}_i$ ($N\left(m_k\left(\mathbf{x}_i\right), s_k^2\left(\mathbf{x}_i\right)\right)$).

If the Kriging variance is small, the CDF becomes equivalent to the indicator function, being 1 if the Kriging mean exceeds the threshold and 0 otherwise. On the other hand, when the variance is high or the predicted response close to the threshold, using the Kriging distribution offers a smoothing effect by giving a number between zero and one instead of a Boolean number.

To address the probability distribution of input variables, we modify the weighted IMSE criterion by integrating the weighted MSE not with a uniform measure, but with the PDF of the input variables:

$$\mathrm{IMSE}_T = \int_D \mathrm{s}_K^2(\mathbf{x}) W(\mathbf{x}) \, \mathrm{d}\mu(\mathbf{x}) = \int_D \mathrm{s}_K^2(\mathbf{x}) W(\mathbf{x}) f(\mathbf{x}) \, \mathrm{d}\mathbf{x} \tag{5–26}$$

where $f(\mathbf{x})$ is the PDF of the law μ with respect to the Lebesgue measure.

5.6 Numerical Examples

In this section, we evaluate the accuracy and efficiency of the method through numerical examples. We consider the fitting of analytical test functions and realizations of random processes with known covariance structures. In the latter case, there is no modeling error when using a Kriging approximation; the error is only due to the lack of information.

5.6.1 Two-Dimensional Example

The first example is the approximation of a two-dimensional parametric function from the optimization literature (*Camelback function*, Chipperfield et al. (1994)). The original function is modified (bounds are different and a negative constant is added) and the target is chosen in order to have two failure regions, one dominating the other. The two-dimensional design space is given as $[1, 1]^2$. The performance function is defined as

$$f(u, v) = \left(4 - 2.1\bar{u}^2 + \frac{1}{3}\bar{u}^4\right)\bar{u}^2 + \frac{2}{3}\bar{u}\bar{v} + \frac{16}{9}\left(-4 + \frac{16}{9}\bar{v}^2\right)\bar{v}^2 - 0.7 \tag{5–27}$$

where $\bar{u} = 1.2u - 0.1$ and $\bar{v} = 0.9v$.

For both numerical integration and optimization, the design space is divided by a 32×32 grid. We present the results for the following configuration:

- Target value T is chosen as 1.3,
- Gaussian-based weight function is used, with parameter $\sigma_\varepsilon = 0.2$,
- Initial DoE consists of the four corners and the center of the domain,
- 11 points are added iteratively to the DoE as described in the previous section.

An isotropic Gaussian covariance function is chosen for the Kriging model. The covariance parameters (process variance σ^2 and range θ) are estimated from the initial 5-point DoE, and re-estimated after each new observation, using the MatLab toolbox GPML [Rasmussen & Williams (2006)]. The final results are presented in Figure 5-3.

Figure 5-3 A) is the plot of the true function, and Figure 5-3 B) is that of the Kriging mean. In the contour plot in Figure 5-3 C), it is shown that there are two critical regions.

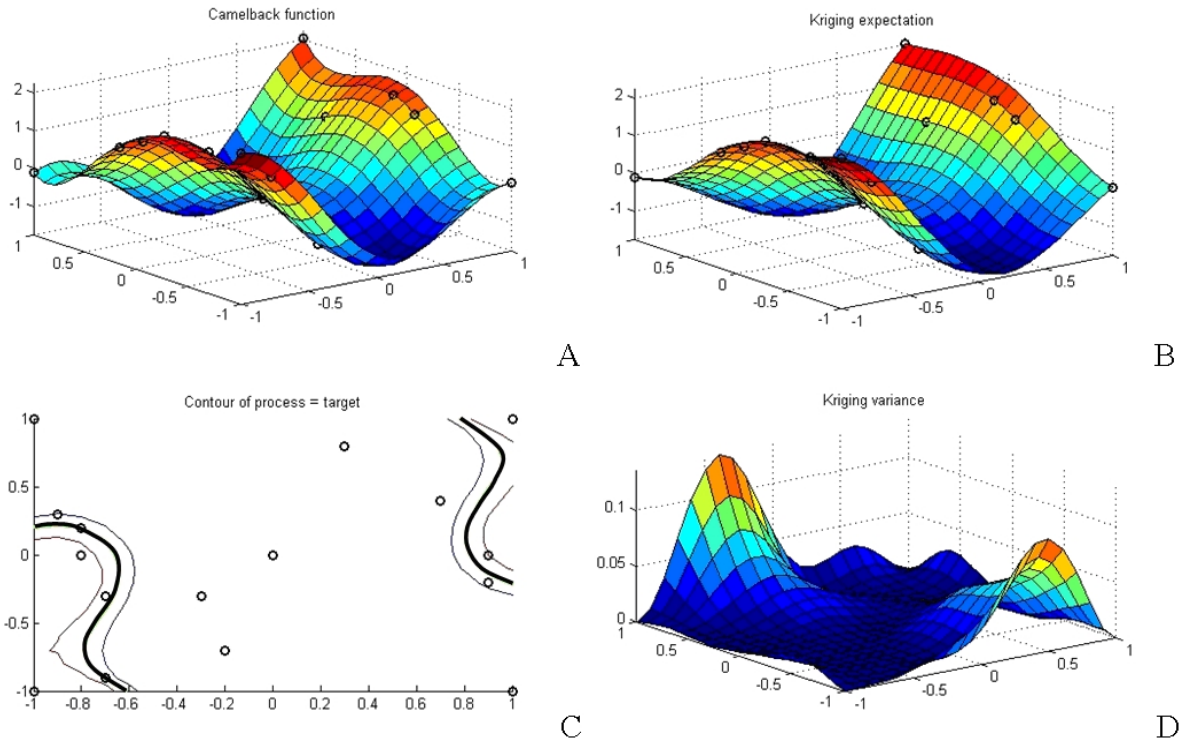

Figure 5-3. Optimal design after 11 iterations. A) True function. B) Kriging expectation. D) Kriging variance. C) Contour lines of the true function at levels $[T - \sigma_\varepsilon, T + \sigma_\varepsilon]$, which delimit the target regions; the bold line corresponds to the target contour. Most of the training points are chosen close to the target region. The Kriging variance is very small in these regions and large in non-critical regions.

After 11 iterations, the sequential strategy used four points to explore the first critical region, three points to explore the second region, and four points for space-filling. As shown in Figure 5-3 D), the Kriging variance becomes small near the critical regions, while it is relatively large in the non-critical region.

Figure 5-4 shows the evolution of the target contour line for the kriging expectation, which is a good indicator of the quality of the surrogate. We see that because the first four iterations (Figure 5-4 B)) are used for space-filling, the Kriging contour line is very different from the actual one. After eight iterations (Figure 5-4 C)), the two target regions are found and additional sampling points are chosen close to the actual contour line. Final state (Figure 5-4 D)) shows that the kriging contour line is close to the actual one.

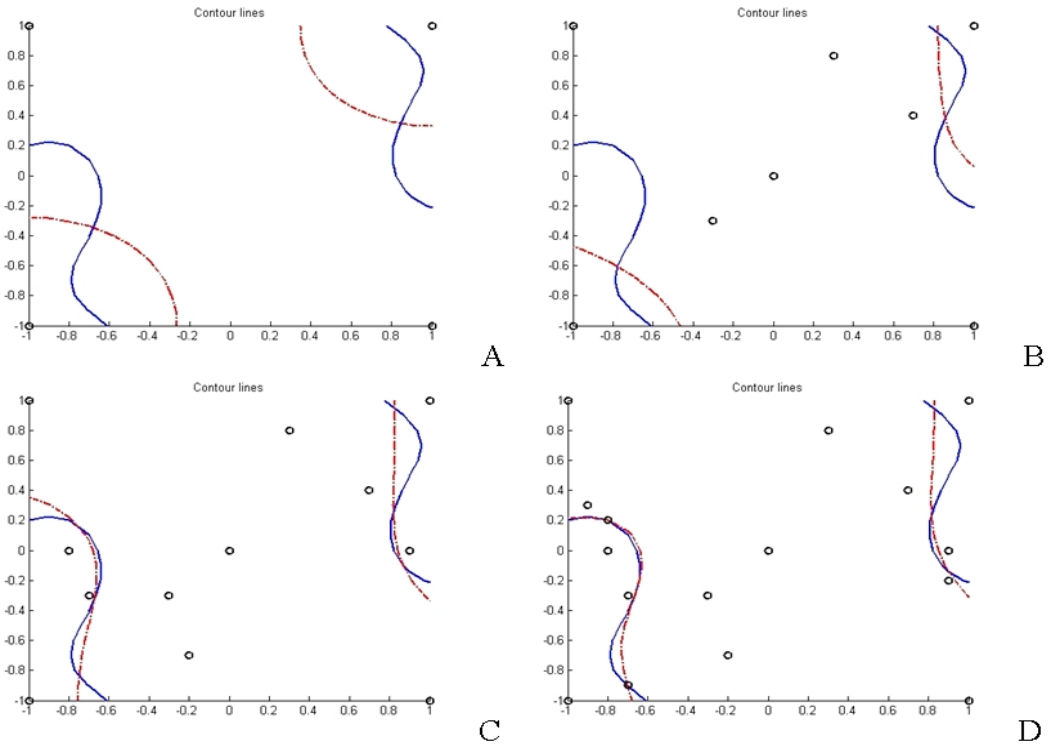

Figure 5-4. Evolution of Kriging target contour line (mixed line) compared to actual (plain line) during the sequential process: A) Initial, B) after four iterations, C) after eight iterations, D) final.

5.6.2 Six-Dimensional Example

In the second example, we consider a realization of a six-dimensional isotropic Gaussian process with Gaussian covariance function. Here, the error in the Kriging model is only due to the lack of data: there is no error in estimating the covariance parameters, and asymptotically (with very large number of observations) the Kriging fits exactly the realization of the Gaussian process. The design space is $[-1, 1]^6$. In order to limit the complexity (number of non-connected target regions) of the target region, we add a linear trend to the Gaussian process. We take $\sigma^2 = 1$, $\theta = 0.1$ and $\beta = [1 \dots 1]$.

The weighted IMSE criterion is computed by Quasi Monte-Carlo integration. The integration points are chosen from a Sobol sequence [Sobol (1976)] to ensure a good space filling property. At each step, the optimization is performed using the population-based optimizer CMA-ES [Hansen & Kern (2004)].

We present the results for the following configurations:

- Target value is chosen as 2
- Gaussian-based weight function is used, with $\sigma_\varepsilon = 0.05$.
- Initial DoE consists of 20 points chosen from Latin-hypercube sampling (LHS)
- 70 points are added iteratively to the DoE.

For comparison purpose, we generate a classical space-filling DoE that consists of 90 LHS points with maximum minimum distance criterion.

First, we represent the error at 10,000 (uniformly distributed) data points (Figure 5-5). The classical space-filling DoE leads to a uniform error behavior, while the optimal DoE lead to large errors when the response is far from the target value, while small errors when it is close to the target.

In order to analyze the error in the target region, we draw the boxplots of the errors for the test points where responses are inside the domains $[-\sigma_\varepsilon, +\sigma_\varepsilon]$ (Figure 5-6 A)) and $[-2\sigma_\varepsilon, +2\sigma_\varepsilon]$ (Figure 5-6 B)). Compared to the space-filling strategy, the optimal design reduces significantly the error. In particular, on both graphs the lower-upper quartiles interval is 2.5 times smaller for the optimal DoE.

5.6.3 Reliability Example

The limit state function is taken as the Camelback function used in the previous section. Let U and V be independent Gaussian variables with zero mean and standard deviation taken at 0.28; i.e., $U, V \sim N\left(0, 0.28^2\right)$. Then, the failure is defined when f becomes greater than 1.3. Thus, the limit state is defined as

$$G = f\left(U, V\right) - 1.3 \tag{5–28}$$

For this example, we generate two adaptive designs: the first is generated sequentially as described previously, with uniform integration measure (Eq. 5–7); the second is generated using the input distribution as integration measure (Eq. 5–26). Both use the four corners and the center of the domain as starting DoE and 11 iterations are performed. For

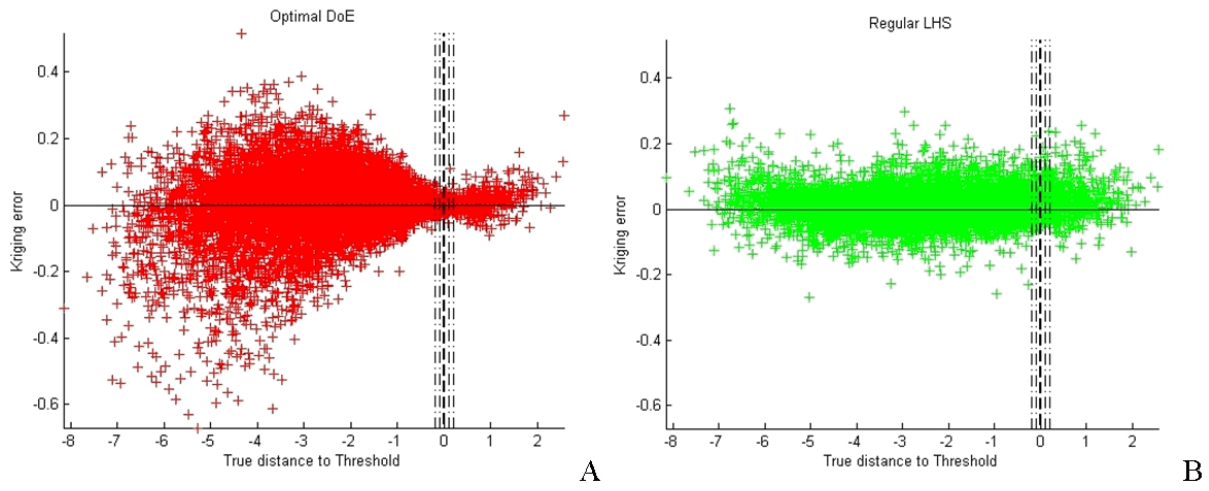

Figure 5-5. Comparison of error distribution for two DoEs: A) optimal DoE and B) classical LHS. The x-axis is the difference between the true function and the threshold, the y-axis is the error. Five vertical bars are drawn at $-2\sigma_\varepsilon$, $-\sigma_\varepsilon$, 0, $+\sigma_\varepsilon$ and $+2\sigma_\varepsilon$ for the target region. The error is on average smaller for the LHS design, but the optimal DoE reduces substantially the error in the target region.

comparison purpose, a 16-point full factorial design is also used. It is found that a Simple Kriging model (UK without linear trend) with isotropic Gaussian covariance function approximates well the function. The covariance parameters are computed using the toolbox GPML for all the DoEs.

Figure 5-7 draws the two optimal designs obtained and the full factorial designs. Both optimal designs concentrate the computational effort on the failure regions and the center of the domain. With uniform measure integration in Figure 5-7 A), the DoE is more space-filling than the one based on the distribution (shown in Figure 5-7 D)). By taking the input distribution into account in Figure 5-7 B), we see that all the observations are located relatively close to the center of the domain. Part of each target regions is not explored, since it is far from the center.

Finally, we perform 10^7 MCS on the three metamodels to compute the probability of failure estimates. 10^7 MCS are also performed directly on the test function to obtain the true probability of failure. Results are reported in Table 5-2. The full-factorial

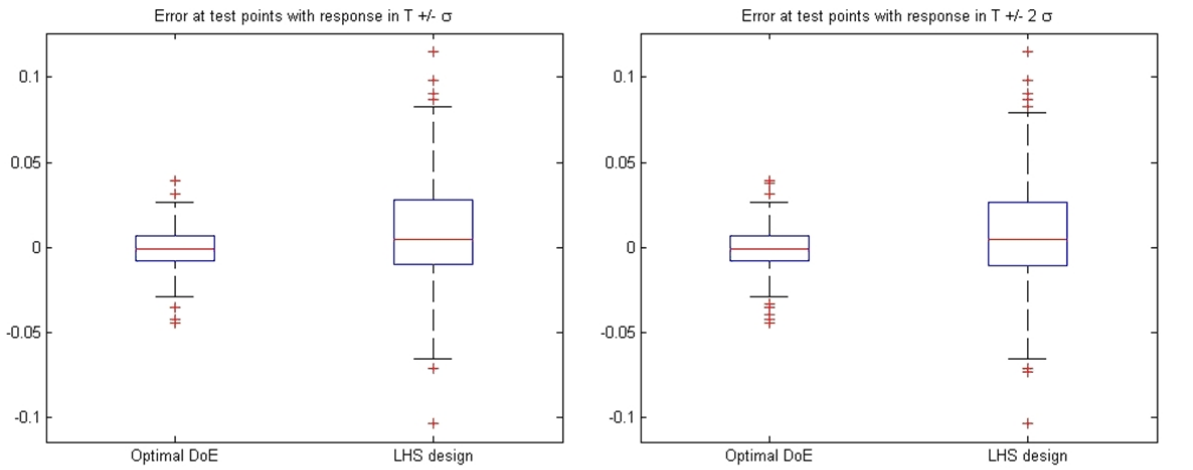

Figure 5-6.
and $[-2\sigma_\varepsilon, +2\sigma_\varepsilon]$.]Boxplots of errors for the LHS and optimal designs for the test points where responses are inside the domains A) $[-\sigma_\varepsilon, +\sigma_\varepsilon]$ and B) $[-2\sigma_\varepsilon, +2\sigma_\varepsilon]$. Error at these points is substantially smaller for the optimal designs for both intervals.

design leads to 77% error, while both optimal designs lead to a small error. Substantial improvement is obtained by taking the input distribution into account.

Table 5-2. Probability of failure estimates for the three DoEs and the actual function based on 10^7 MCS. The standard deviation of all estimates is of the order of 2×10^{-5}.

DoE	Full Factorial	Optimal without input distribution	Optimal with input distribution	Probability estimate based on 10^7 MCS
Probability of failure (%)	0.17	0.70	0.77	0.75
Relative error	77 %	7 %	3 %	

5.7 Concluding Remarks

In this chapter, we have proposed to improve the accuracy of surrogate models by generating designs of experiments adapted to the model application. In particular, we have addressed the issue of choosing a design of experiments when the Kriging metamodel was used to approximate a function accurately around a particular level-set, which occurs in constrained optimization and reliability analysis. We defined an original criterion, which is

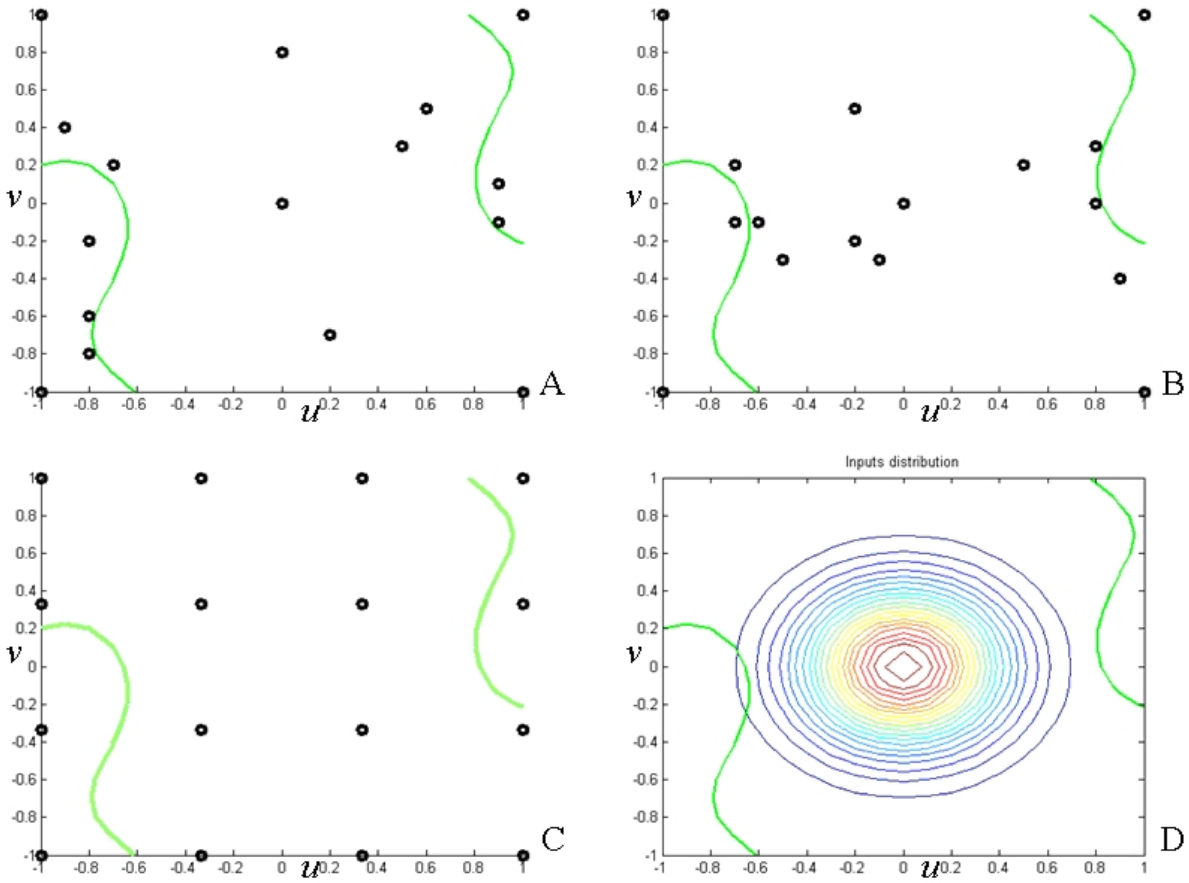

Figure 5-7. Optimal design with A) uniform integration measure, B) input distribution integration measure; C) Full factorial designs with 16 points; D) Input distribution.

based on an explicit trade-off between exploration of regions of interest and reduction of uncertainty of the model, and an sequential procedure to build the DoEs.

Through numerical examples, we showed first that the adaptive DoE was effective for detecting the target regions (where the response was close to the target level-set) and improve locally the accuracy of the surrogate model. Then, the method was applied to a reliability example, and it was found that improving locally the accuracy resulted in great improvement of the accuracy of the reliability estimation.

However, it has been found some limitations to the method, which were not solved here and requires future work to apply the method to a wide range of problems:

- Since it relies on numerical integration, the method can become computationally expensive if a large number of integration points is needed to compute the criterion. We found that for dimensions higher than ten, the criterion minimization becomes critical without the use of complex and problem-dependent numerical procedures, such as dimension reduction or adapted numerical integration.

- Secondly, it is important to recall that it is a *model-believer* strategy, since the criterion is entirely based on the Kriging model. Although sequential strategies allow some correction of the model during the process (through re-estimation of the parameters for instance), the success of the method will strongly depend on the capability of the Kriging model to fit the actual response.

Finally, it seems that the idea of weighted IMSE and sequential strategies to construct DoEs can be applied to many other purposes where there is a need for trade-off between exploration of regions of interest and reduction of the global uncertainty in the metamodel. Here, we defined a weight function to account for the proximity to some target value. Potential applications could be found in optimization, or detection of regions of high variations, etc., the difficulty being in an adapted definition of the weight function.

CHAPTER 6
OPTIMAL ALLOCATION OF RESOURCE FOR SURROGATE MODELING

6.1 Simulators With Tunable Fidelity

A numerical simulator is an approximation to a real phenomenon and is by definition a source of error. The way a simulator response follows the real function of interest is often called *fidelity*. Many engineering applications use two types of simulators, a *low-fidelity* model and a *high-fidelity* model. A typical low-fidelity model is based on great simplification of the system geometry and physics (for instance bars or beams modeling), and a high-fidelity model is typically a finite elements model. High-fidelity models provide an accurate approximation to the function of interest, but are computationally expensive, while low-fidelity models are easy to run but contain large error.

However, many numerical simulators can offer a large range of fidelities, by tuning factors that control the complexity of the model. For instance, the precision of the response of a finite element analysis (FEA) can be controlled by the meshing density or element order. Another example is when the response is obtained using Monte-Carlo methods: the accuracy (measured by the standard deviation or confidence intervals) is inversely proportional to the square root of the number of MC simulations. For both examples, the gain in fidelity is at a price of computational time. This topic has been addressed only recently in the computer experiment community and is usually found under the name of *stochastic simulators* [Kleijnen & van Beers (2005), Boukouvalas & Cornford (2009), Iooss et al. (2008), Ginsbourger (2009)].

When fitting a metamodel to such type of simulators, the sampling strategy may take into account the tunable fidelity. Indeed, when the computational resource is limited, one has to trade-off the fidelity and the number of simulations. Lower fidelity allows a better exploration of the design space, while higher fidelity provides more trust in the simulator responses. Besides, having tunable fidelity is to be considered as an additional degree of freedom: by allocating different computational time for each simulation, the quality of

the surrogate can be improved without additional cost compared to a uniform fidelity situation.

The optimal DoE formulation, as presented in Chapter 2, consists of selecting the points to maximize a criterion of quality for a metamodel construction. Here, we dispose of additional degrees of freedom, since we can choose the number of training point, and tune the model fidelity for each training point (under the constraint of a total computational budget). Elfving (1952) pioneered work in the area of optimal allocation. For a linear model he proposed to repeat experiments at some training points, and allocate a different number of repetitions to each point according to an optimality criterion. Kiefer (1961) generalized this idea of proportioning experiments in order to obtain the most accurate regression coefficients. Fedorov (1972) proposed a continuous version of the problem, and developed iterative strategies to find optimal designs.

This objective of this chapter is to provide efficient strategies for designing the experiments of simulators with tunable fidelity. First, we describe three examples of such type of simulators that model engineering systems. After formalizing the problem of optimal allocation of resource, we review some of the important results of optimal designs for regression. Finally, we propose an original approach for optimal allocation when Kriging models are considered.

6.2 Examples Of Simulators With Tunable Fidelity

6.2.1 Monte-Carlo Based Simulators

We consider functions of the form $f(\mathbf{x}, \mu_{\mathbf{\Theta}})$, that depends on both deterministic variables $\mathbf{x}$ and the distribution $\mu_{\mathbf{\Theta}}$ of some random parameters $\mathbf{\Theta}$. The function $f(\mathbf{x}, \mu_{\mathbf{\Theta}})$ is deterministic, but it is, generally, not known analytically. Hence, we estimate it using Monte-Carlo simulations (MCS). For a given design $\mathbf{x}$, we write:

$$\hat{f}(\mathbf{x}, \theta_{i=1...k}) = \hat{f}\left(\mathbf{x}; \theta_1, \theta_2, ..., \theta_k\right) \tag{6–1}$$

where $\hat{f}$ is the estimator of f and $\theta_1, \theta_2, ..., \theta_k$ are realizations of $\mathbf{\Theta}$.

The estimation of the probability of failure of a system is a typical example of a Monte-Carlo simulator. The limit state $G(\mathbf{x}, \mathbf{\Theta})$ is computed for several realizations of $\mathbf{\Theta}$, and the probability of failure estimate $\hat{P}_f(\mathbf{x})$, which corresponds to $\hat{f}(\mathbf{x}, \theta_{i=1\ldots k})$ in Eq. 6–1 is given by:

$$\hat{P}_f(\mathbf{x}) = \frac{1}{k} \sum_{i=1}^{k} \mathrm{I}\left[G(\mathbf{x}, \theta_i) \geq 0\right] \tag{6–2}$$

where I is the indicator function.

Monte-Carlo methods converge with the square root of the sample size k. That is, when k is chosen sufficiently large, the estimator $\hat{f}$ is normally distributed and its variance is inversely proportional to k:

$$\mathrm{var}\left(\hat{f}(\mathbf{x})\right) = E\left[\hat{f}(\mathbf{x}) - f(\mathbf{x})\right] = \frac{cst}{k} \tag{6–3}$$

For the reliability example, $\hat{P}_f(\mathbf{x})$ follows a binomial law with parameter $p = P_f(\mathbf{x})$, hence its variance is given by:

$$\mathrm{var}\left[\hat{P}_f(\mathbf{x})\right] = \frac{P_f(\mathbf{x})\left(1 - P_f(\mathbf{x})\right)}{k} \tag{6–4}$$

6.2.2 Repeatable Experiments

Repeatable experiments are not in themselves a numerical simulator with tunable fidelity, but can be considered as a discrete version of the problem. Some numerical simulators, and most physical experiments, benefit from repetitions. This is not the case of a finite element analysis for instance: repeating two times the same simulation will give the exact same answer and will not provide any additional information. A numerical simulator that benefits from repetition has typically a response of the form:

$$y_{obs}(\mathbf{x}) = y(\mathbf{x}) + \varepsilon(\mathbf{x}) \tag{6–5}$$

where $y(\mathbf{x})$ is the actual response and the error term $\varepsilon(\mathbf{x})$ is a random variable. Hence:

$$\mathrm{var}\left[y_{obs}(\mathbf{x})\right] = \mathrm{var}\left[\varepsilon(\mathbf{x})\right] \tag{6–6}$$

Now, say the experiment is repeated k times. Assuming that the noise is independent from one observation to another, we define y_{eq} as the single observation equivalent to the k observations ${y_{obs}}^{(j)}(\mathbf{x})$, which is the mean of the k observations:

$$y_{eq}(\mathbf{x}) = \frac{1}{k}\sum_{j=1}^{k} {y_{obs}}^{(j)}(\mathbf{x}) \tag{6–7}$$

The variance of y_{eq} is inversely proportional to the number of repetitions:

$$\mathrm{var}\left[y_{eq}(\mathbf{x})\right] = \frac{\mathrm{var}\left[\varepsilon(\mathbf{x})\right]}{k} \tag{6–8}$$

6.2.3 Finite Element Analysis

The quality of a finite element analysis mostly depends on the meshing chosen to model the structure. The meshing complexity is defined by the element type and the element size, or meshing density. Increasing the element complexity or the density results in a gain in accuracy, but at a price of computational time.

Figure 6-1 shows an example of the evolution of a FEA response when the complexity of the model is tuned to different levels. The FEA used is the torque arm model presented in Chapter 3. The response considered is the maximum Von Mises stress on the structure. The mesh density is a tunable parameter that defines the complexity of the meshing. A density of one corresponds to a crude mesh, while a density of 25 corresponds to a very complex and expensive model. The response for density 25 can be considered as the actual value of the maximum stress.

The graph shows that the simulator error (to the 25-mesh-density reference) decreases with the model complexity. The lowest fidelity model has an error of 24%, while for densities greater than 15 the error is less than 5%. As well as for previous examples, it is possible to relate the error amplitude to the computational effort given for the simulation run and obtain an equation of the form:

$$\mathrm{var}\left[\varepsilon(\mathbf{x})\right] = f(\mathbf{x}, t) \tag{6–9}$$

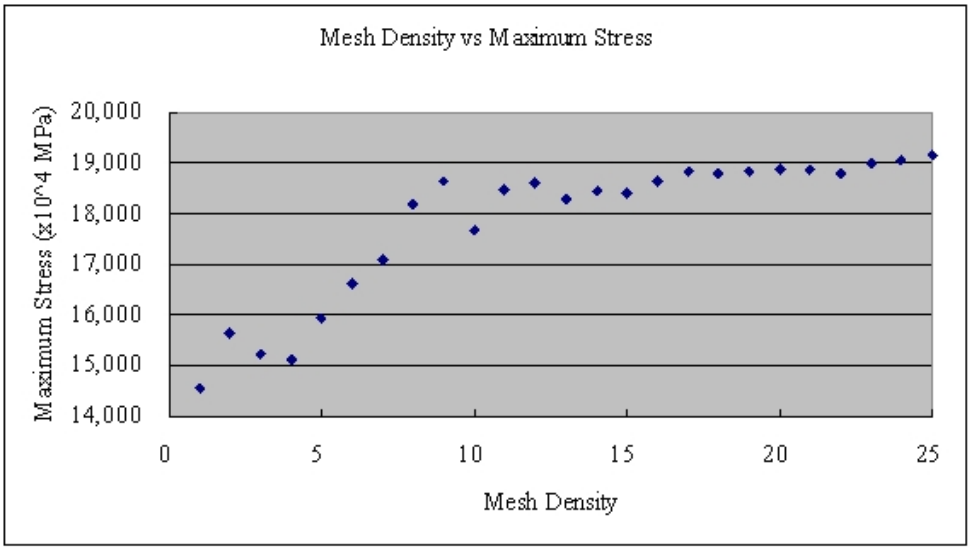

Figure 6-1. Evolution of the response of the FEA for the torque arm example, when the complexity of the model (mesh density) increases.

where f is a function to determine, $\mathbf{x}$ the design parameters and t the computational time.

However, the relations between mesh density, computational effort and error amplitude are complex and problem dependent. It depends on the choice of the elements, the meshing technique, the finite element software method of resolution of the system, etc. Hence, it is impossible to provide a general simple relation between the response variance and the computational time in the general case, and this relation has to be found for a given problem.

6.3 Optimal Allocation Of Resource

A classical design of experiments formulation consists of finding a sampling strategy that maximizes a criterion of interest. The design of experiments is then defined by the sampling point locations. In our framework, the design of experiment must be defined as the combination of training points and computational resource allocated to that point. Then, a design ξ with n points is defined as:

$$\xi = \left\{ \begin{array}{cccc} \mathbf{x}_1, & \dots & , \mathbf{x}_n \\ t_1, & \dots & , t_n \end{array} \right\} \tag{6–10}$$

The $\mathbf{x}_i$'s are training point locations, and the t_i's are real positive numbers that represent the computational time allocated for each training point. The sum of the t_i's is bounded by a constant:

$$0 \leq t_i, \qquad \sum_{i=1}^{n} t_i \leq T_{total} \tag{6–11}$$

T_{total} represents the total computational time available for the design of experiments. Let Φ be a functional of interest to minimize that depends on both training points and computational time. A design ξ^* is called optimal if it achieves:

$$\xi^* = \arg\min \left[\Phi\left(\xi\right)\right] \tag{6–12}$$

Such that:

$$\sum_{i=1}^{n} t_i \leq T_{total}$$

Finding an optimal design is a difficult and complex problem that has been widely addressed in the literature in the framework of regression with repeatable experiments. When the relation between the computational time t and the simulator response variance is unknown or complex, the optimization problem can become very challenging, and no general answer is provided in the literature. In the following, we focus on simulators for which the response variance is inversely proportional to the computational time. This is the case, as seen in Section 6.2.1, of reliability estimates.

In the two following sections, we consider the frameworks of regression and kriging. Results for regression are well-known and its section is mostly devoted to review and bibliography. On the contrary, very little is known for the kriging area, and the approaches we propose are original.

6.4 Application To Regression

6.4.1 Continuous Normalized Designs

In this section, the observations are assumed to be repeatable, and that noise in all observations has the same variance (homoscedastic case). We call n the number of training points and N the number of experiments (counting repetitions), $N \geq n$.

Let r_i be the number of observations at $\mathbf{x}_i$, all observations are denoted y_{ij} ($i = 1, 2, ..., n$; $j = 1, 2, ..., r_i$). The design ξ_N consists of the collection of training points $\mathbf{x}_i$ and numbers of repetitions r_i:

$$\xi_N = \left\{ \begin{array}{cccc} \mathbf{x}_1, & \dots & , \mathbf{x}_n \\ r_1, & \dots & , r_n \end{array} \right\}, \qquad 0 \leq r_i, \qquad \sum_{i=1}^{n} r_i = N \tag{6–13}$$

For a given training point $\mathbf{x}_i$, the equivalent observation (see Section 6.2.2) is denoted by $\bar{y}_i$:

$$\bar{y}_i = r_i^{-1} \sum_{j=1}^{r_i} y_{ij} \tag{6–14}$$

Let σ^2 be the variance of a single observation; assuming independance of the observations, the variance of $\bar{y}_i$ is:

$$\text{var}\left(\bar{y}_i\right) = r_i^{-1}\sigma^2 \tag{6–15}$$

Then, the Fisher's information matrix becomes:

$$\begin{aligned} \mathbf{M}\left(\xi_N\right) &= \mathbf{f}\left(\mathbf{X}\right)^T \mathbf{\Delta}^{-1} \mathbf{f}\left(\mathbf{X}\right) \\ &= \mathbf{f}\left(\mathbf{X}\right)^T \left[\text{diag}\left(\sigma^2 r_1^{-1}, \sigma^2 r_2^{-1}, ..., \sigma^2 r_n^{-1}\right)\right]^{-1} \mathbf{f}\left(\mathbf{X}\right) \\ &= \sigma^{-2} \mathbf{f}\left(\mathbf{X}\right)^T \left[\text{diag}\left(r_1, r_2, ..., r_n\right)\right] \mathbf{f}\left(\mathbf{X}\right) \end{aligned} \tag{6–16}$$

Normalizing by N,

$$\mathbf{M}\left(\xi_N\right) = N\sigma^{-2} \mathbf{f}\left(\mathbf{X}\right)^T \left[\text{diag}\left(r_1/N, r_2/N, ..., r_n/N\right)\right] \mathbf{f}\left(\mathbf{X}\right) \tag{6–17}$$

The Fisher information matrix is proportional to N, and following Fedorov (1972), it is possible to define, without any loss of generality, a *normalized design* ξ as a collection of support points $\mathbf{x}_i$ and their corresponding proportions of experiments p_i (with $p_i = r_i/N$):

$$\xi = \left\{ \begin{array}{cccc} \mathbf{x}_1, & \dots & , \mathbf{x}_n \\ p_1, & \dots & , p_n \end{array} \right\}, \qquad 0 \leq p_i, \qquad \sum_{i=1}^{m} p_i = 1 \tag{6–18}$$

Furthermore, a *continuous normalized design* is defined when p_i can take any real value between 0 and 1. Continuous designs are good approximations of reality for large N. The corresponding Fisher's information matrix is:

$$\mathbf{M}(\xi) = \mathbf{f}(\mathbf{X})^T \left[\text{diag}(p_1, p_2, ..., p_n)\right] \mathbf{f}(\mathbf{X}) = \sum_{i=1}^{n} p_i \mathbf{f}(\mathbf{x}_i)^T \mathbf{f}(\mathbf{x}_i) \tag{6–19}$$

It is important to notice here that such normalization is possible only when the observation noise variance is inversely proportional to computational time. The results described in the following sections only stand when this relation is true.

6.4.2 Some Important Results Of Optimal Designs

At this point, we introduce the dispersion function for linear regression for a prediction point $\mathbf{x}$:

$$d(\mathbf{x}, \xi) = \mathbf{f}(\mathbf{x})^T \mathbf{M}(\xi)^{-1} \mathbf{f}(\mathbf{x}) \tag{6–20}$$

The dispersion function directly relates to the prediction variance by:

$$\text{var}(\hat{y}) = \sigma^2 N^{-1} d(\mathbf{x}, \xi) \tag{6–21}$$

An important result in design optimality is the famous equivalence theorem demonstrated by Kiefer & Wolfowitz (1960). It states that the three following problems are equivalent:

$$\min_{\xi} \quad \det(\mathbf{M}(\xi)) \tag{6–22}$$

$$\min_{\xi} \quad \max_{\mathbf{x}} \quad d(\mathbf{x}, \xi) \tag{6–23}$$

$$\text{find } \xi \text{ such that:} \quad \max_{\mathbf{x}} \quad d(\mathbf{x}, \xi) = p \tag{6–24}$$

p being the number of regression coefficients to estimate.

In practice, it means that D-optimal designs are also G-optimal (and vice-versa), that is designs that minimize the uncertainty on the regression coefficients also minimize the maximum prediction variance, and for normalized optimal designs the value of the maximum prediction variance value is equal to p. However, these results are restricted to

continuous designs; when the total number of observations N is not a lot larger than the number of training points n, the p_i take discrete values and the above theorem does not hold in general.

Another result of great practical relevance is that there exists an optimal design ξ^* that contains no more than n_0 points [see Fedorov (1972)]:

$$n_0 = \frac{p\,(p+1)}{2} + 1 \tag{6–25}$$

Such results are very useful in practice, when algorithms are used to construct optimal designs. With the D-G equivalence, we get the intuition that support points may be taken where the prediction variance is maximal. The latter theorem states that, for linear regression, optimal sampling strategies consist of concentrating the computational resource on a limited number of (well-chosen) training points, rather than using a large number of points.

6.4.3 An Illustration Of A D-Optimal Design

Now, we illustrate D-optimal designs when the response is a second order polynomial with interactions in two dimensions:

$$y = \beta_0 + \beta_1 x_1 + \beta_2 x_2 + \beta_3 x_1^2 + \beta_4 x_2^2 + \beta_5 x_1 x_2 \tag{6–26}$$

The optimal design consists of the full-factorial design with nine points, with the following weights (Fedorov, 1972):

- 14.6 % at the corners
- 8.0 % at the middles of the edges
- 9.6 % at the center

Figure 6-2 represents the optimal design and corresponding prediction variance profile. It can be seen that G-optimality is achieved, since the prediction variance attains its maximum $p = 6$ (see Eq. 6–24) on several locations (center, corners, and middles of the edges). For this model, optimality is achieved by allocating approximately two times more

computational resources to the training points on the corners than to the other training points. Indeed, the corners of the domain are the regions where the uncertainty is likely to be maximal, so it seems logical to compensate for this uncertainty by allocating more resources there.

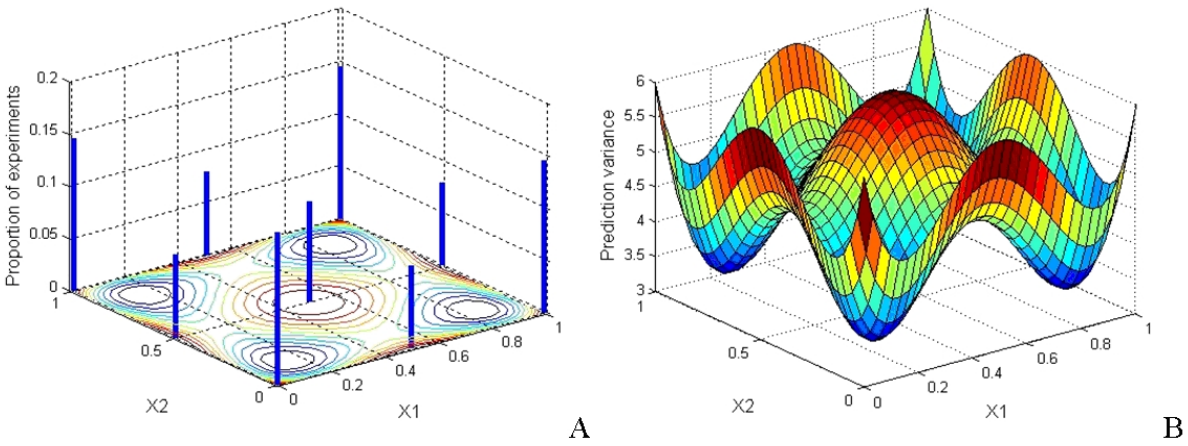

Figure 6-2. A) D-optimal design for a second-order polynomial regression and B) corresponding prediction variance. The vertical bars represent the proportion of computational effort given to each training point.

Figure 6-3 represents the full-factorial design but with homogeneous resource allocation and the corresponding prediction variance. The prediction variance profile shows that such design is not optimal, since the variance is much higher on the corners than on the center of the domain. The maximum prediction variance is 7.25, while it is equal to $p = 6$ for the optimal design.

Finally, Figure 6-4 represents a design with a large number of points uniformly spread on the design region, which is a natural alternative to small designs. Here, we chose a 36-point FF design; the observation noise is very high since only 1/36 of computational time is allocated to each training point. Such design does not appear to be a good solution, since the prediction variance has very high values on the edges of the domain. The maximum prediction variance is 13.45.

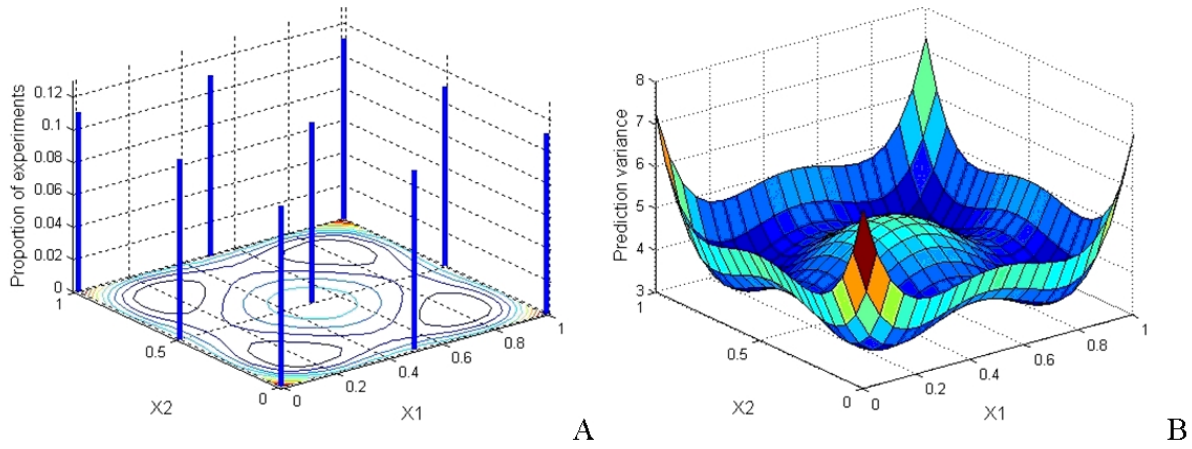

Figure 6-3. A) Full-factorial design with homogeneous allocation of computational effort and B) corresponding prediction variance.

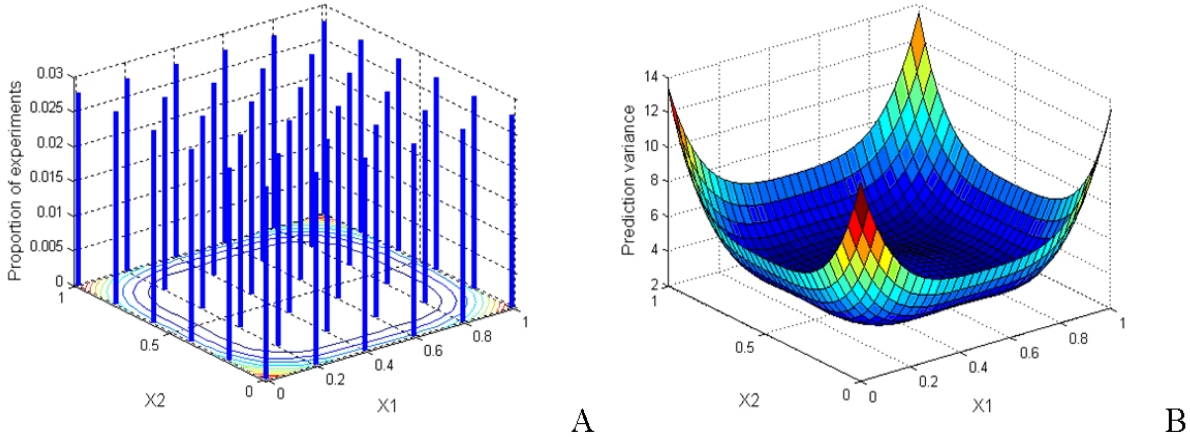

Figure 6-4. A) 36-point Full-factorial design with homogeneous allocation of computational effort and B) corresponding prediction variance.

6.4.4 An Iterative Procedure For Constructing D-Optimal Designs

Many algorithmic procedures have been proposed in the past to generate optimal designs. Here, we detail the first-order algorithm presented by Fedorov in his 1972 book. More refined techniques can be found in Cook & Nachtsheim (1980) Fedorov & Hackl (1997), Wu (1978), Molchanov & Zuyev (2002).

The principle of Fedorov algorithm is to add points sequentially to the design, and to transfer a proportion α of experiments from the existing points to the new one. The procedure is as follows:

Starting from a current design ξ_s obtained after s iterations, the first step is to find one point where the prediction variance is maximal, that is:

$$\mathbf{x}_{new} = \arg\max \left[d\left(\mathbf{x}, \xi\right) \right] \tag{6–27}$$

Then, the new design ξ_{s+1} is:

$$\xi_{s+1} = \left(1 - \alpha\right) \xi_{s+1} + \alpha \xi\left(\mathbf{x}_{new}\right) \tag{6–28}$$

The proportion of experiments for the new point (α) is chosen such that $\det\left[\mathbf{M}\left(\xi_{s+1}\right)\right]$ is maximal, showing the formula [Fedorov & Hackl (1997), p.47]:

$$\alpha_{opt} = \frac{d\left(\mathbf{x}, \xi_S\right) - p}{\left(d\left(\mathbf{x}, \xi_S\right) - 1\right) p} \tag{6–29}$$

The sequence $\{\xi_s\}$ is called optimal in the sense that its criterion value converges to the optimum value:

$$\lim_{s \to \infty} \Phi\left(\xi_s\right) = \Phi\left(\xi^*\right) \tag{6–30}$$

When a very large number of iterations is performed, the resulting design can contain a lot of points. Then, we can reduce the number of points by:

- discarding points with small weights not close to any group of points with high weights
- agglomerating points close to each other (the new point is the barycenter of the points, the weight is the sum of the weights)

6.4.5 Concluding Remarks

The problem of optimal allocation of resource has been widely studied in the regression framework. The remarkable properties of optimal designs allow proposing efficient algorithms to generate such designs. The results are developed for repeatable experiments, but fully apply to any simulator with tunable fidelity that has a response variance error inversely proportional to computational time. When D- or G-optimality are considered, optimal sampling strategies consist of concentrating the computational

resource on a limited number of training points, with non-uniform allocation of resources between points.

6.5 Application To Kriging

6.5.1 Context And Notations

In this section, we consider continuous designs, but with weights p_i's bounded by a constant not equal to one:

$$0 \leq p_i, \qquad \sum_{i=1}^{n} p_i = \frac{1}{\tau^2} \tag{6–31}$$

We will see later that in contrast to the regression case, the quantity $\frac{1}{\tau^2}$ cannot be normalized since it has an non-linear impact on the results. It represents the computational resource available for the design ξ. Here, the weights are the inverse of the variances of the measurement error at $\mathbf{x}_i$:

$$p_i = \frac{1}{\text{var}\left[\varepsilon\left(\mathbf{x}_i\right)\right]} \tag{6–32}$$

Assuming that the error variance is proportional to computational time, Eqs. 6–31 and 6–32 reflects the fact that computational resources remain constant for all ξ. If the design consists of a single support point, the error variance is τ^2; if the design consists of n distinct points with uniform weights, the error variance is uniform, equal to:

$$\text{var}\left(\varepsilon_i\right) = n\tau^2 \tag{6–33}$$

In this section, we always consider that the variances are equal.

The kriging model studied is the simple kriging (SK), which trend consists of a known constant μ (see Section 2.1.3). Then, the SK best predictor is given by the equation:

$$m_K\left(\mathbf{x}\right) = \mu + \mathbf{k}(\mathbf{x})^T {\mathbf{K}_\Delta}^{-1}\left(\mathbf{Y} - \mu\mathbf{1}\right) \tag{6–34}$$

and the SK prediction variance is:

$${s_K}^2\left(\mathbf{x}\right) = \sigma^2 - \mathbf{k}^T\left(\mathbf{x}\right){\mathbf{K}_\Delta}^{-1}\mathbf{k}\left(\mathbf{x}\right) \tag{6–35}$$

Considering a computational budget $1/\tau^2$ and equal variances, the covariance matrix $\mathbf{K}_\Delta$ is given by:

$$\mathbf{K}_\Delta = \mathbf{K} + \mathbf{\Delta} = (k(\mathbf{x}_i, \mathbf{x}_j)) + \begin{pmatrix} n\tau^2 & & 0 \\ & \ddots & \\ 0 & & n\tau^2 \end{pmatrix} \tag{6–36}$$

To analyze the quality of a model fit, we consider the IMSE criterion:

$$IMSE = \int_D {s_K}^2(\mathbf{x})\, d\nu(\mathbf{x}) \tag{6–37}$$

ν being an integration measure, usually taken uniform.

6.5.2 An Exploratory Study Of The Asymptotic Problem

The objective of this study is to quantify the evolution of the quality of the SK model when the number of observations increases, while the computational resource remains the same. In other words, we want to see if it is better using a few accurate observations, or many inaccurate ones.

An exploratory study is performed first. We consider the fit of a two-dimensional stationary processes in $D = [0, 1]^2$. The first process has a Gaussian covariance function (smooth), the second has an exponential covariance function (irregular).

We choose $\sigma^2 = 1$ and $\tau^2 = 10^{-3}$ for both processes, a range of $\theta = 3.1$ for the gaussian covariance and $\theta = 2$ for the exponential. We consider several sample sizes n from 10 to 150. For each sample size, we generate 500 designs $\xi_n^{(p)}$, the $\mathbf{x}_i$ being uniformly taken in D, the p_i being equal to $n\tau^2$. Then, we compute the IMSE criterion for each $\xi_n^{(p)}$, using numerical integration on a 32×32 grid. Figure 6-5 shows the evolution of the mean, 90% confidence interval and minimum IMSE criterion (over the 500 designs) with respect to m, for both covariance functions. Note that the IMSE criterion is independent of the observations, so the results depend only on the covariance structure and parameters.

We see that the mean and minimum IMSE decrease when the number of observations increases. Both quantities seem to converge to a non-zero constant. The confidence

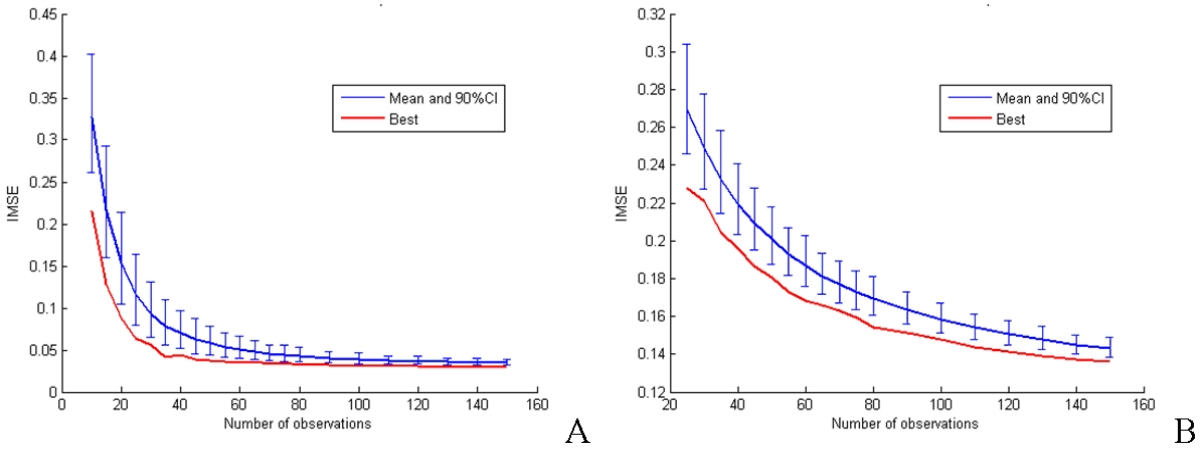

Figure 6-5. Evolution of the IMSE with respect to the number of observations for uniform random designs with A) Gaussian covariance, B) Exponential covariance.

interval width also decreases. Hence, we can conclude, for these two examples, that it is preferable for a constant computational budget to have a large number of points with large variances spread all over the design domain, rather than a few accurate ones.

Besides, the designs with large number of points are more robust, since the confidence interval decreases when the number of observations increases. This is logical since, with a small number of points, having an observation at a wrong location has a strong influence on the global accuracy of the model.

Thus, the goal is to study the behavior of $s_K^2(\mathbf{x})$ and the IMSE when n tends to infinity, the $\mathbf{x}_i$ being uniformly spread onto the design domain D. In particular, we aim at finding analytical expressions of both variance and IMSE, which can be used for comparison to designs with a finite number of support points.

6.5.3 Asymptotic Prediction Variance And IMSE

We assume that the observations are taken randomly according to the measure μ. μ can be either continuous on the design domain D, or discrete. Typically in the first case, μ is the uniform measure on D; then, each training point is taken randomly with uniform distribution on D (which is the case of the example of the previous section). Asymptotically, when the number of observations n tends to infinity, the training points

are taken everywhere on D. Inversely, a discrete measure μ is defined as the sum of Dirac functions, with positive weights such that their sum equals one:

$$\mu = p_1 \delta_{\mathbf{x}_1} + \ldots + p_k \delta_{\mathbf{x}_k} \tag{6–38}$$

With: $p_i \geq 0$, $1 \leq i \leq k$ and $\sum p_i = 1$.

Each observation is taken randomly on the set $\{\mathbf{x}_1, \ldots, \mathbf{x}_k\}$ with probability p_i. When n tends to infinity, the design of experiments is equivalent to a continuous normalized design with training points $\{\mathbf{x}_1, \ldots, \mathbf{x}_k\}$ and noise variances τ^2/p_i.

6.5.3.1 General result

Theorem. The observations are taken randomly according to the measure μ. When the number of observations m tends to infinity, the prediction variance and IMSE tend to:

$$s^2_{K\infty}(\mathbf{x}) = \sigma^2 - \sum_{p\geq 0}^{\infty} \frac{{\lambda_p}^2}{\tau^2 + \lambda_p} \left(\phi_p(\mathbf{x})\right)^2 \tag{6–39}$$

$$IMSE_\infty = \sigma^2 - \sum_{p\geq 0}^{\infty} \frac{{\lambda_p}^2}{\tau^2 + \lambda_p} \int_D \left(\phi_p(\mathbf{x})\right)^2 d\nu(\mathbf{x}) \tag{6–40}$$

where λ_p are the eigenvalues of the Hilbert-Schmidt integral operator associated with the covariance function $k(\mathbf{x}, \mathbf{y})$ (see appendix B), and ϕ_p are the natural representatives of the eigenfunctions $\tilde{\phi}_p$ of the operator, defined by:

$$\phi_p(\mathbf{x}) = \frac{1}{\lambda_p} \int_D k(\mathbf{x}, \mathbf{y}) \tilde{\phi}_p(\mathbf{y}) d\mu(\mathbf{y}), \qquad \mathbf{x} \in D$$

We recall that the spectral decomposition has the following properties:

- $k(\mathbf{x}, \mathbf{y}) = \sum_{p\geq 0} \lambda_p \tilde{\phi}_p(\mathbf{x}) \tilde{\phi}_p(\mathbf{y}), \qquad \mu \otimes \mu$ almost everywhere
- $\left(\tilde{\phi}_p\right)_p$ an orthonormal family:

$$\int_D \left(\tilde{\phi}_p(\mathbf{x})\right)^2 d\mu(\mathbf{x}) = 1, \qquad \int_D \tilde{\phi}_p(\mathbf{x}) \tilde{\phi}_q(\mathbf{x}) d\mu(\mathbf{x}) = 0 \qquad p \neq q$$

- $\lambda_p \tilde{\phi}_p(\mathbf{x}) = \int_D k(\mathbf{x}, \mathbf{y}) \tilde{\phi}_p(\mathbf{y}) d\mu(\mathbf{y}), \qquad \mathbf{x} \in supp(\mu)$

If μ and ν coincide:. The $IMSE_\infty$ expression reduces to:

$$IMSE_\infty = \sigma^2 - \sum_{p\geq 0}^{\infty} \frac{{\lambda_p}^2}{\tau^2 + \lambda_p} \tag{6–41}$$

Proof:. Two different proofs are proposed depending on the nature of the kernel. (1) If the kernel can be defined as a finite sum of basis functions and coefficients:

$$k(\mathbf{u}, \mathbf{v}) = \sigma_1^2 f_1(\mathbf{u}) f_1(\mathbf{v}) + \ldots + \sigma_l^2 f_l(\mathbf{u}) f_l(\mathbf{v})$$

Then, the number of non-null eigenvalues of the spectral decomposition is finite and the proof is algebraic.

(2) The general case, to which belong the usual Kriging kernels, requires a more complex proof. The proofs are given in Appendix B.1 and Appendix B.2, respectively.

Remarks:. Finding the spectral decomposition of the covariance function is a classical problem. Depending on the kernel considered, the decomposition can be well-known, easy to derive or inexistent (in particular, an analytical form of the decomposition of the Gaussian covariance function seems not to exist). In many case, the series $(\lambda_p)_p$ decrease rapidly, so the series for $s^2_{K\infty}$ and $IMSE_\infty$ are well approximated by its first q terms, typically: $10 \leq q \leq 100$.

6.5.3.2 A direct application: space-filling designs

We consider the case where the user wants to learn the function uniformly on D; the measure ν of integration for the IMSE is the uniform measure. Typically, space-filling designs are used for that purpose, so the measure μ of distribution of the observations is also the uniform measure on D. In that case, the asymptotic MSE and IMSE have simple form:

$$s^2_{K\infty}(\mathbf{x}) = \sum_{p\geq 0} \frac{\tau^2 \lambda_p}{\tau^2 + \lambda_p} (\phi_p(\mathbf{x}))^2 \tag{6–42}$$

$$IMSE_\infty = \sum_{p\geq 0}^{\infty} \frac{\tau^2 \lambda_p}{\tau^2 + \lambda_p} \tag{6–43}$$

In that case, they can be easily computed numerically. This value constitutes the limit of the IMSE of a space-filling DoE, when the number of observations tends to infinity, and can be used for a stopping criterion when building the design.

Let $(\mathbf{x}_n)_{n\in\mathbf{N}^*}$ be a space-filling series, for instance a Sobol or a Niederreiter sequence, k an initial number of points and α a positive number. Then, we can build a space-filling design by adding points of the series to the DoE until the corresponding IMSE is close enough to the asymptotic value, as we show in the following examples.

6.5.4 Examples

6.5.4.1 Brownian motion

We consider the fitting of a one-dimensional Brownian motion in the space . The covariance function associated with the Brownian motion is:

$$k\left(x,y\right)=\sigma^2\min(x,y) \tag{6–44}$$

Note that this covariance function is not stationary (since it depends on x and y and not only $|x-y|$). However the kriging model remains the same. The eigenvalues and eigenfunctions associated with the covariance are:

$$\lambda_p=\left(\frac{2\sigma}{\pi(2p+1)}\right)\qquad \phi_p(x)=\sqrt{2}\sin\frac{(2p+1)\pi x}{2} \tag{6–45}$$

Thus, the asymptotical prediction variance and IMSE are:

$$s^2_{K\infty}(\mathbf{x}) = \tau^2\sum_{p\geq 0}\frac{2}{1+\left(\frac{\tau}{\sigma}\right)^2\left[\frac{\pi(2p+1)}{2\sigma}\right]^2}\sin^2\left(\frac{(2\mathrm{p}+1)\,\pi x}{2}\right) \tag{6–46}$$

$$IMSE_\infty = \tau^2\sum_{p\geq 0}\frac{\sigma^2}{\sigma^2+\left[\frac{\pi\tau(2p+1)}{2\sigma}\right]^2} \tag{6–47}$$

We illustrate this result on a numerical example. We take $\mu=0$, $\sigma^2=1$ and $\tau^2=2\times10^{-3}$. Figure 6-6 shows one realization of a Brownian motion, two Kriging models based on four and 19 noisy data, respectively, and the prediction variance for the two models, and the analytical function (using the 50 first terms of the series) for an infinite

dataset. The variances of the observation noises are equal to $n\tau^2$, that is, 0.008 and 0.038, respectively.

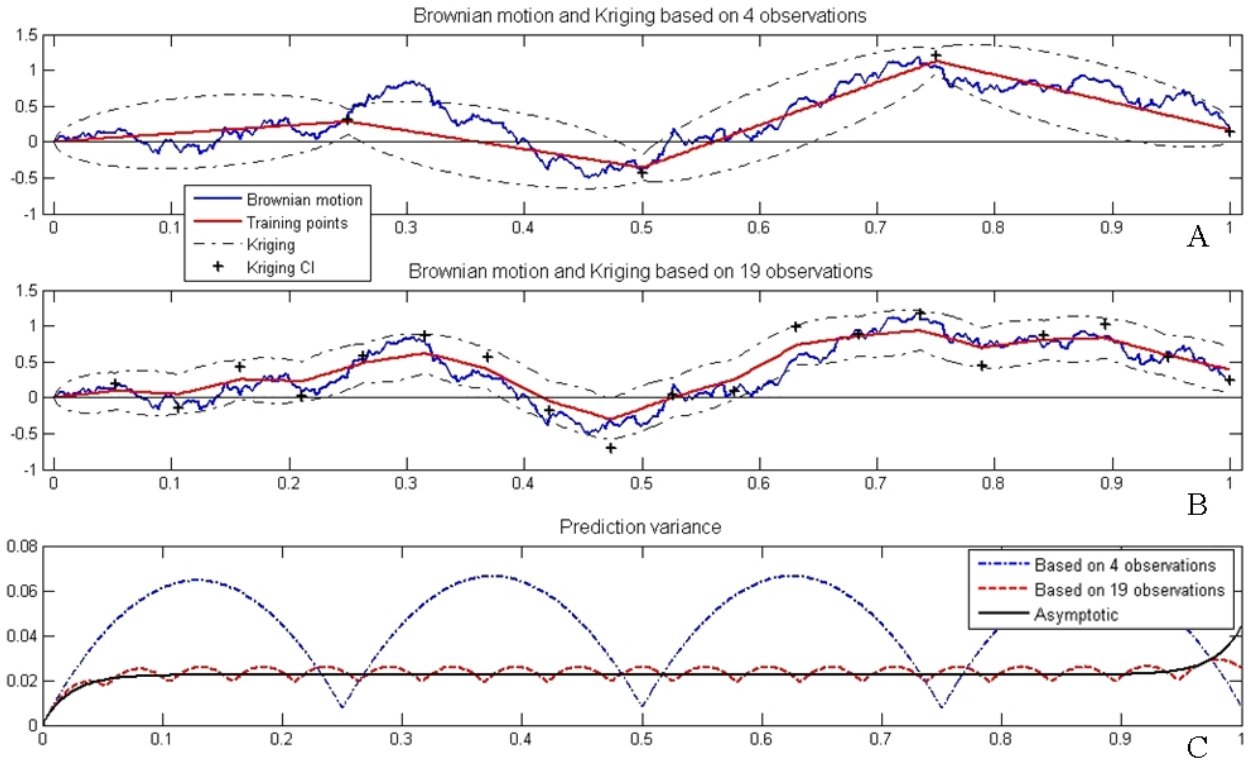

Figure 6-6. Illustration of the MSE function for a Brownian motion ($\sigma^2 = 1$, $\tau^2 = 0.002$). A) Realization of a Brownian motion and the Kriging model based on 4 noisy data; B) Kriging based on 19 noisy data; C) prediction variance function for the two models, and asymptotic value.

Since the noise variance is small, the 4-observation based Kriging (Figure 6-6 A)) almost interpolates the true function. However, the Kriging mean is very inaccurate when away from the observation. As a consequence, the prediction variance (Figure 6-6 C)) is close to zero at the observation points and is maximal at mid-distances between two observations. Since the response is known at $x = 0$ ($g(0) = 0$), the prediction variance is equal to zero.

The 19-observation based Kriging (Figure 6-6 B)) is a better approximation to the real function, even though the observation noise is much higher to satisfy the constraint of a constant computational budget (see Eq. 6–31)(indeed, some observation points [black

cross] are not close to the true function). When increasing the number of observations, the prediction variance tends to a constant (except on the boundaries), which is logical since the information is uniformly spread into the domain.

Table 6-1 shows the IMSE values for the three models. We can see that for a constant computational budget, the IMSE can be considerably reduced by spreading the information uniformly on the prediction domain. The IMSE for the 4-point model is two times larger than the asymptotic value. On the other hand, the difference between the 19-point model and the asymptotic value is only 4%. Since having more observations increases the computational burden, one can decide that a DoE with 19 observations is sufficient in terms of IMSE.

Table 6-1. IMSE values for the two Kriging models and the asymptotic model.

	Kriging based on 4 observations	Kriging based on 19 observations	Asymptotic
IMSE	0.0461	0.0233	0.0224

6.5.4.2 Orstein-Uhlenbeck process

Now, we consider the fitting of a one-dimensional Gaussian process in the space $D = [0, 1]$, with the following covariance function:

$$k(x, y) = \sigma^2 \exp\left(-\frac{1}{\theta}|x - y|\right) \tag{6–48}$$

The associated decomposition is (see appendix C for calculations):

$$\phi_p(x) = C_p\left(\theta\rho_p \cos(\rho_p x) + \sin(\rho_p x)\right) \tag{6–49}$$

With: $\rho_p = \sqrt{\frac{2\theta - \lambda_p}{\theta^2 \lambda_p}}$.

The ρ_p are the roots of the equation:

$$2u\theta \cos(u) + \left(1 - \theta^2 u^2\right) \sin(u) = 0 \tag{6–50}$$

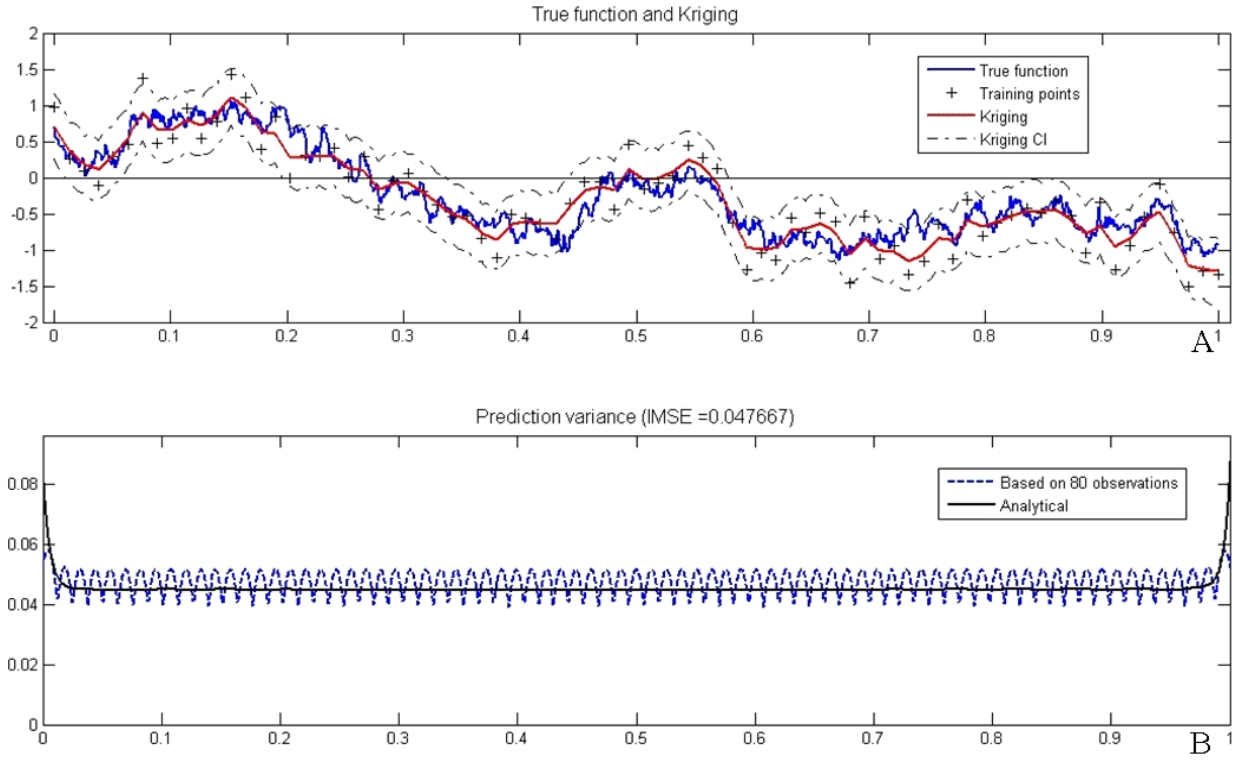

Figure 6-7. Illustration of the MSE function for a Gaussian process (GP) with exponential covariance function ($\sigma^2 = 1$, $\theta = 0.2$ and $\tau^2 = 0.002$). A) Realization of a GP and the Kriging model based on 80 noisy data; B) MSE function based on the 80 data, and asymptotic value.

Such equation does not have explicit analytical solutions and must be solved numerically. However, when p is large (> 10), the roots are well approximated by:

$$\rho_p = (p-1)\,\pi \tag{6–51}$$

The eigenvalues are obtained from the roots of the equation:

$$\lambda_p = \frac{2\theta}{1+\theta^2\rho_p^2} \tag{6–52}$$

The constant C_p is chosen so that ϕ_p is normalized:

$$C_p = \frac{2\rho_p}{\rho_p\left(1+\rho_p^2\theta^2\right) - \left(1+\rho_p^2\theta^2\right)\sin\left(\rho_p\right)\cos\left(\rho_p\right) + 2\rho_p\theta(\sin\left(\rho_p\right))^2} \tag{6–53}$$

Figure 6-7 illustrates this result for the parameter values $\sigma^2 = 1$, $\theta = 0.2$ and $\tau^2 = 0.002$. For comparison, a model based on 80 data is represented, which is found to be a good approximation to an infinite dataset.

6.5.5 Application To The Robust Design Of Gears With Shape Uncertainty

In this section, we apply the asymptotic results on Kriging to the optimization of gears under shape uncertainty. For the sake of equilibrium and homogeneity, the study is only briefly described here. All the details can be found in Appendix D.

Although gears have been designed for a long time, controlling gears performance under teeth shape uncertainties is a recent, difficult and important design objective: teeth shape variations result from manufacturing (e.g., heat treatment) and from wear and induce, in particular, noise. The objective of this study is to design gears so that the noise is minimum when there is shape uncertainty.

Gear design typically involves a large number of geometrical parameters (see Figure 6-8) and several performance measures. In this study, gear analysis is done with the help of the *Filengrene* software [Meyer (2008)], which provide many outputs as well as shape modification capabilities. Uncertainties can be taken into account by using classical Monte-Carlo techniques. Here, departures from the theoretical shape profile are defined with the use of Gaussian processes and given as inputs for the analysis. Multiple runs with different shape departures allow the propagation of uncertainty to the outputs.

Minimizing the noise when the shape is uncertain is computationally intensive: even though the computational time for a given profile is small (about 2 CPU seconds per gears analysis) it is not possible to directly include the Monte Carlo simulations inside an optimization loop because the computational costs are multiplied by each other: for 100 Monte Carlo simulations and 1,000 optimization steps, a single run would take 100*1,000 = 56 CPU hours. To alleviate the computational issue, we use a Kriging model to approximate the objective function. We take advantage of the asymptotic study by generating a design of experiment as large as possible.

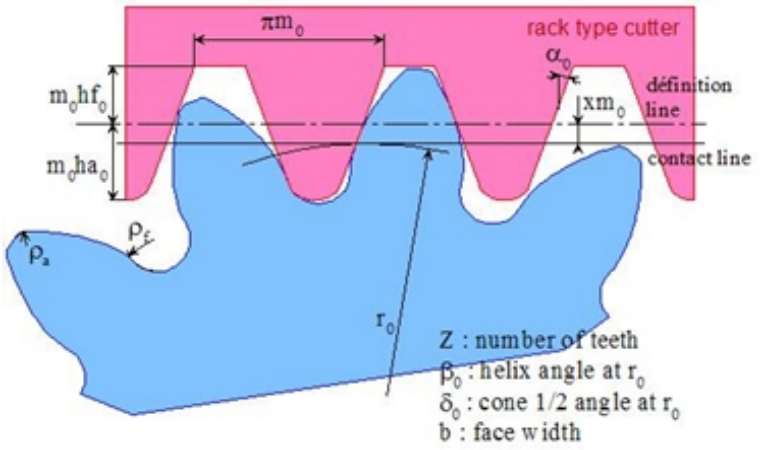

Figure 6-8. Gears parameters definitions.

The objective function is chosen as the 90^{th} percentile of the Static Transmission Error (STE, returned by *Filengrene*). To ensure good properties of the percentile estimate (in particular, normality), a minimum of 25 samples is needed. Due to computational limitations, the number of calls cannot exceed 90,000. So we choose to compute 3,000 responses based on 30 MCS each. However, the design space being of six dimensions, 3,000 observations is not enough to fill it densely, so this DoE is sub-optimal. This illustrates well the trade-off to be made between theoretical results and practice.

Results showed that the Kriging-based strategy allowed to find acceptable designs even if the observation noise was very high due to limited computational resources. The Kriging-based design is depicted in Figure 6-9. The chosen sampling strategy allowed to perform global optimization and detect the region of optimality, but failed to achieve fine convergence (which may require adaptive sampling).

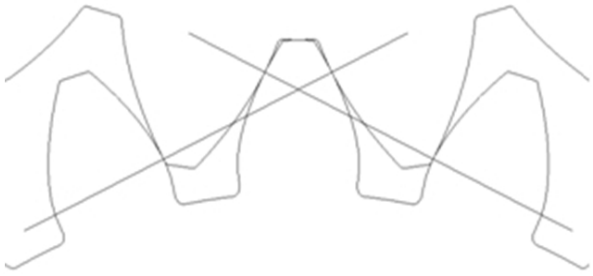

Figure 6-9. Optimum robust design found using the kriging metamodel.

6.5.6 Concluding Comments

In this section, we found empirically that using a very large number of observations with very low fidelity was an optimal solution to minimize the uncertainty in the simple kriging model, when space-filling designs are used. We found that this kind of designs asymptotically converge to a bound. However, it has to be kept in mind that this sampling strategy is not yet proven to be optimal. Anyway we can conclude that, contrarily to regression where optimal designs have a finite number of support points, it seems better to spread as much as possible the computational resource rather than concentrate it on a few training points.

CHAPTER 7
CONCLUSION

7.1 Summary And Learnings

The use of surrogate modeling as a helping tool for learning, prediction and design of engineering systems is an efficient and computationally attractive solution. However, dealing with the uncertainties associated with a surrogate model is a challenging but crucial issue to the success of the surrogate-based strategy.

The two primary objectives of this work were the following: (1) Propose and discuss alternatives to compensate for the error and uncertainty in surrogate models in order to provide safe estimates that limit the risk of weak design; (2) Explore the sampling strategies in order to minimize the uncertainty of surrogate models.

First, it was showed that uncertainty can be compensated by adding bias to the surrogate models in order to increase the chance that they are safe, using constant or pointwise margins, designed by taking advantage of error distribution measures given by the model, or by model-independent measures of accuracy of the model. Since the conservative predictions are biased, the problem can be considered as a multi-objective optimization, and results are presented in the form of Pareto fronts between accuracy and conservativeness. It was found that the efficiency of the different methods depend on the ability of the surrogate model to reflect the system response. When error measures given by the model are reasonably accurate, their use outperforms model-independent measures to reduce large unsafe errors. On the other hand, model-independent measures, in particular cross-validation, are found to be more robust and efficient when the number of observations is sufficiently large (regardless of sparsity).

Then, a simple methodology was proposed to estimate the uncertainty in a reliability measure based on Monte-Carlo simulations. Using the bootstrap method, we were able to quantify the level of bias needed to ensure a prescribed probability to be on the safe side for the analysis. The procedure was applied to the design of a laminate composite under

cryogenic and mechanical stress. It was found that fitting a surrogate based on datasets that were biased to compensate for their uncertainty allowed to obtain a satisfying design, even when the available information was very limited by computational resources. Compared to traditional methods of reliability estimates, equivalent levels of safety was obtained with a reduction of computational cost of several orders of magnitude.

The choice of the observations used to fit the model (design of experiment) was addressed by two different ways. In a first time, it was shown that substantial gain can be obtained by considering the surrogate model in an objective-based approach. In particular, a methodology was proposed to construct designs of experiments adapted to the frameworks of reliability assessment and constrained optimization, so that the model accurately approximates the vicinity of a boundary in design space defined by a target value of the function approximated by the surrogate. The method was applied to a reliability example, and it was found that improving locally the accuracy resulted in great improvement of the accuracy of the reliability estimation.

Finally, a global approach to uncertainty reduction in surrogate modeling was proposed to address the issue of surrogates based on simulators with tunable fidelity. This situation is, in particular, encountered in the framework of reliability-based design optimization. Solutions differ depending on the surrogate model considered. For regression models, classical results of design optimality show that substantial reduction of uncertainty can be achieved by allocating different computational resources - hence different uncertainty levels in the responses - to a few chosen simulations. For kriging models, it was found that the best way to reduce uncertainty in the model is to spread the information as much as possible, by using very large datasets with very large levels of uncertainty. This result was supported by theoretical asymptotic studies of the kriging model.

7.2 Perspectives

Ensuring high levels of conservativeness is, as we have seen, at a price of a substantial increase of error, which leads to overdesign. In an engineering context, such approach is recommended for preliminary analysis, which would be followed by more refined (and expensive) procedures. More generally, the efficiency of conservative strategies are very dependent on the sampling strategies used to generate the observations. Possible prolongation of this work might include a combined use of conservative predictions and sequential strategies in order to limit the risk of overdesign.

The adapted design strategy proposed in Chapter 5 was tested on academic problems of reasonable complexity. Its application on real-life problems might lead to additional problems and discussion, which were only mentioned here. In particular, one might think of measuring the influence of the quality of the metamodel on the efficiency of the method, the combined use of space-filling and adapted strategies for increased robustness, or numerical solutions to overcome computational issues. Secondly, it seems that the idea of weighted IMSE and sequential strategies to construct DoEs can be applied to many other purposes where there is a need for trade-off between exploration of regions of interest and reduction of the global uncertainty in the metamodel. Here, we defined a weight function to account for the proximity to some target value. Potential applications could be found in optimization, or detection of regions of high variations, etc., the challenge being in an adapted definition of the weight function.

We discussed in Chapter 6 optimal strategies of allocation of resource for simulators with tunable fidelity. We showed that, in particular, reliability analysis belongs to this framework. It is also potentially applicable to a wide range of problems, in particular Finite Element Analysis or Computational Fluid Dynamics codes. Future research may aim at relating this work to studies of convergence of numerical models (depending on meshing, complexity of elements, etc.), in order to estimate the relation between computational time and error and propose optimal strategies for these problems. In

addition, we proposed in this work some links to functional analysis and spectral theory when considering optimal allocation for the Kriging model. It seems that this way offers many potential prolongations for the theory of design of experiments, which might lead to exactly optimal strategies, or numerical methods to generate designs.

APPENDIX A
ALTERNATIVES FOR CONSERVATIVE PREDICTIONS

In this appendix, we detail two alternatives to produce conservative predictions using surrogate modeling.

A.1 Biased Fitting Estimators

A.1.1 Biased Fitting Models

We propose here to include bias during the fitting process in order to produce conservative predictions. To do so, we constrain the predicted response to be on one side of the DOE responses; that is, the errors between prediction and actual response are positive at DOE points. Such method do not apply to interpolation techniques since the error is by definition null at data points. For polynomial regression, the conservative coefficients $\hat{\beta}_{\text{cons}}$ are the solution of the following constrained optimization model:

$$\begin{aligned} \underset{\hat{\beta}_{\text{cons}}}{\text{Minimize}} \quad & \text{MSE} = \frac{1}{n}\sum_{i=1}^{n}\left[\hat{y}\left(\mathbf{x}_i\right) - y\left(\mathbf{x}_i\right)\right]^2 \\ \text{s.t.} \quad & \hat{y}\left(\mathbf{x}_i\right) - y\left(\mathbf{x}_i\right) \geqslant 0, \quad i = 1, ..., n \end{aligned} \tag{A–1}$$

Then, the biased fitting conservative estimate is given by:

$$\hat{y}_{\text{BF}}\left(\mathbf{x}\right) = \mathbf{f}^T\left(\mathbf{x}\right)\hat{\beta}_{\text{cons}} \tag{A–2}$$

In order to control the level of bias, we propose two alternatives. The first is constraint relaxation, that allows a given amount of constraint violation denoted as δ:

$$\begin{aligned} \underset{\hat{\beta}_{\text{cons}}}{\text{Minimize}} \quad & \text{MSE} \\ \text{s.t.} \quad & \hat{y}\left(\mathbf{x}_i\right) - y\left(\mathbf{x}_i\right) + \delta \geqslant 0, \quad i = 1, ..., n \end{aligned} \tag{A–3}$$

A positive δ will reduce the bias in the fitting. δ can also be chosen negative in order to be more conservative than with no constraint relaxation.

The second alternative is to reduce the number of constraints, that is, to constrain the errors to be positive only at a selected number of points (constraint selection). The

constraints selected are those *a priori* easier to be satisfied, that is, where the error from the unbiased fit is minimal.

The procedure to select these points is as follow:

- Compute the unbiased estimates using classical regression
- Compute the errors and sort them by ascending order
- Select the points corresponding to the k smallest errors
- Solve the following optimization problem:

$$\begin{aligned} &\underset{\hat{\beta}_{\text{cons}}}{\text{Minimize}} \quad \text{MSE} \\ &\text{s.t.} \quad \hat{y}\left(\mathbf{x}_i\right) - y\left(\mathbf{x}_i\right) + \delta \geqslant 0, \quad i = 1, ..., k \end{aligned} \tag{A–4}$$

where the $\mathbf{x}_i$ are sorted in ascending order according to errors and $1 \leq k \leq n$.

In the following, the two above-referenced biased-fitting alternatives are entitled *constraint relaxation* and *constraint selection*, respectively.

Remark. The biased fitting strategy requires the solving of a constrained optimization problem to obtain the coefficients $\hat{\boldsymbol{\beta}}$ instead of using an analytical function. However, this optimization problem is quite simple to solve, since the criterion is convex (least squares), and the constraints are linear.

A.1.2 Results And Comparison To Other Methods

Here, we compare the two biased fitting strategies to the constant safety margin (CSM) strategy on the Branin-Hoo function, in the experimental setup described in Section 3.3.2.2. First, we compare the two strategies for biased fitting estimates. The range of the constraint relaxation is chosen as [-3; 15]; the proportion of selected constraints is chosen between 0 and 1. The graphs of performance are shown in Figure A-1.

Both methods seem to provide similar results; the difference for high percentiles on the left figure is here due to numerical noise. Using constraint selection does not allow

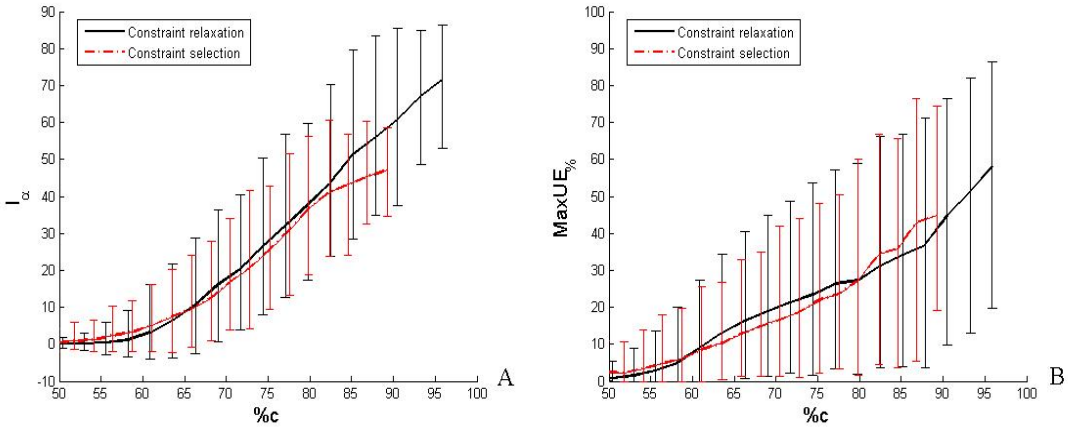

Figure A-1. Average results for Biased fitting with constraint relaxation (plain black) and constraint selection (mixed grey) on the Branin-Hoo function. A) $\%c$ vs. l_alpha; B) $\%c$ vs. $MaxUE_{\%}$.

obtaining very conservative estimates: indeed, using all the 17 constraints leads to a 85% conservativeness. On the other hand, with constraint relaxation, using a negative shift allows to be more conservative. On the right graph, we see that a high proportion of conservative estimates does not prevent for having large unconservative errors: for instance, for a 90% conservativeness, the maximum unconservative error is reduced by 40% only.

Now, we compare biased fitting and CSM strategies. Figure A-2 shows the graphs of performance for the CSM estimator and the biased fitting estimator with constraint relaxation.

The two estimators have similar trends, but biased fitting results with higher variability. Indeed, this method is a lot more sensitive to the DOE, since a single constraint can have a large influence on the shape of the response.

A.2 Indicator Kriging

A.2.1 Description Of The Model

Indicator Kriging (IK) is a surrogate-based alternative to provide conservative estimates. Instead of estimating the value of response, IK estimates the probability that the response exceeds a given value (cut-off). In other words, IK provides an estimate of

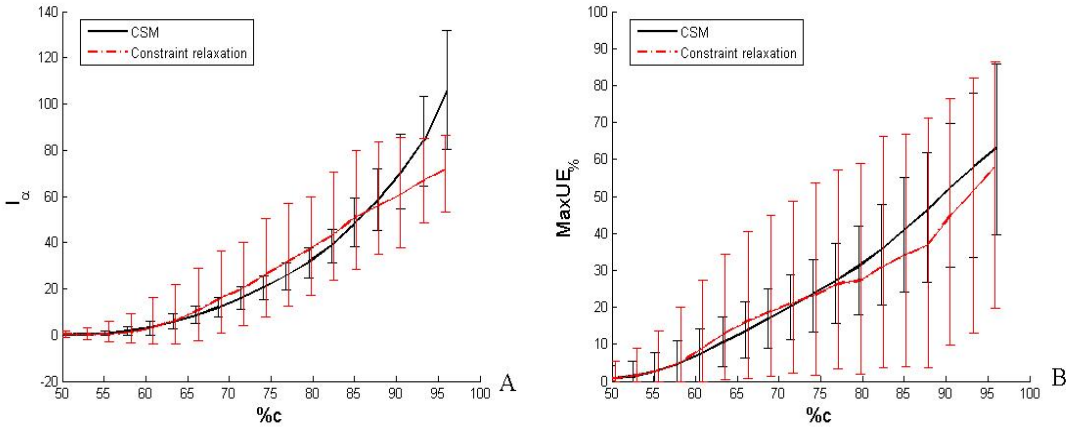

Figure A-2. Average results for CSM (plain black) and Biased fitting with constraint selection (mixed grey). A) $\%c$ vs. l_alpha; B) $\%c$ vs. $MaxUE_{\%}$.

the conditional cumulative distribution function (CCDF) at a particular cut-off c. The key idea of IK is to code the observed responses into probabilities of exceeding the cut-off. When the response is deterministic (without observation noise), the probability is either 0 or 1. The indicator coding at a sampled location $\mathbf{x}_i$ is written:

$$\begin{aligned} I_i = I\left(c; \mathbf{x}_i | \left\{y_1, y_2, ..., y_n\right\}\right) &= \mathrm{P}\left(y(\mathbf{x}_i) > c\right) \\ &= \begin{cases} 1 & if \quad y(\mathbf{x}_i) > c \\ 0 & otherwise \end{cases} \end{aligned} \tag{A–5}$$

At an unsampled location $\mathbf{x}$, the probability is estimated by the Kriging prediction based on the indicator data:

$$\hat{P}\left(y\left(\mathbf{x}\right) > c\right) = \hat{y}_{IK}\left(\mathbf{x}\right) \tag{A–6}$$

where $\hat{y}_{IK}$ is the Kriging estimate based on $\{I_1, I_2, ..., I_n\}$ instead of $\{y_1, y_2, ..., y_n\}$.

For a given set of cut-offs $\{c_1, c_2, ..., c_q\}$ and prediction location $\mathbf{x}$, we obtain a corresponding set of probabilities $\{P_1, P_2, ..., P_q\}$. We use these discrete probabilities to fit a continuous approximation of the CCDF of the response at and build confidence intervals. IK is often qualified as a 'non-parametric' approach since it does not rely on a pre-specified distribution model. Note that it is an expensive procedure compared to a classical kriging model since it may require a large number of kriging models.

Post-processing is necessary to transform the IK set of values into a usable discrete CDF. Indeed, there is no constraint during the procedure to have values only inside $[0, 1]$ or that CDF estimates vary monotonically with cut-offs. We use here one of the methods proposed in the GSLIB user's guide [Deutsch & Journel (1997)]. First, values out of the interval [0, 1] are replaced by 0 or 1. Then, the original IK-derived percentiles are perturbed by running an optimization that minimizes the perturbation while ensuring all order relations.

The $(1-\alpha)\%$ conservative estimator is the $(1-\alpha)^{th}$ percentile of this distribution, given by the inverse of the CDF. This percentile is interpolated from the set of probability (like for the bootstrap method). Here, we use linear interpolation.

A.2.2 Application To The Torque Arm Analysis

Since it requires a large number of points, IK is applied to the analysis of the torque arm only. A rational quadratic function is used for covariance; the parameters of the function are re-estimated for each cut-off using the toolbox GPML. A total of 100 cutoffs are used for the distribution estimation.

In this section, we compare IK to the regular Kriging with error distribution (ED). First, we compare the performances of the unbiased metamodels: without margin for Kriging and with a target of 50% conservativeness for IK. Table A-1 reports their e_{RMS}, $\%c$ and $MaxUE$ based on the 1,000 test points.

Table A-1. Statistics based on 1,000 test points for the unbiased surrogates.

Surrogate	e_{RMS}	$\%c$	$MaxUE$
IK	22.9	45.6%	228.9
Kriging	14.5	51.6%	60.7

For unbiased predictions, IK has an error a lot larger than Kriging. The e_{RMS} is two times larger and the $MaxUE$ almost three times. Here, it appears that the IK procedure, with conversion into boolean number, CDF normalization and interpolation, results in substantial loss in accuracy.

In order to have a fair comparison between IK and Kriging, we compare unscaled quantities, e_{RMS} and $MaxUE$, instead of l_α and $MaxUE_{\%}$. Figure A-3 shows the graphs of performance for the two conservative estimators.

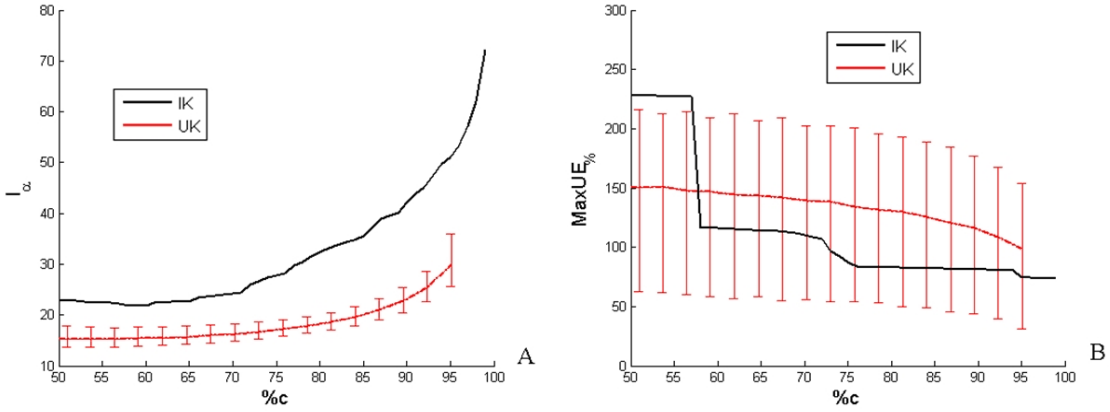

Figure A-3. Average results for Indicator Kriging (IK, plain black) and ED with Kriging (UK, mixed grey). A) $\%c$ vs. l_α; B) $\%c$ vs. $MaxUE_{\%}$.

On the left graph (Figure A-3 A)), we see that the rate of increase of e_{RMS} of the IK is very small up to $\%c = 70\%$. However, it is not enough to compensate for the initial value of e_{RMS} and be competitive with the UK estimator. Figure A-4 shows the fidelity to target conservativeness for both estimators. Despite very large errors compared to classical Kriging, Indicator Kriging is found to be very accurate regarding fidelity.

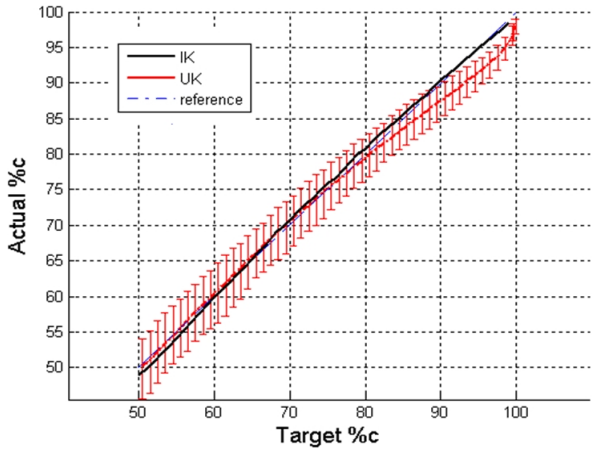

Figure A-4. Target vs. actual $\%c$ for IK (plain black) and Kriging with ED (mixed gray).

APPENDIX B
DERIVATION OF THE ASYMPTOTIC KRIGING VARIANCE

This appendix shows the derivation of the asymptotic formula of the kriging variance described in Chapter 6.

On all these calculations, we assume that the observations are distributed according to the probability μ. If μ is the uniform measure on the design region D, it means that the observations are uniformly spread on D. If μ is a Dirac function, all the observations are taken on a single location.

We propose two different proofs, depending on the nature of the kernel. For kernels of finite dimension, the proof is algebraic. The general case is more complex, and the proof is formal.

B.1 Kernels Of Finite Dimension

The covariance kernel is assumed to be of the form of a finite sum of basis functions and coefficients:

$$k(\mathbf{u},\mathbf{v}) = f(\mathbf{u})\mathbf{\Gamma} f(\mathbf{v})^T \tag{B–1}$$

With: $f(\mathbf{u}) = [f_1(\mathbf{u}),\ldots,f_p(\mathbf{u})]$.

$\mathbf{\Gamma}$ can be diagonal for instance, hence the kernel is of the form:

$$k(\mathbf{u},\mathbf{v}) = \sigma_1^2 f_1(\mathbf{u}) f_1(\mathbf{v}) + \ldots + \sigma_p^2 f_p(\mathbf{u}) f_p(\mathbf{v}) \tag{B–2}$$

For simplification purpose, we will assume in the following that $\mathbf{\Gamma}$ is always diagonal.

We recall the equation of the kriging prediction variance, based on m observations with homogeneous nugget effect equal to $m\tau^2$:

$${s_K}^2(\mathbf{x}) = k(\mathbf{x},\mathbf{x}) - \mathbf{k}^T(\mathbf{x})\left(\mathbf{K}+\mathbf{\Delta}\right)^{-1}\mathbf{k}(\mathbf{x}) \tag{B–3}$$

With:

$$\mathbf{K}+\mathbf{\Delta}=\left(k\left(\mathbf{x}_i,\mathbf{x}_j\right)\right)_{1\leq i,j\leq m}+\begin{pmatrix} m\tau^2 & & 0 \\ & \ddots & \\ 0 & & m\tau^2 \end{pmatrix}$$

Then, with covariance function as defined in Eq. B–1, the kriging variance can be expressed as:

$$s_K^2(\mathbf{x})=f(\mathbf{u})\mathbf{\Gamma}f(\mathbf{u})^T-f\left(\mathbf{x}\right)\mathbf{\Gamma}f\left(\mathbf{X}\right)^T\left[m\tau^2\mathbf{I}_m+f\left(\mathbf{X}\right)\mathbf{\Gamma}f\left(\mathbf{X}\right)^T\right]^{-1}f\left(\mathbf{X}\right)\mathbf{\Gamma}f\left(\mathbf{x}\right)^T \quad \text{(B–4)}$$

with the convention:

$$f\left(\mathbf{X}\right)=\begin{bmatrix} f_1\left(\mathbf{x}_1\right) & \dots & f_p\left(\mathbf{x}_1\right) \\ \vdots & & \\ f_1\left(\mathbf{x}_m\right) & \dots & f_p\left(\mathbf{x}_m\right) \end{bmatrix}.$$

Then, by factorization we obtain:

$$s_K^2(\mathbf{x})=f\left(\mathbf{x}\right)\left[\mathbf{\Gamma}-\mathbf{\Gamma}f\left(\mathbf{X}\right)^T\left[m\tau^2\mathbf{I}_m+f\left(\mathbf{X}\right)\mathbf{\Gamma}f\left(\mathbf{X}\right)^T\right]^{-1}f\left(\mathbf{X}\right)\mathbf{\Gamma}\right]f\left(\mathbf{x}\right)^T \quad \text{(B–5)}$$

So the prediction variance is of the form:

$$s_K^2(\mathbf{x})=f\left(\mathbf{x}\right)\mathbf{M}^{-1}f\left(\mathbf{x}\right)^T \quad \text{(B–6)}$$

with:

$$\mathbf{M}^{-1}=\mathbf{\Gamma}-\mathbf{\Gamma}f\left(\mathbf{X}\right)^T\left[m\tau^2\mathbf{I}_m f\left(\mathbf{X}\right)\mathbf{\Gamma}f\left(\mathbf{X}\right)^T\right]^{-1}f\left(\mathbf{X}\right)\mathbf{\Gamma}.$$

$\mathbf{M}^{-1}$ is of dimension $p\times p$.

Using the equality [Fedorov & Hackl (1997), p. 107]

$$\left(\mathbf{A}+\mathbf{B}\mathbf{B}^T\right)^{-1}=\mathbf{A}^{-1}-\mathbf{A}^{-1}\mathbf{B}\left(\mathbf{I}+\mathbf{B}^T\mathbf{A}^{-1}\mathbf{B}\right)^{-1}\mathbf{B}^T\mathbf{A}^{-1}, \quad \text{(B–7)}$$

with $\mathbf{A}=\frac{1}{m\tau^2}\mathbf{\Gamma}$ and $\mathbf{B}=f\left(\mathbf{X}\right)^T$, $\mathbf{M}^{-1}$ can be simplified to:

$$\mathbf{M}^{-1}=\left(\frac{1}{m\tau^2}f\left(\mathbf{X}\right)^T f\left(\mathbf{X}\right)+\mathbf{\Gamma}^{-1}\right)^{-1} \quad \text{(B–8)}$$

The prediction variance is then:

$$s_K^2(\mathbf{x}) = f(\mathbf{x}) \left(\frac{1}{m\tau^2} f(\mathbf{X})^T f(\mathbf{X}) + \mathbf{\Gamma}^{-1} \right)^{-1} f(\mathbf{x})^T \tag{B–9}$$

Now, we want to consider the case when $m \to +\infty$. We have by definition:

$$\frac{1}{m} f(\mathbf{X})^T f(\mathbf{X}) = \left(\frac{1}{m} \sum_{i=1}^{m} f_k(\mathbf{x}_i) f_l(\mathbf{x}_i) \right)_{1 \leq k,l \leq p} \tag{B–10}$$

When $m \to +\infty$, we get by the strong law of large numbers:

$$\frac{1}{m} f(\mathbf{X})^T f(\mathbf{X}) \to \left(\langle f_k, f_l \rangle_\mu \right)_{1 \leq k,l \leq p} \tag{B–11}$$

where:

$$\langle f_k, f_l \rangle_\mu = \int_D f_k(\mathbf{x}) f_l(\mathbf{x}) \, d\mu(\mathbf{x})$$

We define the Gram matrix $\mathbf{G}_\mu$ such that:

$$\mathbf{G}_\mu = \left(\langle f_k, f_l \rangle_\mu \right)_{1 \leq k,l \leq p} \tag{B–12}$$

By continuity, we obtain:

$$s_K^2(\mathbf{x}) \to s_{K\infty}^2(\mathbf{x}) = f(\mathbf{x}) \left[\frac{\mathbf{G}_\mu}{\tau^2} + \mathbf{\Gamma}^{-1} \right]^{-1} f(\mathbf{x})^T \tag{B–13}$$

Equation B–13 shows that, even if the number of observations tends to infinity, the prediction variance can be expressed as a function of the inverse of a $p \times p$ matrix. Hence, the complexity of the calculations is driven by the dimension of the kernel instead of the number of observations, which is counter-intuitive regarding the original form of the prediction variance (Eq. 2–23).

Now, we introduce the Hilbert-Schmidt integral operator $T_{k,\mu}$ associated with the kernel k and measure μ:

$$\begin{array}{rccc} T_{k,\mu}: & L^2(\mu) & \to & L^2(\mu) \\ & g & \mapsto & T_{k,\mu} g : \mathbf{x} \mapsto \int\limits_D k(\mathbf{x}, \mathbf{y}) \, g(\mathbf{y}) \, d\mu(\mathbf{y}) \end{array} \tag{B–14}$$

By using Eq. B–2:

$$\begin{aligned} T_{k,\mu}g(\mathbf{x}) &= \int_D k(\mathbf{x},\mathbf{y})g(\mathbf{y})d\mu(\mathbf{y}) \\ &= \sum_{k=1}^{p}\sigma_k^2\left[\int_D f_k(\mathbf{y})g_(\mathbf{y})\right]f_k(\mathbf{x}) \\ &= \sum_{k=1}^{p}\sigma_k^2\langle f_k,g\rangle_\mu f_k(\mathbf{x}) \end{aligned} \tag{B–15}$$

Equation B–15 shows that the image of $T_{k,\mu}$ is generated by p functions $f_k(\mathbf{x})$. Hence, $T_{k,\mu}$ is an operator of finite rank r, $r \leq p$ and it admits a spectral decomposition $\phi_1, \phi_2, \ldots \phi_r$ and $\lambda_1 \geq \lambda_2 \geq \ldots \geq \lambda_r$ such that:

- $(\phi_j)_j$ an orthonormal family:

$$\int_D (\phi_j(\mathbf{x}))^2 d\mu(\mathbf{x}) = 1 \qquad \text{and} \qquad \int_D \phi_i(\mathbf{x})\,\phi_j(\mathbf{x})\,d\mu(\mathbf{x}) = 0, \quad i \neq j$$

- $T_{k,\mu}\phi_j = \lambda_j\phi_j$

Remark:. The rank r depends on both $(f_i)_i$ and μ. In particular, when μ is a weighted sum of Dirac functions, $L^2(\mu)$ is of dimension $q = Card(supp(\mu))$. The image of $T_{k,\mu}$ being a vector subspace of $L^2(\mu)$, its dimension r is bounded by q. For the extreme case where $\mu = \delta_{\mathbf{x}^*}$ (single Dirac function), we have $r = 1$, even if the covariance is defined by a large number p of basis functions. In practice, most of the time $r = \min(p, q)$.

Now:

$$\begin{aligned} \lambda_j\phi_j(\mathbf{x}) &= \int k(\mathbf{x},\mathbf{y})\phi_j(\mathbf{y})d\mu(\mathbf{y}) \\ &= \sum_{k=1}^{p}\sigma_k^2\langle f_k,\phi_j\rangle_\mu f_k(\mathbf{x}) \end{aligned} \tag{B–16}$$

We define the $p \times r$ matrix $\mathbf{A} = (a_{jk})_{1\leq j\leq p, 1\leq k\leq r}$ such that:

$$a_{jk} = \langle f_k, \phi_j\rangle_\mu$$

Then:

$$\lambda_j \phi_j(\mathbf{x}) = \sum_{k=1}^{p} \sigma_k^2 a_{kj} f_k(\mathbf{x}) \tag{B–17}$$

$$\Lambda \boldsymbol{\phi}(\mathbf{x})^T = \mathbf{A}^T \boldsymbol{\Gamma} \mathbf{f}(\mathbf{x})^T \tag{B–18}$$

With: $\Lambda = \text{diag}\left([\lambda_1, \ldots, \lambda_r]\right)$.

We multiply both sides of Eq. B–18 by $\boldsymbol{\phi}(\mathbf{x})$, and integrate with respect to the measure μ:

$$\int \Lambda \boldsymbol{\phi}(\mathbf{x})^T \boldsymbol{\phi}(\mathbf{x}) d\mu(\mathbf{x}) = \int \mathbf{A}^T \boldsymbol{\Gamma} \mathbf{f}(\mathbf{x})^T \boldsymbol{\phi}(\mathbf{x}) d\mu(\mathbf{x})$$

Since $(\phi_j)_j$ is an orthonormal basis, the left-hand-side reduces to Λ. Then, we obtain the equality:

$$\Lambda = \mathbf{A}^T \boldsymbol{\Gamma} \mathbf{A} \tag{B–19}$$

Similarly, by multiplying both sides of Eq. B–18 by $\boldsymbol{f}(\mathbf{x})$ and integrating, we obtain:

$$\begin{aligned} \Lambda \mathbf{A}^T &= \mathbf{A}^T \boldsymbol{\Gamma} \mathbf{G}_\mu \\ \mathbf{G}_\mu &= \mathbf{A} \mathbf{A}^T \end{aligned} \tag{B–20}$$

Now, using the equality of Eq. B–7 we obtain:

$$\begin{aligned} \mathbf{M}^{-1} &= \left(\frac{1}{n\tau^2} \mathbf{A}^T \mathbf{A} + \boldsymbol{\Gamma}^{-1} \right)^{-1} \\ &= \boldsymbol{\Gamma} - \boldsymbol{\Gamma} \mathbf{A} \left[\tau^2 \mathbf{I}_r + \mathbf{A}^T \boldsymbol{\Gamma} \mathbf{A} \right]^{-1} \mathbf{A}^T \boldsymbol{\Gamma} \\ &= \boldsymbol{\Gamma} - \boldsymbol{\Gamma} \mathbf{A} \left[\tau^2 \mathbf{I}_r + \boldsymbol{\Lambda} \right]^{-1} \mathbf{A}^T \boldsymbol{\Gamma} \end{aligned} \tag{B–21}$$

Then:

$$\begin{aligned} s_{K\infty}^2(\mathbf{x}) &= f(\mathbf{x}) \boldsymbol{\Gamma} f(\mathbf{x})^T - f(\mathbf{x}) \boldsymbol{\Gamma} \mathbf{A} \left[\tau^2 \mathbf{I}_r + \boldsymbol{\Lambda} \right]^{-1} \mathbf{A}^T \boldsymbol{\Gamma} f(\mathbf{x})^T \\ &= k(\mathbf{x}, \mathbf{x}) - \boldsymbol{\phi}(\mathbf{x}) \boldsymbol{\Lambda} \left[\tau^2 \mathbf{I}_r + \boldsymbol{\Lambda} \right]^{-1} \boldsymbol{\Lambda} \boldsymbol{\phi}(\mathbf{x})^T \end{aligned} \tag{B–22}$$

Now:

$$\begin{aligned}\boldsymbol{\Lambda}\left[\tau^2\mathbf{I}_r+\boldsymbol{\Lambda}\right]^{-1}\boldsymbol{\Lambda} &= \boldsymbol{\Lambda}\left(diag\left(\frac{1}{\tau^2+\lambda_k}\right)\right)\boldsymbol{\Lambda}\\ &= diag\left(\frac{{\lambda_k}^2}{\tau^2+\lambda_k}\right)\end{aligned} \tag{B–23}$$

Finally:

$$s^2_{K\infty}(\mathbf{x}) = k(\mathbf{x},\mathbf{x}) - \sum_{k=1}^{r}\frac{\lambda_k^2}{\lambda_k^2+\tau^2}\phi_k(\mathbf{x})^2 \tag{B–24}$$

B.2 General Case

The demonstration is organized as follow: first, the classical kriging equations are given for a finite number of observations m. After transformations, the kriging variance is expressed when m tends to infinity using the law of great numbers. Then, the theory of Hilbert-Schmidt operators and their spectral decomposition are introduced. Finally, the kriging variance expression is simplified using the spectral decomposition to obtain the formula.

First, we recall the equation of the kriging prediction variance, based on m observations with homogeneous nugget effect equal to $m\tau^2$:

$${s_K}^2(\mathbf{x}) = \sigma^2 - \mathbf{k}^T(\mathbf{x})\left(\mathbf{K}+\boldsymbol{\Delta}\right)^{-1}\mathbf{k}(\mathbf{x}) \tag{B–25}$$

With:

$$\mathbf{K}+\boldsymbol{\Delta} = \left(k(\mathbf{x}_i,\mathbf{x}_j)\right)_{1\le i,j\le m} + \begin{pmatrix} m\tau^2 & & 0\\ & \ddots & \\ 0 & & m\tau^2\end{pmatrix}$$

We decompose $\left(\mathbf{K}+\boldsymbol{\Delta}\right)^{-1}$ in Taylor series, using:

$$\left(\mathbf{I}+\mathbf{H}\right)^{-1} = \mathbf{I}-\mathbf{H}+\mathbf{H}^2-\mathbf{H}^3+... = \sum_{p=0}^{\infty}(-1)^p\mathbf{H}^p$$

Here we have:

$$\mathbf{K}+\boldsymbol{\Delta} = m\tau^2\left[\mathbf{I}+\frac{\mathbf{K}}{m\tau^2}\right]$$

Hence:

$$(\mathbf{K}+\mathbf{\Delta})^{-1}=\frac{1}{m\tau^2}\sum_{p=0}^{\infty}(-1)^p\frac{\mathbf{K}^p}{(m\tau^2)^p} \tag{B–26}$$

Note that this decomposition is correct when the spectral radius of $\mathbf{K}$ is smaller than $m\tau^2$. However, it has been found empirically that the results of this proof stand when this asumption is not met. Yet, we have not found how to relax this hypothesis.

Using the decomposition of Eq. B–26, the prediction variance in Eq. B–25 becomes:

$${s_K}^2(\mathbf{x})=\sigma^2-\sum_{p\geq 0}(-1)^p\frac{1}{(m\tau^2)^{p+1}}\mathbf{k}^T(\mathbf{x})\,\mathbf{K}^p\mathbf{k}(\mathbf{x})$$

We expand the quadratic form on the right-hand side:

$$\begin{aligned}\mathbf{k}^T(\mathbf{x})\,\mathbf{K}^p\mathbf{k}(\mathbf{x}) &= \sum_{i,j}k(\mathbf{x},\mathbf{x}_i)(\mathbf{K}^p)_{ij}k(\mathbf{x}_j,\mathbf{x})\\ &= \sum_{i_1,\ldots,i_{p+1}}k(\mathbf{x}_i,\mathbf{x}_{i_1})\,k(\mathbf{x}_{i_1},\mathbf{x}_{i_2})\ldots k\left(\mathbf{x}_{i_p},\mathbf{x}_{i_{p+1}}\right)k\left(\mathbf{x}_{i_{p+1}},\mathbf{x}\right)\end{aligned}$$

When $m\to+\infty$, we obtain, by the law of large numbers:

$$\frac{1}{m^{p+1}}\sum_{i_1,\ldots,i_{p+1}}k(\mathbf{x},\mathbf{x}_{i_1})\,k(\mathbf{x}_{i_1},\mathbf{x}_{i_2})\ldots k\left(\mathbf{x}_{i_p},\mathbf{x}_{i_{p+1}}\right)k\left(\mathbf{x}_{i_{p+1}},\mathbf{x}\right)\to$$

$$\int_{D^{p+1}}k(\mathbf{x},\mathbf{u}_1)\,k(\mathbf{u}_1,\mathbf{u}_2)\ldots k(\mathbf{u}_p,\mathbf{u}_{p+1})\,k(\mathbf{u}_{p+1},\mathbf{x})\,d\mu(\mathbf{u}_1)\ldots d\mu(\mathbf{u}_{p+1})$$

Thus:

$${s_K}^2_\infty(\mathbf{x})=\sigma^2-\sum_{p\geq 0}(-1)^p\frac{1}{(\tau^2)^{p+1}}\int_{D^{p+1}}k(\mathbf{x},\mathbf{u}_1)\,k(\mathbf{u}_1,\mathbf{u}_2)\ldots k(\mathbf{u}_p,\mathbf{u}_{p+1})\,k(\mathbf{u}_{p+1},\mathbf{x})\,d\mu(\mathbf{u}_1)\ldots d\mu(\mathbf{u}_{p+1})$$

Let us introduce the notation:

$$\kappa_{p+2}(\mathbf{x},\mathbf{x})=\int_{D^{p+1}}k(\mathbf{x},\mathbf{u}_1)\,k(\mathbf{u}_1,\mathbf{u}_2)\ldots k(\mathbf{u}_p,\mathbf{u}_{p+1})\,k(\mathbf{u}_{p+1},\mathbf{x})\,d\mu(\mathbf{u}_1)\ldots d\mu(\mathbf{u}_{p+1}) \tag{B–27}$$

Then:

$${s_K}^2_\infty(\mathbf{x})=\sigma^2-\sum_{p\geq 0}(-1)^p\frac{\kappa_{p+2}(\mathbf{x},\mathbf{x})}{(\tau^2)^{p+1}} \tag{B–28}$$

At this point, we introduce the Hilbert-Schmidt integral operator $T_{k,\mu}$ associated with the kernel k:

$$\begin{array}{rccc} T_{k,\mu}: & L^2(D) & \rightarrow & L^2(D) \\ & f & \mapsto & T_{k,\mu}f : \mathbf{x} \mapsto \int\limits_D k(\mathbf{x},\mathbf{y})\, f(\mathbf{y})\, d\mu(\mathbf{y}) \end{array} \tag{B–29}$$

Mercer's theorem states that the kernel function k can be represented on $L^2(\mu \otimes \mu)$ in an orthogonal basis $(\phi_n)_n$ of $L^2(\mu)$ consisting of the eigenfunctions of $T_{k,\mu}$ such that the corresponding sequence of eigenvalues $\{\lambda_n\}_n$ is nonnegative [Riez & Nagy (1952), p. 242]:

$$k(\mathbf{u},\mathbf{v}) = \sum_{n\geq 0} \lambda_n \phi_n(\mathbf{u})\, \phi_n(\mathbf{v}), \qquad \mathbf{u},\mathbf{v} \in \operatorname{supp}(\mu) \tag{B–30}$$

With:

- $(\phi_n)_n$ an orthonormal basis:

$$\int\limits_D (\phi_n(\mathbf{x}))^2 d\mu(\mathbf{x}) = 1 \qquad \text{and} \qquad \int\limits_D f_i(\mathbf{x})\, f_j(\mathbf{x})\, d\mu(\mathbf{x}) = 0, \quad i \neq j$$

- $\lambda_n \geq 0, \quad \lambda_1 \geq \lambda_2 \geq \lambda_3 \geq ...$
- $T_{k,\mu}\phi_n = \lambda_n \phi_n$

The p^{th} power of $T_{k,\mu}$ ($T_{k,\mu}$ applied p times) has the same eigenfunctions and its eigenvalues are ${\lambda_n}^p$. Its associated kernel is (for $p > 1$):

$$\kappa_p(\mathbf{u},\mathbf{v}) = \int\limits_{D^{p-1}} k(\mathbf{u},\mathbf{u}_1)\, k(\mathbf{u}_1,\mathbf{u}_2) ... k(\mathbf{u}_{p-2},\mathbf{u}_{p-1})\, k(\mathbf{u}_{p-1},\mathbf{v})\, d\mu(\mathbf{u}_1) ... d\mu(\mathbf{u}_{p-1})$$

For instance, for $p = 2$:

$$\begin{aligned} T_{k,\mu}^2 &= T_{k,\mu}(T_{k,\mu}f)(\mathbf{x}) = \int\limits_D k(\mathbf{x},\mathbf{u}_1)\, T_{k,\mu}f(\mathbf{u}_1)\, d\mu(\mathbf{u}_1) \\ &= \int\limits_D k(\mathbf{x},\mathbf{u}_1) \left[\int\limits_D k(\mathbf{y},\mathbf{u}_2)\, f(\mathbf{u}_2)\, d\mu(\mathbf{u}_2) \right] d\mu(\mathbf{u}_1) \\ &= \int\int\limits_{D^2} k(\mathbf{x},u_1)\, k(\mathbf{u}_1,\mathbf{u}_2)\, f(\mathbf{u}_2)\, d\mu(\mathbf{u}_2)\, d\mu(\mathbf{u}_1) \end{aligned}$$

$$
\begin{aligned}
&= \int_D \left[\int_D k(\mathbf{x}, \mathbf{u}_1)\, k(\mathbf{u}_1, \mathbf{u}_2)\, d\mu(\mathbf{u}_1) \right] f(\mathbf{u}_2)\, d\mu(\mathbf{u}_2) \\
&= \int_D \kappa_2(\mathbf{x}, \mathbf{u}_2)\, f(\mathbf{u}_2)\, d\mu(\mathbf{u}_2)
\end{aligned}
$$

For $\mathbf{u}, \mathbf{v} \in \operatorname{supp}(\mu)$, we have the spectral decomposition of the kernel κ_p:

$$
\kappa_p(\mathbf{u}, \mathbf{v}) = \sum_{n \geq 0} {\lambda_n}^p \phi_n(\mathbf{u})\, \phi_n(\mathbf{v}) \tag{B–31}
$$

Now, from Eq. B–27:

$$
\begin{aligned}
\kappa_{p+2}(\mathbf{x}, \mathbf{x}) &= \int_{D^{p+1}} k(\mathbf{x}, \mathbf{u}_1)\, k(\mathbf{u}_1, \mathbf{u}_2) \ldots k(\mathbf{u}_p, \mathbf{u}_{p+1})\, k(\mathbf{u}_{p+1}, \mathbf{x})\, d\mu(\mathbf{u}_1) \ldots d\mu(\mathbf{u}_{p+1}) \\
&= \int_{D^2} k(\mathbf{x}, \mathbf{u}_1) \left[\int_{D^{p-1}} k(\mathbf{u}_1, \mathbf{u}_2) \ldots k(\mathbf{u}_p, \mathbf{u}_{p+1})\, d\mu(\mathbf{u}_2) \ldots d\mu(\mathbf{u}_p) \right] k(\mathbf{u}_{p+1}, \mathbf{x})\, d\mu(\mathbf{u}_1)\, d\mu(\mathbf{u}_{p+1}) \\
&= \int_{D^2} k(\mathbf{x}, \mathbf{u}_1) \left[\kappa_p(\mathbf{u}_1, \mathbf{u}_{p+1}) \right] k(\mathbf{u}_{p+1}, \mathbf{x})\, d\mu(\mathbf{u}_1)\, d\mu(\mathbf{u}_{p+1})
\end{aligned}
$$

The kernel κ_p is evaluated on the support of μ, we can replace it by its spectral representation (Eq. B–31):

$$
\begin{aligned}
\kappa_{p+2}(\mathbf{x}, \mathbf{x}) &= \int_{D^2} k(\mathbf{x}, \mathbf{u}_1) \left[\sum_{n \geq 0} {\lambda_n}^p \phi_n(\mathbf{u}_1)\, \phi_n(\mathbf{u}_{p+1}) \right] k(\mathbf{u}_{p+1}, \mathbf{x})\, d\mu(\mathbf{u}_1)\, d\mu(\mathbf{u}_{p+1}) \\
&= \sum_{n \geq 0} {\lambda_n}^p \int_{D^2} k(\mathbf{x}, \mathbf{u}_1)\, \phi_n(\mathbf{u}_1)\, \phi_n(\mathbf{u}_{p+1})\, k(\mathbf{u}_{p+1}, \mathbf{x})\, d\mu(\mathbf{u}_1)\, d\mu(\mathbf{u}_{p+1}) \\
&= \sum_{n \geq 0} \left[{\lambda_n}^p \left(\int_D k(\mathbf{x}, \mathbf{u}_1)\, \phi_n(\mathbf{u}_1)\, d\mu(\mathbf{u}_1) \right) \left(\int_D \phi_n(\mathbf{u}_{p+1})\, k(\mathbf{u}_{p+1}, \mathbf{x})\, d\mu(\mathbf{u}_{p+1}) \right) \right]
\end{aligned}
$$

By definition, we have:

$$
T_{k,\mu} \phi_n(\mathbf{x}) = \lambda_n \phi_n(\mathbf{x}) \quad \text{and} \quad \int_D k(\mathbf{x}, \mathbf{y})\, \phi_n(\mathbf{y})\, d\mu(\mathbf{y}) = \lambda_n \phi_n(\mathbf{x})
$$

Finally:

$$
\kappa_{p+2}(\mathbf{x}, \mathbf{x}) = \sum_{n \geq 0} \left[{\lambda_n}^p \left(\lambda_n \phi_n(\mathbf{x}) \right) \left(\lambda_n \phi_n(\mathbf{x}) \right) \right]
$$

$$\kappa_{p+2}(\mathbf{x},\mathbf{x}) = \sum_{n\geq 0} {\lambda_n}^{p+2} (\phi_n(\mathbf{x}))^2 \tag{B–32}$$

Then, we put Eq. B–32 into Eq. B–28:

$${s_K}^2_{\infty}(\mathbf{x}) = \sigma^2 - \sum_{p\geq 0} (-1)^p \frac{1}{(\tau^2)^{p+1}} \sum_{n\geq 0} {\lambda_n}^{p+2} (\phi_n(\mathbf{x}))^2$$

$${s_K}^2_{\infty}(\mathbf{x}) = \sigma^2 - \sum_{n\geq 0} \lambda_n (\phi_n(\mathbf{x}))^2 \sum_{p\geq 0} (-1)^p \frac{{\lambda_n}^{p+1}}{(\tau^2)^{p+1}}$$

The second sum corresponds to a Taylor extension:

$$\sum_{p\geq 0} (-1)^p \frac{{\lambda_n}^{p+1}}{(\tau^2)^{p+1}} = \sum_{p\geq 0} (-1)^p \left(\frac{\lambda_n}{\tau^2}\right)^{p+1} = 1 - \frac{1}{1+\frac{\lambda_n}{\tau^2}}$$

Hence:

$${s_K}^2_{\infty}(\mathbf{x}) = \sigma^2 - \sum_{n\geq 0} \lambda_n \left(1 - \frac{1}{1+\frac{\lambda_n}{\tau^2}}\right) (\phi_n(\mathbf{x}))^2$$

$${s_K}^2_{\infty}(\mathbf{x}) = \sigma^2 - \sum_{n\geq 0} \left(\frac{{\lambda_n}^2}{\tau^2+\lambda_n} (\phi_n(\mathbf{x}))^2\right) \tag{B–33}$$

B.3 The Space-Filling Case

In the space-filling case, μ is the uniform measure on D. When uniform accuracy over the design domain is wanted, the integration measure used for the IMSE is also uniform:

$$IMSE = \int_D {s_K}^2(\mathbf{x})\, d\mu(\mathbf{x})$$

In the case when the two measures coincide, the IMSE can be expressed in simple form. For any $\mathbf{x}$ in supp(μ), we have:

$$\sum_{n\geq 0} \lambda_n (\phi_n(\mathbf{x}))^2 = \sigma^2$$

Here, supp(μ) = D, so this equality is correct for any $\mathbf{x} \in D$. Then:

$${s_K}^2_{\infty}(\mathbf{x}) = \sigma^2 - \sum_{n\geq 0} \lambda_n \left(1 - \frac{1}{1+\frac{\lambda_n}{\tau^2}}\right) (\phi_n(\mathbf{x}))^2$$

$$
\begin{aligned}
&= \sigma^2 - \sum_{n\geq 0} \lambda_n (\phi_n(\mathbf{x}))^2 + \sum_{n\geq 0} \left(\frac{\lambda_n}{1+\frac{\lambda_n}{\tau^2}} \right) (\phi_n(\mathbf{x}))^2 \\
&= = \sum_{n\geq 0} \frac{\tau^2 \lambda_n}{\tau^2+\lambda_n} (\phi_n(\mathbf{x}))^2 \qquad \text{(B–34)}
\end{aligned}
$$

Besides:

$$
\int_D (\phi_n(\mathbf{x}))^2 d\mu(\mathbf{x}) = 1
$$

When integrating the prediction variance to compute the IMSE, we obtain:

$$
\begin{aligned}
IMSE_\infty &= \int_D {s_K}^2{}_\infty(\mathbf{x})\, d\mu(\mathbf{x}) \\
&= \sum_{n\geq 0} \frac{\tau^2 \lambda_n}{\tau^2+\lambda_n} \int_D (\phi_n(\mathbf{x}))^2 d\mu(\mathbf{x}) \\
&= \sum_{n\geq 0}^{\infty} \frac{\tau^2 \lambda_n}{\tau^2+\lambda_n} \qquad \text{(B–35)}
\end{aligned}
$$

APPENDIX C
SPECTRAL DECOMPOSITION OF THE ORSTEIN-UHLENBECK COVARIANCE FUNCTION

We consider the following kernel:

$$k\left(x,y\right)=\sigma^{2}\exp\left(-\frac{1}{\theta}\left|x-y\right|\right)$$

An eigenfunction f with corresponding eigenvalue λ for that kernel verifies:

$$Kf\left(y\right)=\sigma^{2}\int_{0}^{y}\exp\left(-\frac{y-x}{\theta}\right)f\left(x\right)dx+\sigma^{2}\int_{y}^{1}\exp\left(-\frac{x-y}{\theta}\right)f\left(x\right)dx=\lambda f\left(y\right)$$

By differentiating this equation two times with respect to y we find:

$$Kf"\left(y\right)=\frac{1}{\theta^{2}}Kf\left(y\right)-\frac{2\sigma^{2}}{\theta}f\left(y\right)$$

However:

$$Kf\left(x\right)=\lambda f\left(x\right)$$

$$Kf"\left(x\right)=\lambda f"\left(x\right)$$

Thus:

$$\lambda f"\left(x\right)=\frac{\lambda}{\theta^{2}}f\left(x\right)-\frac{2\sigma^{2}}{\theta}f\left(x\right)$$

$$f"\left(x\right)=-\left(\frac{2\sigma^{2}\theta-\lambda}{\lambda\theta^{2}}\right)f\left(x\right)$$

We deduce that f is of the form:

$$f\left(x\right)=A\cos\left(\rho x\right)+B\sin\left(\rho x\right) \tag{C–1}$$

And:

$$\rho=\sqrt{\frac{2\sigma^{2}\theta-\lambda}{\lambda\theta^{2}}} \tag{C–2}$$

Now, we replace f by its trigonometric form of Eq. C–1 in the integral equation, and λ by:

$$\lambda=\frac{2\sigma^{2}\theta}{1+\rho^{2}\theta^{2}}$$

We have:

$$Kf(x)-\lambda f(x)=\sigma^2\int_0^1\exp\left(-\frac{|x-y|}{\theta}\right)\left[A\cos(\rho x)+B\sin(\rho x)\right]dx-\frac{2\sigma^2\theta}{1+\rho^2\theta^2}\left[A\cos(\rho x)+B\sin(\rho x)\right]$$

After simplifications, we obtain:

$$Kf(x)-\lambda f(x)=\frac{\sigma^2\theta}{1+\rho^2\theta}\left[\alpha e^{-\frac{x}{\theta}}+\beta e^{\frac{x}{\theta}}\right]$$

With:

$$\begin{cases}\alpha=-A+B\rho\theta\\ \beta=e^{-\frac{1}{\theta}}\left[A\left(\rho\theta\sin(\rho)-\cos(\rho)\right)-B\left(\sin(\rho)+\rho\theta\cos(\rho)\right)\right]\end{cases}$$

This expression is null for any x only if both α and β are equal to zero:

$$\frac{\theta}{1+\rho^2\theta}\left[\alpha e^{-\frac{x}{\theta}}+\beta e^{\frac{x}{\theta}}\right]=0\quad\Leftrightarrow\quad\begin{cases}\alpha=0\\ \beta=0\end{cases}$$

We deduce from $\alpha=0$ that:

$$A=\rho\theta B$$

So, the eigenfunction is of the form:

$$f(x)=C\left(\theta\rho\cos(\rho x)+\sin(\rho x)\right)$$

C is a normalization constant so that $\int_0^1 f^2(x)=1$.

Besides, from $\beta=0$ we obtain:

$$\rho\theta\left(\rho\theta\sin(\rho)-\cos(\rho)\right)-\left(\sin(\rho)+\rho\theta\cos(\rho)\right)=0$$

$$2\rho\theta\cos(\rho)+\left(1-\theta^2\rho^2\right)\sin(\rho)=0 \tag{C–3}$$

The roots of this equation define all the eigenvalues and eigenfunctions of the problem. However, this equation does not have analytical solution and must be found numerically.

Figure C-1 represents the function $g(u) = 2u\theta\cos(u) + (1-\theta^2u^2)\sin(u)$. We see that $g(u)$ is pseudo-periodic. When u is relatively large ($\theta^2u^2 - 1 \gg 2u\theta$), the roots are well approximated by:

$$u^* = n\pi, \qquad n \in \mathbf{N} \tag{C–4}$$

Finally, the spectral decomposition associated with the exponential covariance is:

$$f_p(x) = C_p\left(\theta\rho_p\cos(\rho_p x) + \sin(\rho_p x)\right) \qquad \lambda_p = \frac{2\sigma^2\theta}{1+\theta^2\rho_p^2} \tag{C–5}$$

With:

$$\rho_p = \sqrt{\frac{2\sigma^2\theta - \lambda_p}{\theta^2\lambda_p}}$$

$$C_p = \frac{2\rho_p}{\rho_p\left(1+\rho_p^2\theta^2\right) - \left(1+\rho_p^2\theta^2\right)\sin(\rho_p)\cos(\rho_p) + 2\rho_p\theta(\sin(\rho_p))^2}$$

The ρ_p are the roots of the equation:

$$2u\theta\cos(u) + \left(1-\theta^2u^2\right)\sin(u) = 0$$

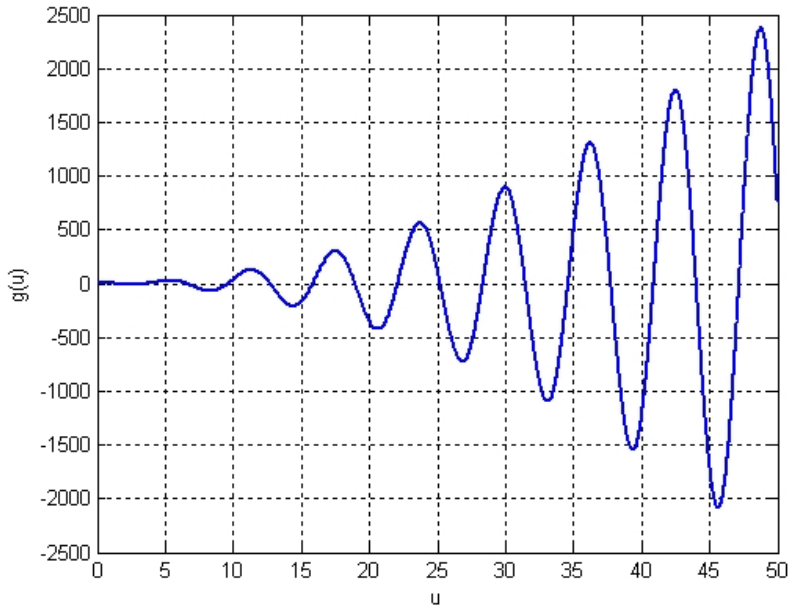

Figure C-1. Representation of the function $g(u) = 2u\theta\cos(u) + (1-\theta^2u^2)\sin(u)$. The roots of this equation are the eigenvalues of the exponential covariance kernel.

APPENDIX D
GEARS DESIGN WITH SHAPE UNCERTAINTIES USING MONTE-CARLO SIMULATIONS AND KRIGING

This appendix proposes an engineering application to the theoretical results found in Chapter 6. In particular, it uses an optimal design strategy for Kriging to help the optimization of an expensive simulator based on Monte-Carlo methods. The objective is the optimization of helical involute gears for geometrical feasibility, contact ratio, teeth sliding velocity, stresses and static transmission error (STE), with teeth shape subject to random perturbations due to wear.

D.1 Introduction

Gears are a fundamental mechanical system involved when torques must be transmitted with high efficiencies, which is the case of transmissions in cars, windmills, and other special machines. Although gears have been designed for a long time, controlling gears performance under teeth shape uncertainties is a recent, difficult and important design objective : teeth shape variations result from manufacturing (e.g., heat treatment) and from wear and induce, in particular, noise.

The applicative objective of this article is to design helical gears so as to account for teeth shape inaccuracies. Computational challenges that are familiar in Reliability Based Design Optimization (RBDO) accompany this problem: the teeth in gears are moving solids in contact with each other whose detailed simulation by finite elements is computationally intensive. With the added computational cost of accounting for shape uncertainties (through Monte Carlo simulations, reliability index calculation or polynomial chaos expansion), the robust design of these systems requires careful methodological developments.

Gears design is traditionally approached by parameterizing the shape of the teeth as helical and involute Colbourne (1987). Most gears in use today are chosen in standardized tables and are non-optimal. In Kapelevich & Kleiss (2002), helical involute gears are designed for geometrical feasibility and large contact ratio by semi-analytical approaches.

In Li et al. (1996), the size of helical gear sets is minimized where the gears stress analysis is based on standardized AGMA formula. A finite element analysis of the gears was implemented in Li et al. (2002) and served to optimize the pressure angle for minimum von Mises stresses. Modified teeth shapes were proposed in Li et al. (2002) to make the gears less sensitive to shape and positions perturbations. The gears performance criteria were bearing contact, transmission error and stress state.

In the present article, gears are designed for geometrical feasibility, contact ratio, teeth sliding velocity, stresses and Static Transmission Error (STE). Efficient stress and STE analyses are performed using Hertz contact formula and beam theory. Teeth wear is described by superposing Archard's wear model Kahraman et al. (2005) and random material removal. Gears design is decomposed into i) the optimization of the 11 involute parameters for deterministic responses ii) the optimization of the crowning to control teeth shape random perturbations, i.e., to minimize the 90th percentile of the STE variation, ΔSTE. ΔSTE is one of the primary origins of the noise made by gears Driot & Perret-Liaudet (2006).

From a methodological standpoint, it is not computationally affordable to calculate the ΔSTE percentile by simple Monte Carlo simulations at each optimization step. A Kriging metamodel of the percentile is built before the optimization. The optimization uses the Kriging prediction of ΔSTE instead of the computationally intensive Monte Carlo simulations, but other optimization criteria, which are not subject to uncertainties, are calculated with the original gears model.

The contributions of this work are twofold: firstly, a complete formulation of the gears optimum design problem, involving the 90th percentile of the STE variation, is solved; secondly, a methodology for robust design based on Kriging as a substitute for the Monte-Carlo simulations is proposed. The noise in the statistical estimator of the performance is taken into account in the Kriging metamodel through its "nugget" intensity. The Kriging approach is compared to an alternative method where the STE

variation for the average wear is minimized. The comparison is made in terms of the achieved 90% percentile of the STE variation.

D.2 Problem Formulation

D.2.1 Gears Analysis

Geometrical gears analysis is based on classical involute helical representation [Colbourne (1987), Meyer (2008)]. Twelve design variables are considered, some of which are illustrated in D-1: Z_p, the number of teeth of pinion 1; x_p and x_r the addendum modification coefficients of the two pinions; ha_{0p} and ha_{0r} the cutting tool addendum of the two pinions, hf_{0p} and hf_{0r} the cutting tool dedendum of the pinions; ρ_{ap} and ρ_{ar} the tip fillet radiuses, ρ_{fp} and ρ_{fp} the root fillet radiuses; β_0 the helix angle.

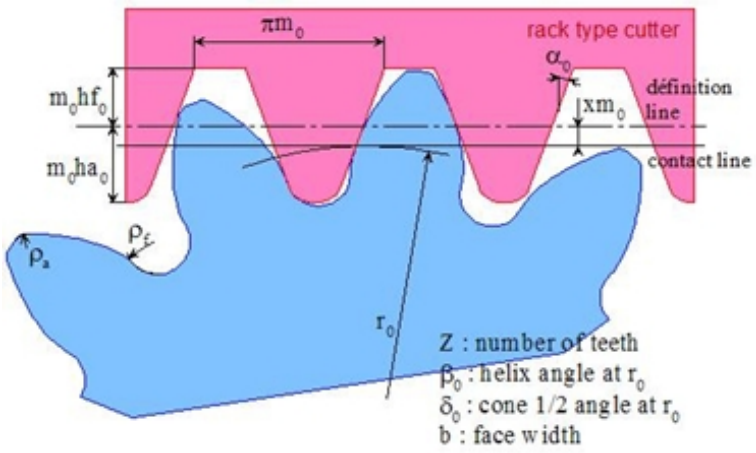

Figure D-1. Gears parameters definitions.

The optimization criteria are:

- the contact ratio, r_c, i.e., the average number of teeth in contact, which is related to gears silence;
- the specific slip ratio, g_s, which is a measure of the tangential velocity of a tooth with respects to the tooth in contact and which is related to wear;
- the maximum contact pressure between teeth, F (using Hertz's model for contact between cylinders) ;
- σ_{vm}, the maximum von Mises stresses (at the teeth root);

- ΔSTE, the difference between the maximum and the minimum of the Static Transmission Error.

The STE describes the gears position errors due to teeth deformations under loads and due to teeth shape errors. It is estimated by a fast model based on Hertz contact and beam theories. All these aspects of gears analysis were implemented in the Filengrene software Meyer (2008).

Wear profiles are perturbed Archard's profiles. They are generated by multiplying Archard's profile (proportional to $F * V$, where F is the contact pressure and V the relative sliding velocity) by a Gaussian random processes Cressie (1993), $\mathbf{\Theta}$, as described in D-2. The Gaussian processes have mean 1, a range of 0.2 *rad* and a variance of 0.01.

The randomness in the wear profiles represents uncertainties in the load and number of cycles each gear will endure, hence inducing deviations (in amplitude and shape) from the nominal Archard's profile. Shape perturbations due to wear mainly affect the STE amplitude, ΔSTE, which is therefore a random function of the design variables, x, and the wear profiles, $\Delta STE(x, \mathbf{\Theta})$. All other gears design criteria (contact and specific slip ratios, stresses, etc.) are deterministic functions of x since they are marginally affected by shape variations of the order of 1 m. A deterministic optimization criterion is obtained from ΔSTE by taking its 90th percentile, $P^{90}_{\Delta STE(x)}$. Such a criterion is natural when optimizing a random response because it ensures that 90% of the actual systems (gears here) will achieve the declared $P^{90}_{\Delta STE(x)}$ performance. Computing this percentile involves Monte-Carlo simulations (MCS), which will be detailed in Section D.3.

D.2.2 Gears Optimization Formulation

Even though the Filengrene gears simulator is rapid (about 2 CPU seconds per gears analysis) it is not possible to directly include the Monte Carlo simulations inside the optimization loop because the computational costs are multiplied by each other: for 100 Monte Carlo simulations and 1,000 optimization steps (which is an underestimation of the needed cost for globally optimizing in 11 dimensions), a single run would take 100*1,000

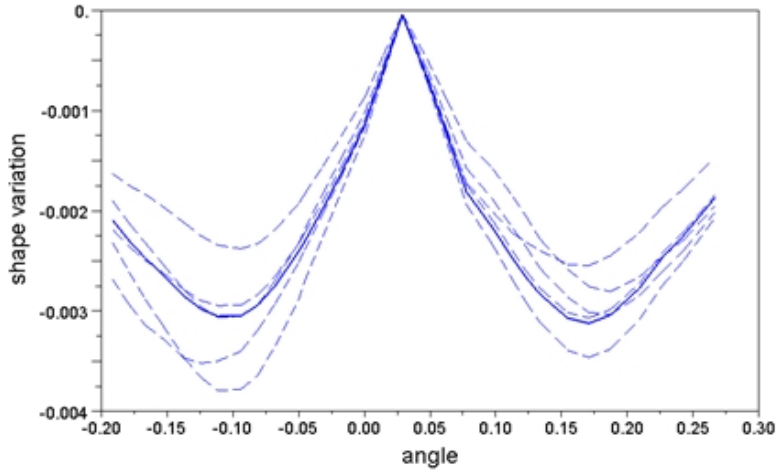

Figure D-2. Profile wear (mm) vs. angle (rad). The central continuous line corresponds to $-0.1 * F * V$, i.e. wear according to Archard's model. F is the contact pressure and V the relative sliding velocity. Wears (dashed lines) are Gaussian random processes multiplied by Archard's model : $\mathbf{\Theta} * (-0.1 * F * V)$. Wear is then proportional to $F * V$ curves with a maximum of $5\mu m$.

= 56 CPU hours. To tackle the computational cost barrier, designing gears is first formulated as a deterministic problem in 11 variables, and then as a robust optimization problem in 6 variables. The initial deterministic optimization permits to fix 11-6=5 variables and provides an entry-level design to compare to.

D.2.2.1 Deterministic Sub-problem

The gears teeth involute shape is described by the 12 variables introduced earlier : Z_p, x_p, x_r, ha_{0p}, ha_{0r}, hf_{0p}, hf_{0r}, ρ_{ap}, ρ_{ar}, ρ_{fp}, ρ_{fp} and β_0. Z_p, the number of teeth of the pinion, is the only integer variable. It is taken out of the formulation by setting its value a priori : with only one integer variable, optimizing the number of teeth boils down to repeating the procedure described in this article for various values of Z_p.

Let therefore $\mathbf{x}$ be the 11 design variables of the deterministic problem,

$$\mathbf{x} = [x_p, x_r, ha_{0p}, ha_{0r}, hf_{0p}, hf_{0r}, \rho_{ap}, \rho_{ar}, \rho_{fp}, \rho_{fr}, \beta_0] \tag{D–1}$$

The deterministic gears design problem is,

$$\mathrm{Min}\Delta\mathrm{STE}\,(\mathbf{x}) \tag{D–2}$$

such that there is no teeth interference and

$$r_c > 1.25, \qquad g_s < 2, \qquad \sigma_{vm} < Re, \qquad F < P_{hertz}^{max}, \tag{D–3}$$
$$-1 \leq x_p, x_r \leq 2, \qquad 0.8 \leq ha_{0p}, ha_{0r}, hf_{0p}, hf_{0r} \leq 1.7,$$
$$0 \leq \rho_{ap}, \rho_{ar} \leq m_0, \qquad 0.05m_0 \leq \rho_{fp}, \rho_{fr} \leq m_0 \qquad \text{and} 0 \leq \mathrm{b}_0 \leq 30$$

The number of teeth of the second pinion and the module are not part of the variables vector because they are solved by satisfying two equality constraints. The gears ratio (0.9) yields

$$Z_r = \text{integer}\,(Z_p/0.9) \tag{D–4}$$

m_0, the module (a scale factor) is calculated by solving a non linear equation stating that the distance between the gears centers is equal to 110 mm. The details of this equation are beyond the scope of this article. Other working data are : pressure angle $\alpha_0 = 18deg$, the torque transmitted by the pinion is 200 Nm, the material is a 20 NC 6 cemented steel ($E = 200GPa$, $\nu = 0.29$, $Re = 980MPa$, $P_{hertz}^{max} = 1550MPa$) and the gears thickness is 10 mm.

The deterministic sub-problem is handled with the Covariance Matrix Adaptation Evolution Strategy, CMA-ES Hansen & Kern (2004), which is the state-of-the-art evolutionary optimizer. Constraints are treated by a static linear penalization of the objective function, i.e., by minimizing

$$f_p\,(x) = \frac{\Delta EST}{\Delta_{ref}} + p\times\left[\left(1 - \frac{r_c}{1.25}\right)^+ + \left(\frac{g_s}{2} - 1\right)^+ + \left(\frac{\sigma_{vm}}{R_e} - 1\right)^+ + \left(\frac{F}{P_{hertz}^{\max}} - 1\right)^+\right] \tag{D–5}$$

where $(...)^+ = \max(0, ...)$ and $p = 10$. CMA-ES is a stochastic optimizer, it is therefore not sensitive to the slope discontinuity at 0 introduced by our penalization scheme. This penalization scheme has, on the other hand, the advantage when compared to quadratic penalty functions of allowing convergence to feasible solutions at a finite, reasonably small values of p Le Riche & Guyon (2002).

Gears simulations are not possible for every choice of the design variables: for example, there are configurations when the involute equation cannot be solved. These cases are handled by setting the objective function equal to a large number (100 here), which makes the final penalized objective function non-continuous. This is another reason for using a zero order optimizer such as CMA-ES. Note that other evolutionary optimizers (CMA-ES only handles continuous variables) are also often applied to gears design because the number of teeth is an integer variable [Missoum et al. (1999), Deb & Jain (2003)].

Bounds on the variables are handled by repeating the probabilistic CMA-ES point generations until an in-bound point is proposed. Of course, out-of-bounds points are rejected without further analysis, so the numerical cost of this strategy is negligible when compared to gears analyses.

D.2.2.2 Robust Optimization Sub-Problem

The robust optimization sub-problem is much more computationally intensive than the deterministic sub-problem because it involves estimating at each optimization step the 90% percentile of ΔSTE. Two strategies are proposed to decrease the computational cost : reducing the design space dimension and approximating percentiles with Kriging (see Section 3). The reduction in dimension is achieved by considering the 6 design variables $\mathbf{x} = [x_p, x_r, ha_{0p}, ha_{0r}, hf_{0p}, hf_{0r}]$, while the rest of the variables, ρ_{ap}, ρ_{ar}, ρ_{fp}, ρ_{fr} and β_0, are set equal to their deterministic optimal values. The reasons for this reduction are that i) the fillet radiuses have a more local influence than the addendum and dedendum and ii) the effect of the helix angle is almost completely decoupled from the effects of the other parameters (it acts in another dimension) : 0 could eventually be tuned a posteriori.

The effect of teeth shape fluctuations due to wear is controlled by solving:

$$\mathrm{Min} P^{90}{}_{\Delta STE}(\mathbf{x}) \tag{D–6}$$

by changing $\mathbf{x} = [x_p, x_r, ha_{0p}, ha_{0r}, hf_{0p}, hf_{0r}]$ such that there is no teeth inference and

$$r_c > 1.25, \qquad g_s < 2, \qquad \sigma_{vm} < Re, \qquad F < P^{max}_{hertz}, \tag{D–7}$$

$$-1 \leq x_p, x_r \leq 2, \qquad 0.8 \leq ha_{0p}, ha_{0r}, hf_{0p}, hf_{0r} \leq 1.7$$

The next section describes how we proceed to calculate the 90th percentile.

D.3 Percentile Estimation Through Monte-Carlo Simulations And Kriging

D.3.1 Computing Percentiles Of ΔSTE

In Section D.2, we described wear profiles as random processes modifying Archard's profiles. Hence, ΔSTE is a random variable, whose distribution can be estimated by Monte Carlo simulations (MCS). To do so, we first generate a large number (k) of wear profiles, $\theta_1, \theta_2, ..., \theta_k$ (again, details of the random wear profiles generation were given in D-2. For each of these profiles, we compute the corresponding $\Delta\text{STE}(\mathbf{x}, \theta_i)$. Then, the 90th percentile $P^{90}_{\Delta STE(\mathbf{x})}$ is estimated from the sample $\{\Delta\text{STE}(\mathbf{x}, \theta_1), ..., \Delta\text{STE}(\mathbf{x}, \theta_k)\}$. We call $\hat{P}^{90}(\mathbf{x}^i; \quad \theta_1, \theta_2, ..., \theta_k)$ such an estimate. A preliminary study is performed on four designs to choose k, the number of MCS (see D-1). For each design, 500 MCS are performed. Using a Lilliefors test Kenney & Keeping (1954), we find that all the samples $\{\Delta\text{STE}(\mathbf{x}_i, \theta_1), ..., \Delta\text{STE}(\mathbf{x}_i, \theta_k)\}$, $i = 1, \ldots, 4$, follow normal distributions. Hence, we assume that ΔSTE is normally distributed for any design $\mathbf{x}$.

Table D-1. Preliminary statistical analysis of four designs.

Design	x_p	x_r	ha_{0p}	ha_{0r}	hf_{0p}	hf_{0r}	$Mean(\Delta STE)$	$SD(\Delta STE)$	$\hat{P}^{90}$
1	0.49	0.49	1.20	1.11	1.00	1.09	5.82	0.41	6.34
2	0.00	0.20	1.02	1.00	0.90	1.00	6.22	0.66	7.06
3	1.10	1.00	1.30	1.40	0.90	0.90	7.30	0.44	7.87
4	0.40	-0.40	1.70	1.00	0.90	1.60	6.66	0.45	7.24

The normality of the samples allows us to increase the accuracy of the estimated percentile. Indeed, an unbiased estimate $\hat{P}^{90}$ of $P^{90}_{\Delta STE(\mathbf{x})}$ is then

$$\hat{P}^{90} = m + 1.28s \tag{D–8}$$

where

$$m = \frac{1}{k}\sum_{i=1}^{k} \Delta STE(\mathbf{x}, \theta_i), \quad \text{and}$$

$$s = \sqrt{\frac{1}{k-1}\sum_i \left[\Delta STE\left(\mathbf{x}, \theta_\mathbf{i}\right) - m\right]^2}.$$

The variance of $\hat{P}^{90}$ can now be expressed analytically. Since m and s are independent random variables,

$$\mathrm{var}\left(\hat{\mathrm{P}}^{90}\right) = \mathrm{var}\left(\mathrm{m}\right) + 1.28^2 \mathrm{var}\left(\mathrm{s}\right) \tag{D–9}$$

Let $\sigma^2_{\Delta STE}$ denote the actual variance of $\Delta STE\left(\mathbf{x}, \theta\right)$. We have Kenney & Keeping (1954):

$$var\left(m\right) = \frac{\sigma^2_{\Delta STE}}{k} \tag{D–10}$$

$$var\left(s^2\right) = \frac{2\sigma^4_{\Delta STE}}{k-1} \tag{D–11}$$

It can be shown using a first order Taylor expansion that the variance of s is approximately equal to

$$var\left(s\right) = \frac{\sigma^2_{\Delta STE}}{2}\left(1 - \sqrt{\frac{k-3}{k-1}}\right) \tag{D–12}$$

Finally,

$$var\left(\hat{P}^{90}\right) = \sigma^2_{\Delta STE}\left[\frac{1}{k} + \frac{1.28^2}{2}\left(1 - \sqrt{\frac{k-3}{k-1}}\right)\right] \tag{D–13}$$

Estimating a percentile requires a large number of calls to the gears simulation. To reduce this computational cost, we approximate the percentile by a Kriging metamodel based on noisy observations (see Section 2.1.3.2). We make the assumption that the $\hat{P}^{90}$ estimate is equal to the true function $P^{90}_{\Delta STE(\mathbf{x})}$ plus a random noise (due to the Monte Carlo sampling process):

$$\hat{P}^{90}\left(\mathbf{x}^i; \quad \theta_1, \theta_2, ..., \theta_k\right) = P^{90}_{\Delta STE}\left(\mathbf{x}^i\right) + \varepsilon^i \tag{D–14}$$

The variance of ε^i is defined here as the variance of the estimated percentile as in Eq. D–13.

D.3.2 Design Of Experiments

We have seen that each observation $\hat{P}^{90}$ requires k calls to the gears simulator. Hence, a design of experiments (DoE) of size n requires $k \times n$ calls. Due to computational limitations, the number of calls cannot exceed 90,000. Both numbers must be chosen to ensure best trade-off between:

- Space-filling
- Reasonable variance of each estimate
- Affordable computational time.

A larger n ensures a better filling of the design space, while a larger k reduces the variance of each observation. We showed in Chapter 6 that for the Kriging model, it is more accurate to have large variance and large DoEs. Hence, we choose k as small as possible. However, the hypothesis of normality of the error do not stand for very small samples ($k < 25$), so we choose $k = 30$, and $n = 3,000$.

The preliminary analysis already discussed in D-1 provides us with large ΔSTE samples at four design points, which can be used to validate our choice of k. D-2 shows the variability of the percentile estimates, $var\left(\hat{P}^{90}\right)$, from D–13 assuming only 30 MCS are performed (the true variance $\sigma^2_{\Delta STE}$ is replaced by its accurate estimate based on 500 MCS).

Table D-2. Variability of percentile estimates based on $k = 30$ Monte Carlo simulations.

Design	$var\left(\hat{P}^{90}\right)$	$SD\left(\hat{P}^{90}\right)$	$\hat{P}^{90}$
1	0.010	0.10	6.34
2	0.027	0.16	7.06
3	0.012	0.11	7.87
4	0.013	0.11	7.24

For all four designs, we see that the standard deviations are very small compared to the mean value, so $k = 30$ is sufficient.

To ensure good space-filling properties, the training point locations are chosen from a Latin Hypercube Sampling (LHS) optimized for a maximum minimum distance (maximin)

criterion. To each training point corresponds three response values: the ΔSTE with no wear, the ΔSTE with wear taken from the nominal Archard's profile (written ΔSTE_A), and the 90th percentile of ?STE with random wear (estimated by $\hat{P}^{90}_{\Delta STE}$). Out of the 3,000 points, 825 are found as infeasible designs by the Filengrene software, so the final DoE consists of 2,175 observations. D-3 summarizes the values taken by the observations.

Table D-3. Observation values of the DoE.

	Mean	Range
ΔSTE (no wear)	4.83	[0.49 ; 42.70]
ΔSTE_A (Archard's profile)	7.31	[1.47 ; 37.75]
$\hat{P}^{90}_{\Delta STE}$	8.20	[2.12 ; 39.67]

D.3.3 Data Analysis: Is A Robust Optimization Approach Really Necessary?

First, to validate our approach, we look at the correlations between the responses. Indeed, there is no evidence a priori that the optimal design for the deterministic problem D–2 is different from the robust optimal design D–6.

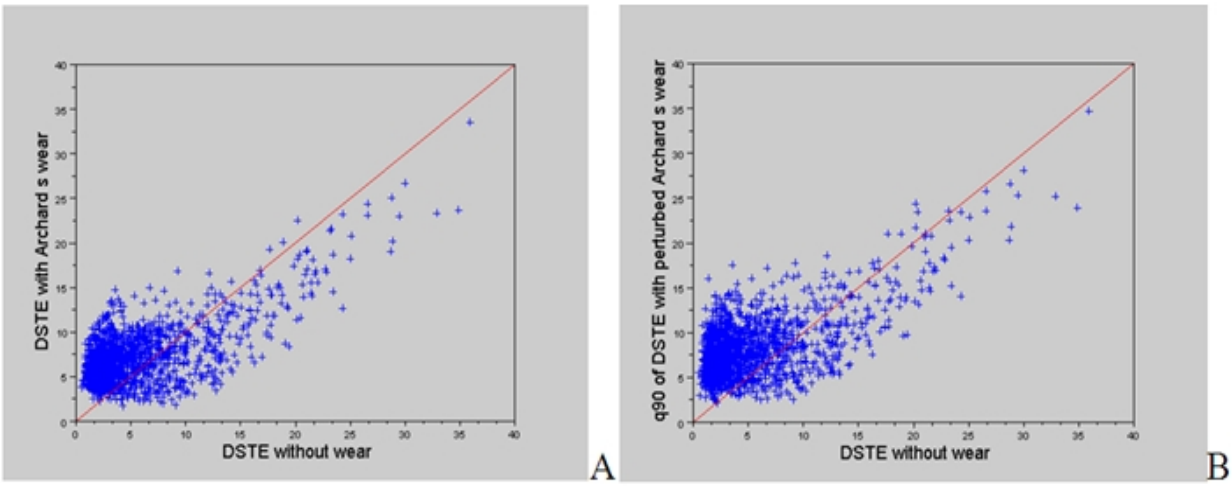

Figure D-3. ΔSTE without wear vs. ΔSTE with Archard's wear profile (ΔSTE_A, A), and vs. the 90% percentile of ΔSTE with randomly perturbed Archard's wear (B).

From D-3, we see that the ΔSTE with no wear differ in shape and amplitude from the ΔSTE with wear. Hence, the deterministic and robust optimizations are likely to have different solutions. On the contrary, ΔSTE from the nominal Archard's profile and

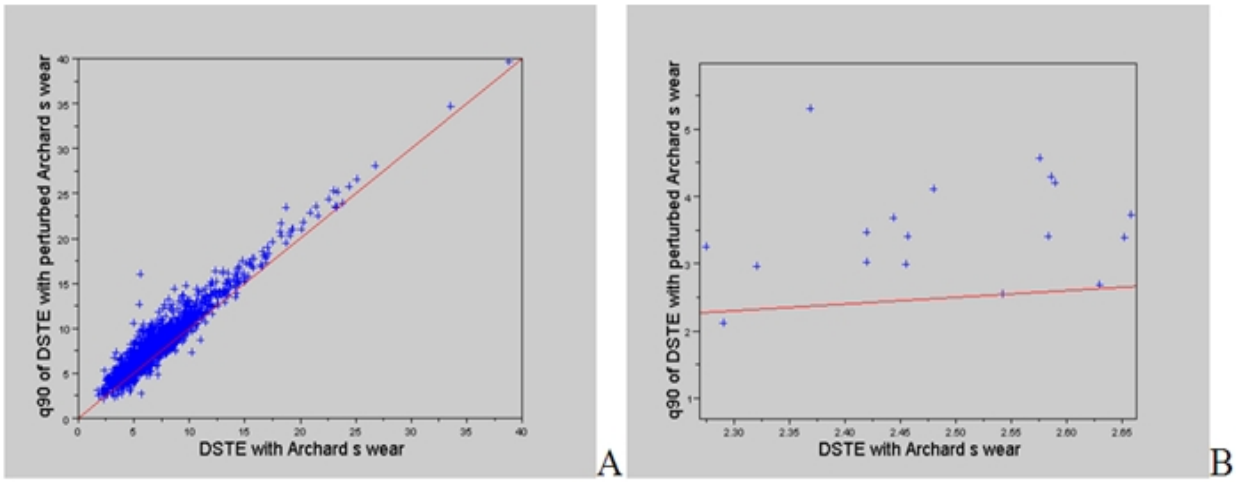

Figure D-4. ΔSTE_A (with Archard's wear profile) vs. $\hat{P}^{90}_{\Delta STE}$ (30 Monte Carlo simulations). A: full scale, B: zoom.

the percentile from the stochastic profile are strongly correlated, the percentile being shifted by a margin. So it seems that for large scale optimization, the two problems are equivalent. However, for small values of ΔSTE (D-4, A), the correlation is weaker. It is difficult to determine if the difference is due to the noise in $\hat{P}^{90}$ or not.

To refine the analysis, we pick six points out of the 2,175 observations that have similar values of ΔSTE with Archard's wear (ΔSTE_A between 2.4 and 2.5) but correspond to different designs. At each design, we run 500 MCS to have an accurate estimate of the percentile (so the noise is negligible). The values of the accurate percentile estimates and the ΔSTE with deterministic wear are reported in D-4.

Table D-4. Comparison of six designs with similar ΔSTE_A.

Design	x_p	x_r	ha_{0p}	ha_{0r}	hf_{0p}	hf_{0r}	$\Delta STE(Archard)$	P^{90}
1	0.25	1.37	1.37	0.85	1.31	0.80	2.42	3.03
2	0.18	0.69	1.54	1.01	1.08	1.05	2.44	3.07
3	-0.21	1.11	0.90	1.23	1.61	0.90	2.46	3.34
4	-0.02	1.10	1.03	0.81	1.41	1.00	2.42	3.21
5	0.15	0.71	1.44	1.07	1.63	1.16	2.48	2.88
6	-0.12	-0.08	1.25	1.19	1.63	1.61	2.45	2.84

From D-4, we see that P^{90} and ΔSTE do not always behave similarly. For instance, designs 1 and 4 have the same best ΔSTE_A out of the 6 selected designs, but they have

the third and fifth P^{90}. Design 5 is the worst design in terms of ΔSTE_A, but the second best in terms of P^{90}. This shows that optimizing ΔSTE with nominal (Archard) and stochastic wear is likely to lead to different solutions.

D.4 Optimization Results

D.4.1 Optimization Without Wear

The penalized objective function $f_p(\mathbf{x})$ [Eq. D–5] has been minimized with the CMA-ES algorithm. The penalty parameter p was set to 10 and $\Delta_{ref} = 0.5$. The 11 design variables were scaled by their range, the initial CMA-ES "step size" was 0.3, there were 10 parents and 5 child designs at each CMA-ES iteration, and the runs were 12,000 analyses long with a restart (taking the best-so-far design as new starting point and re-setting the step size to 0.3) at 6,000 analyses. The optimization was repeated from three initial points randomly chosen inside the bounds. One of these initial (therefore non optimal) design point is presented in D-5. The best performing gear out of the three optimizations, which we consider as the optimum of the deterministic gears design formulation, is given in D-6. Comparison of the starting and optimal designs show that, at the deterministic optimum, the teeth mesh has no play and the helix angle is at its upper bound. Large helix angles induce forces in the gears axes direction, but the induced axis force is not a criterion of the current design formulation [Eq. D–2]. The optimum STE profile has four modes (i.e., four maxima) for one mesh period, versus one for the starting design shown in D-5. Each mode corresponds to a teeth pair entering or leaving contact. It is likely that larger teeth numbers would be optimal for minimizing the static transmission error variation by enabling more modes in a mesh period.

D.4.2 Optimization With Wear Based On A Kriging Metamodel

Designing gears while accounting for probabilistic wear has been formulated in Eq. D–6 by replacing the variation in static transmission error, ΔSTE, by its 90th percentile, $\hat{P}^{90}_{\Delta STE}$. Section D.3 has explained how $\hat{P}^{90}_{\Delta STE}(\mathbf{x})$ can be estimated by Monte Carlo simulations at a reasonable number ($n = 2175$) of design points $\mathbf{x}$'s and then

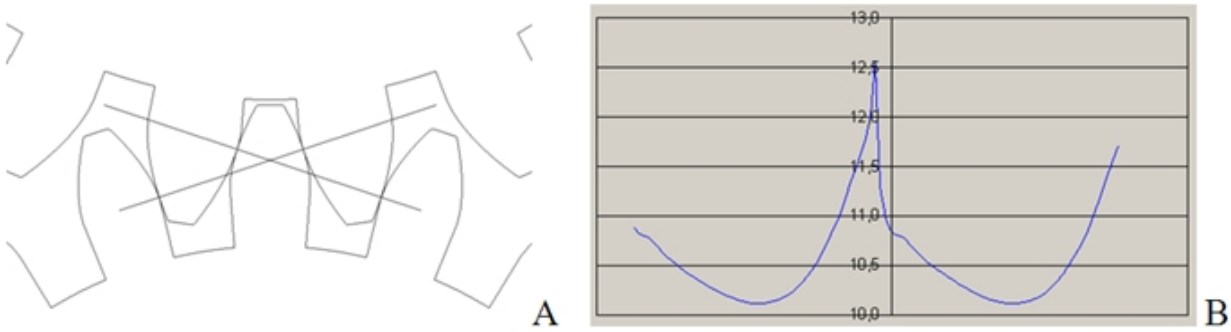

Figure D-5. Example of an optimization run starting design. Gears cross-section (A) and static transmission error (STE) in μm (B). $x_p = -0.2, x_r = 0.2, ha_{0p} = 1.5, ha_{0r} = 1.4, hf_{0p} = 1.3, hf_{0r} = 1.17, \rho_{ap} = 0.2, \rho_{ar} = 0.1, \rho_{fp} = 0.05, \rho_{fr} = 0.1, \beta_0 = 10, r_c = 2, g_s = 592, \sigma_{vm} = 1556, F = 11683, \Delta STE = 2.45$. Although there are no teeth interferences, this design is infeasible w.r.t. the maximum slip ratio, the maximum von Mises stress and the contact pressure. All dimensions but the STE are in mm, stresses are in MPa. The STE is plotted for one meshing period.

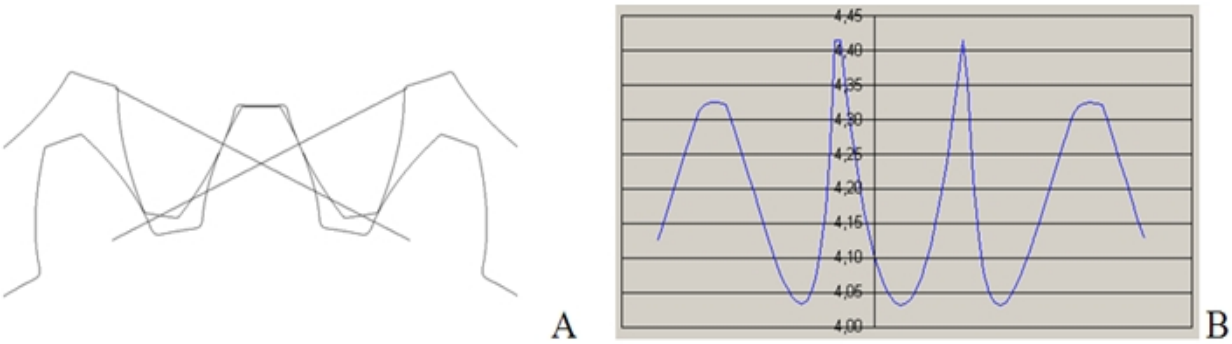

Figure D-6. Optimum design without wear. Gears cross-section (A) and STE in μm (B). $x_p = 0.49, x_r = 0.49, ha_{0p} = 1.20, ha_{0r} = 1.11, hf_{0p} = 1.00, hf_{0r} = 1.09, \rho_{ap} = 0.0003, \rho_{ar} = 0.19, \rho_{fp} = 0.64, \rho_{fr} = 0.23, \beta_0 = 30$.
$r_c = 1.66, g_s = 1.47, \sigma_{vm} = 443, F = 938, \Delta STE = 0.38$. The design is feasible. All dimensions but the STE are in mm, stresses are in MPa. The STE is plotted for one meshing period.

approximated by an ordinary Kriging metamodel. A basic idea of our approach to robust optimization with Kriging is, first, to make the costly Monte Carlo simulations before the optimization iterations and estimate the percentiles at the sampled points, then learn them with a Kriging metamodel which, finally, replaces the percentile estimation during the optimization. Although Kriging provides a complete Gaussian probability density function at each point $\mathbf{x}$, we only use here the Kriging mean, $m_K(\mathbf{x})$, for two reasons. Firstly, contrarily to global optimization methods based on Kriging such as EGO Jones et al. (1998), we do not iteratively update the Kriging model. We are therefore not interested in its uncertainty $s_K^2(\mathbf{x})$. Secondly, the data points gathered in $\hat{P}^{90}$ and learned by the Kriging model are noisy since estimated from 30 Monte Carlo simulations. The Kriging mean with nugget effect, $m_K(\mathbf{x})$, acts as a filter of the observations noise.

All other optimization constraints, r_c, g_s, σ_{vm} and F, are calculated by a single call to the gears simulator because they are mainly insensitive to wear. To sum up, the robust optimization problem with Kriging solved is,

$$Min \quad m_{OK}(\mathbf{x}) \tag{D–15}$$

by changing $\mathbf{x} = [x_p, x_r, ha_{0p}, ha_{0r}, hf_{0p}, hf_{0r}]$ such that there is no teeth interference and

$$\begin{aligned} &r_c > 1.25, \qquad g_s < 2, \qquad \sigma_{vm} < Re, \qquad F < P_{hertz}^{max}, \\ &-1 \leq x_p, x_r \leq 2, \qquad 0.8 \leq ha_{0p}, ha_{0r}, hf_{0p}, hf_{0r} \leq 1.7, \end{aligned} \tag{D–16}$$

Like in the deterministic optimization problem, the constraints were handled by minimizing the penalized objective function D–5 where ΔEST was replaced by m_K. The problem was solved using the CMA-ES optimization algorithm with the same settings as in the deterministic optimization of Section D.4.1, including the search length, restart and variables bounds handling. However, there are only six unknowns in the

robust problem, the other variables being fixed at their deterministic optimal value, $\rho_{ap} = 0.0003, \rho_{ar} = 0.19, \rho_{fp} = 0.64, \rho_{fr} = 0.23, \beta_0 = 30$.

The best design found when solving Eq. D–15 is described in D-7. We will henceforth refer to it as the "Kriging design".

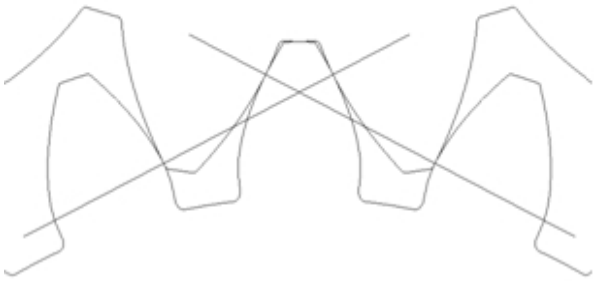

Figure D-7. Optimum robust design found using the kriging metamodel.

D.4.3 Optimization With Wear Based On A Deterministic Noise Representative

An alternative formulation of the gears design problem with wear is to solve replace the percentile estimation by a single, deterministic, instance of wear. Here, this instance is simply chosen as the average of the wear profiles, i.e., a non-perturbed Archard's wear profile since the perturbation are centered on it. The design problem solved with Archard's wear is,

$$Min \quad \Delta STE_A(\mathbf{x}) \tag{D–17}$$

by changing $\mathbf{x} = [x_p, x_r, ha_{0p}, ha_{0r}, hf_{0p}, hf_{0r}]$ such that there is no teeth interference and

$$\begin{aligned} r_c > 1.25, \qquad g_s < 2, \qquad \sigma_{vm} < Re, \qquad F < P_{hertz}^{max}, \\ -1 \leq x_p, x_r \leq 2, \qquad 0.8 \leq ha_{0p}, ha_{0r}, hf_{0p}, hf_{0r} \leq 1.7, \end{aligned} \tag{D–18}$$

Note that the numerical cost of evaluating the objective function ΔSTE_A involves two calls to the gears simulator: a first call to evaluate the contact forces and sliding rates,

and a second call to remove material from the teeth surfaces and recalculate all gears performance criteria. This numerical cost is twice that of the deterministic formulation but it is much lower than a complete Monte Carlo simulation. Equation D–17 is solved with the CMA-ES optimizer is the same fashion as all other optimization problems discussed in this article. The optimum design for this problem, called "Archard's design", is described in D-8.

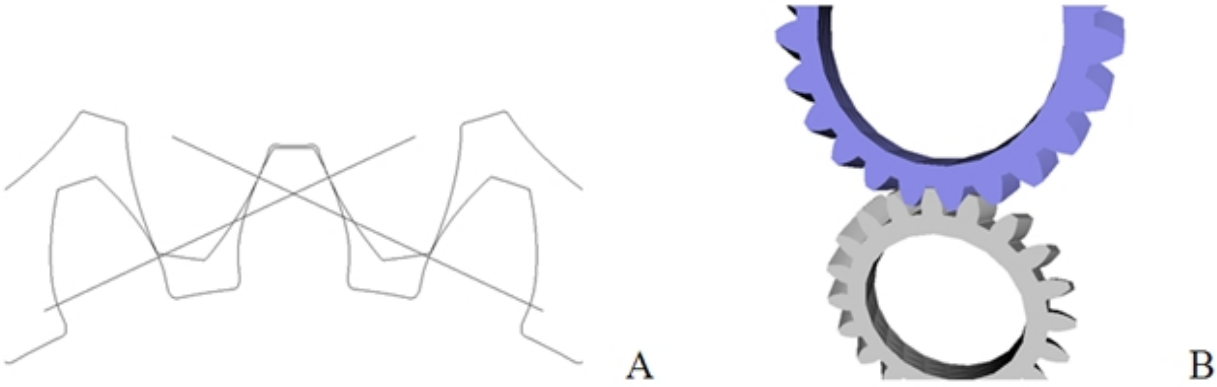

Figure D-8. Optimum design with Archard's wear. A) 2D cross-section, B) 3D drawing.

D.4.4 Comparison Of Approaches

The four methods that have been seen up to now for designing gears are now compared :

- Neglecting wear and solving Eq. D–2. The solution to this deterministic problem was shown in D-6. The numerical cost of the method is one call to the gears simulator per optimization analysis (objective function and constraints).
- Replacing Monte Carlo simulations with a Kriging metamodel, as stated in Eq. D–15. The obtained optimum design was described in D-7. The numerical cost of the procedure is one call to the gears simulator plus one call to the metamodel (negligible) per optimization analysis. In addition, there is an initial cost for calculating the design of experiments ($k \times n$ simulations) and inverting the $n \times n$ Kriging covariance matrix.
- Optimizing the static transmission error for a deterministic nominal wear profile (Archard's profile). This formulation is stated in Eq. D–17 and the resulting design described in D-8. Each optimization analysis costs two calls to the gears simulator.

- Designing the gears by selecting the best point of the initial maximin latin hypercube design of experiments (DoE). There are n points where k Monte Carlo simulations (MCS) are performed for a total cost of $k \times n$ simulations. Note that this DoE was used to build the Kriging metamodel. The so-called "empirical MCS design" is described in D-9.

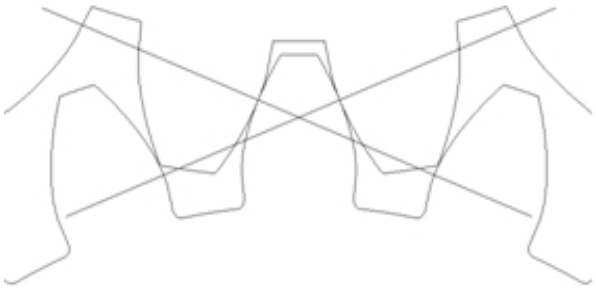

Figure D-9. Empirical MCS design, i.e., best design of the original latin hypercube set of points with 30 Monte Carlo simulations per point.

D-5 summarizes the designs associated to each approach. The last column (P^{90}) is the targeted design criterion, estimated with 500 Monte Carlo analyses. It is clear from D-5 that neglecting wear from the ΔSTE calculation (row 1) leads to designs with poor ΔSTE performance in the presence of wear. Accounting for wear (compare rows 2 to 4 to row 1) decreases the pinion addendum modification coefficient x_p and increases its counterpart x_r. It also increases the teeth heights (ha's and hf's). Minimizing the Kriging wear prediction is an improvement over neglecting wear. This method yielded a design that was not present in the initial DoE, but its P^{90} performance is similar to that of the best design in the DoE. This is because the initial 6-dimensional design space is quite large for fitting a metamodel with about 2000 data points.

The Kriging P^{90} prediction at the Kriging optimum design is of poor quality (1.97 versus 3.37 μm). This is another piece of evidence that optimizing with a metamodel requires an iterative enrichment of the DoE around the optimum design area (other examples can be found in, e.g., Jones et al. (1998)). The overall best design was the Archard's design. For long optimization runs, it is also the most expensive method out of

the ones considered here since each evaluation of the objective function needs two gears simulations. Nevertheless, for the 3*12,000 analyses long optimization runs performed here, this extra-cost remains inferior to that of building the Kriging database (3,000*30 analyses). In robust optimization problems where i) the number of variables is of the order of 10 or less and ii) one knows a noise sample leading to a reliable design, the representative noise sample approach is to be preferred.

Table D-5. Comparison of optimum gears for various formulations: without wear, with Archard's wear, with Kriging percentile approximation, and with Monte Carlo simulations (best point of LHS). All these designs are feasible.

Design	Numerical cost (in simulation call)	x_p	x_r	ha_{0p}	ha_{0r}	hf_{0p}	hf_{0r}	ΔSTE	P^{90}
Without wear	1 per analysis	0.49	0.49	1.20	1.11	1.00	1.09	0.38	6.38
Archard's wear	2 per analysis	-0.028	0.86	1.26	1.32	1.20	0.81	1.49	2.64
Kriging	1 per analysis + initial DoE	0.20	1.26	1.44	1.49	1.27	0.92	1.97	3.37
Monte Carlo	Initial DoE	-0.004	0.37	1.37	1.51	1.27	0.87	2.69	3.29

D.5 Conclusions And Perspectives

This article represents a first step in the optimization of gears while accounting for random teeth wear through the static transmission error (STE). Two robust optimization approaches have been proposed where the statistical estimation of the performance (here a 90% percentile of the STE variation) is replaced either by a Kriging metamodel or by fixing the noise to an adequate value (here the average wear profile). This study confirms that the Kriging approach is feasible because we observed that it leads to reasonable designs. However, it is seen that the Kriging metamodel needs to be updated to allow a convergence to optimal designs. This is the methodological perspective of this article. The optimization with the wear profile fixed at its average value leads to the overall best design and is the currently advised method for solving the stated gears design problem. Regarding gears design, the results presented here should be completed by varying the number of teeth and considering teeth profile corrections.

REFERENCES

Acar, E., & Haftka, R. (2005). The Effects of uncertainty control measures on the weight saving from composite laminates at cryogenic temperatures. In *Proceedings of ASME-IDECT-2005,September, Long Beach, California*.

Acar, E., Kale, A., & Haftka, R. (2007). Comparing Effectiveness of Measures That Improve Aircraft Structural Safety. *Journal of Aerospace Engineering*, *20*, 186.

Ben-Haim, Y., & Elishakoff, I. (1990). *Convex models of uncertainty in applied mechanics*. North-Holland.

Bennett, J., & Botkin, M. (1986). *The optimum shape: Automated structural design*. Plenum Pub Corp.

Boukouvalas, A., & Cornford, D. (2009). Learning heteroscedastic Gaussian processes for complex datasets. Tech. rep., Technical report, Neural Computing Research Group, Aston University.

Box, G., & Draper, N. (1986). *Empirical model-building and response surface*. Wiley Series in Probability and Mathematical Statistics.

Chernick, M. (1999). *Bootstrap methods: A practitioner's guide*. Wiley New York.

Chipperfield, A., Fleming, P., Pohlheim, H., & Fonseca, C. (1994). Genetic algorithm toolbox users guide. *ACSE Research Report*, *512*.

Choi, K., Du, L., Youn, B., & Gorsich, D. (2005). Possibility-based design optimization method for design problems with both statistical and fuzzy input data. *6th World Congresses of Structural and Multidisciplinary Optimization, Rio de Janeiro, Brazil*.

Colbourne, J. (1987). *The geometry of involute gears*. Springer Verlag, New York.

Cook, R., & Nachtsheim, C. (1980). A comparison of algorithms for constructing exact D-optimal designs. *Technometrics*, (pp. 315–324).

Cressie, N. (1993). Statistics for spatial data: Wiley Series in Probability and Mathematical Statistics. *Find this article online*.

Currin, C., Mitchell, T., Morris, M., & Ylvisaker, D. (1991). Bayesian prediction of deterministic functions, with applications to the design and analysis of computer experiments. *Journal of the American Statistical Association*, (pp. 953–963).

Deb, K., & Jain, S. (2003). Multi-speed gearbox design using multi-objective evolutionary algorithms. *Journal of Mechanical Design*, *125*, 609.

Deutsch, C., & Journel, A. (1997). GSLIB: Geostatistical software library and user's guide. *Applied geostatistics*, *2*.

Dixon, L., & Szego, G. (1978). *Towards Global Optimisation 2*. North-Holland.

Driot, N., & Perret-Liaudet, J. (2006). Variability of modal behavior in terms of critical speeds of a gear pair due to manufacturing errors and shaft misalignments. *Journal of Sound and Vibration*, *292*(3-5), 824–843.

Du, L., Choi, K., Youn, B., & Gorsich, D. (2006). Possibility-based design optimization method for design problems with both statistical and fuzzy input data. *Journal of Mechanical Design*, *128*, 928.

Du, X., Sudjianto, A., & Huang, B. (2005). Reliability-based design with the mixture of random and interval variables. *Journal of mechanical design*, *127*(6), 1068–1076.

Efron, B. (1982). The jackknife, the bootstrap and other resampling plans. In *CBMS-NSF regional conference series in applied mathematics*, vol. 38, (p. 92). Siam.

Elfving, G. (1952). Optimum allocation in linear regression theory. *The Annals of Mathematical Statistics*, (pp. 255–262).

Elishakoff, I. (1991). An idea of the uncertainty triangle. *The Shock and Vibration Digest*, (p. 1).

Elishakoff, I. (2004). *Safety factors and reliability: friends or foes?*. Kluwer Academic Pub.

Enevoldsen, I., & Sørensen, J. (1994). Reliability-based optimization in structural engineering. *Structural Safety*, *15*(3), 169–196.

Engelund, S., & Rackwitz, R. (1993). A benchmark study on importance sampling techniques in structural reliability. *Structural Safety*, *12*(4), 255–276.

Fedorov, V. (1972). *Theory of optimal experiments*. New York: Academic press.

Fedorov, V., & Hackl, P. (1997). *Model-oriented design of experiments*. Springer.

Ginsbourger, D. (2009). *Metamodeles Multiples pour l'Approximation et l'Optimisation de Fonctions Numeriques Multivariables*. Ph.D. thesis, Ecole Nationale Superieure des Mines de Saint Etienne.

Goel, T., Haftka, R., Papila, M., & Shyy, W. (2006). Generalized pointwise bias error bounds for response surface approximations. *International journal for numerical methods in engineering*, *65*(12).

Haldar, A., & Mahadevan, S. (2000). *Probability, reliability and statistical methods in engineering design*. Wiley New York.

Hansen, N., & Kern, S. (2004). Evaluating the CMA evolution strategy on multimodal test functions. *Lecture Notes in Computer Science*, (pp. 282–291).

Holton, G. (2003). *Value-at-risk: theory and practice*. Academic Press.

Iooss, B., Ribatet, M., & Marrel, A. (2008). Global Sensitivity Analysis of Stochastic Computer Models with joint metamodels. *Arxiv preprint arXiv:0802.0443*.

Isaaks, E., & Srivastava, R. (1989). An introduction to applied geostatistics.

Jin, R., Chen, W., & Sudjianto, A. (2002). On sequential sampling for global metamodeling in engineering design. In *Proceedings of DETC*, vol. 2. Citeseer.

Jones, D., Schonlau, M., & Welch, W. (1998). Efficient global optimization of expensive black-box functions. *Journal of Global Optimization*, *13*(4), 455–492.

Kahraman, A., Bajpai, P., Assistant, G., Anderson, N., & Engineer, S. (2005). Influence of tooth profile deviations on helical gear wear. *Journal of Mechanical Design*, *127*, 656.

Kapelevich, A., & Kleiss, R. (2002). Direct gear design for spur and helical involute gears. *Gear Technology*, *19*(5), 29–35.

Kenney, J., & Keeping, E. (1954). *Mathematics of statistics, part one*. D. Van Nostrand Company, Inc., Princeton, NJ.

Khuri, A., & Cornell, J. (1996). *Response surfaces: designs and analyses*. CRC.

Kiefer, J. (1961). Optimum designs in regression problems, II. *The Annals of Mathematical Statistics*, (pp. 298–325).

Kiefer, J., & Wolfowitz, J. (1960). The equivalence of two extremum problems. *Canad. J. Math*, *12*, 363–366.

Kim, N., Ramu, P., & N.V., Q. (2006). Tail Modeling in Reliability-Based Design Optimization for Highly Safe Structural Systems. In *Proceedings of 47th AIAA/ASME/ASCE/AHS/ASC Structures, Structural Dynamics and Materials Conference*.

Kleijnen, J., & Van Beers, W. (2004). Application-driven sequential designs for simulation experiments: Kriging metamodelling. *Journal of the Operational Research Society*, *55*(8), 876–883.

Kleijnen, J., & van Beers, W. (2005). Robustness of Kriging when interpolating in random simulation with heterogeneous variances: some experiments. *European Journal of Operational Research*, *165*(3), 826–834.

Kurtaran, H., Eskandarian, A., Marzougui, D., & Bedewi, N. (2002). Crashworthiness design optimization using successive response surface approximations. *Computational mechanics*, *29*(4), 409–421.

Kwon, Y., & Berner, J. (1997). Matrix damage of fibrous composites: effects of thermal residual stresses and layer sequences. *Computers and Structures*, *64*(1-4), 375–382.

Le Riche, R., & Guyon, F. (2002). Dual evolutionary optimization. *Lecture notes in computer science*, (pp. 281–294).

Lee, J., Yang, Y., & Ruy, W. (2002). A comparative study on reliability-index and target-performance-based probabilistic structural design optimization. *Computers and Structures*, *80*(3-4), 257–269.

Li, C., Chiou, H., Hung, C., Chang, Y., & Yen, C. (2002). Integration of finite element analysis and optimum design on gear systems. *Finite Elements in Analysis & Design*, *38*(3), 179–192.

Li, X., Symmons, G., & Cockerham, G. (1996). Optimal design of involute profile helical gears. *Mechanism and machine theory*, *31*(6), 717–728.

Lin, Y., Luo, D., Bailey, T., Khire, R., Wang, J., & Simpson, T. W. (2008). Model Validation and Error Modeling to Support Sequential Sampling. In *Proceedings of the ASME Design Engineering Technical Conferences - Design Automation Conference, New York, NY, DETC2008/DAC-49336*.

Marrel, A. (2008). *Mise en oeuvre et utilisation du metamodele processus gaussien pour l'analyse de sensibilite de modeles numeriques: Application a un code de transport hydrogeologique*. Ph.D. thesis, INSA Toulouse.

Martin, J., & Simpson, T. (2004). A Monte Carlo simulation of the Kriging model. In *10th AIAA/ISSMO Symposium on Multidisciplinary Analysis and Optimization*, (pp. 2004–4483).

Matheron, G. (1969). Le krigeage universel. *Cahiers du centre de morphologie mathematique*, *1*.

McKay, M., Beckman, R., & Conover, W. (2000). A comparison of three methods for selecting values of input variables in the analysis of output from a computer code. *Technometrics*, (pp. 55–61).

Melchers, R. (1987). *Structural reliability: analysis and prediction*. Ellis Horwood.

Meyer, A. (2008). Filengrene: A Software for gears analysis and manufacturing.

Missoum, S., Hernandez, P., & Grdal, Z. (1999). Optimization of a gearbox using mathematical programming and genetic algorithms. In *Proceedings of the 3rd World Congress of Structural and Multidisciplinary Optimization, Buffalo, New-York, USA*, (pp. 487–490).

Molchanov, I., & Zuyev, S. (2002). Steepest descent algorithms in a space of measures. *Statistics and Computing*, *12*(2), 115–123.

Mourelatos, Z., Kuczera, R., & Latcha, M. (2006). An Efficient Monte Carlo Reliability Analysis using Global and Local Metamodels. In *Proceedings of 11th AIAA/ISSMO multidisciplinary analysis and optimization conference, September, Portsmouth, VA*.

Myers, R., & Montgomery, D. (1995). Response surface methodology: process and product optimization using designed experiments. *John Wiley&Sons, New York*.

Neal, D., Matthews, W., & Vangel, M. (1992). Uncertainty in Obtaining High Reliability fro Stress-Strength Models. In *Proceedings of the 9th DOD-/NASA/FAA Conference on Fibrious Composites in Structural Design*, vol. 1, (pp. 503–521).

Niederreiter, H. (1992). *Random number generation and quasi-Monte Carlo methods*. Society for Industrial Mathematics.

Nikolaidis, E., Chen, S., Cudney, H., Haftka, R., & Rosca, R. (2004). Comparison of probability and possibility for design against catastrophic failure under uncertainty. *Journal of Mechanical Design*, *126*, 386.

Oakley, J. (2004). Estimating percentiles of uncertain computer code outputs. *Applied statistics*, (pp. 83–93).

Oakley, J., & O'Hagan, A. (2004). Probabilistic sensitivity analysis of complex models: a Bayesian approach. *Journal of the Royal Statistical Society. Series B, Statistical Methodology*, (pp. 751–769).

Osio, I., & Amon, C. (1996). An engineering design methodology with multistage Bayesian surrogates and optimal sampling. *Research in Engineering Design*, *8*(4), 189–206.

Qu, X., & Haftka, R. (2004). Reliability-based design optimization using probabilistic sufficiency factor. *Structural and Multidisciplinary Optimization*, *27*(5), 314–325.

Qu, X., Haftka, R., Venkataraman, S., & Johnson, T. (2003). Deterministic and reliability-based optimization of composite laminates for cryogenic environments. *AIAA journal*, *41*(10), 2029–2036.

Rackwitz, R. (2000). Reliability analysis past, present and future. In *8th ASCE Speciality Conference on Probabilistic Mechanics and Structural Reliability*.

Rajashekhar, R., & Ellingwood, B. (1993). A new look at the response surface approach for reliability analysis. *Structural Safety*, (pp. 205–220).

Ramu, P., Kim, N., & Haftka, R. (2007). Error Amplification in Failure Probability Estimates of Small Errors in Response Surface Approximations. *SAE SP*, *2119*, 37.

Ranjan, P., Bingham, D., & Michailidis, G. (2008). Sequential experiment design for contour estimation from complex computer codes. *Technometrics*, *50*(4), 527–541.

Rasmussen, C., & Williams, C. (2006). *Gaussian processes for machine learning*. Springer.

Riez, F., & Nagy, B. (1952). Leçons d'Analyse Fonctionnelle.

Sacks, J., Schiller, S., & Welch, W. (1989a). Designs for computer experiments. *Technometrics*, (pp. 41–47).

Sacks, J., Welch, W., Mitchell, T., & Wynn, H. (1989b). Design and analysis of computer experiments. *Statistical science*, (pp. 409–423).

Santner, T., Williams, B., & Notz, W. (2003). *The design and analysis of computer experiments*. Springer.

Scheidt, C. (2006). *Analyse statistique d'experiences simulees: Modelisation adaptative de reponses non regulieres par krigeage et plans d'experiences, Application a la quantification des incertitudes en ingenierie des reservoirs petroliers*. Ph.D. thesis, Universite Louis Pasteur Strasbourg.

Shan, S., & Wang, G. (2004). Space exploration and global optimization for computationally intensive design problems: a rough set based approach. *Structural and Multidisciplinary Optimization*, *28*(6), 427–441.

Shewry, M., & Wynn, H. (1987). Maximum entropy sampling. *Journal of Applied Statistics*, *14*(2), 165–170.

Smarslok, B., Alexander, D., Haftka, R., Carraro, L., & Ginsbourger, D. (2008). Separable Monte Carlo Simulation Applied to Laminated Composite Plates Reliability. In *4th Multidisciplinary Design Optimization Specialist Conference*. American Institute of Aeronautics and Astronautics.

Sobol, I. (1976). Uniformly distributed sequences with an additional uniform property. *Zh. Vychisl. Mat. Mat. Fiz*, *16*, 1332–1337.

Starnes Jr, J., & Haftka, R. (1979). Preliminary design of composite wings for buckling, strength, and displacement constraints. *Journal of Aircraft*, *16*(8), 564–570.

Stein, M. (1999). *Interpolation of spatial data: Some theory for kriging*. Springer.

Steinberg, D., & Hunter, W. (1984). Experimental design: review and comment. *Technometrics*, (pp. 71–97).

Stine, R. (1985). Bootstrap prediction intervals for regression. *Journal of the American Statistical Association*, (pp. 1026–1031).

Tu, C., & Barton, R. (1997). Production yield estimation by the metamodel method with a boundary-focused experiment design. In *ASME Design Engineering Technical Conference*. American Society Of Mechanical Engineers.

Turner, C., Campbell, M., & Crawford, R. (2003). Generic sequential sampling for meta-model approximations. In *ASME 2003 Design Engineering Technical Conferences and Computers and Information in Engineering Conference*, (pp. 2–6).

Vazquez, E., & Piera-Martinez, M. (2006). Estimation of the volume of an excursion set of a Gaussian process using intrinsic kriging. *URL http://arxiv.org/abs/math.ST/0611273*.

Venter, G., Haftka, R., & Starnes, J. (1998). Construction of response surface approximations for design optimization. *AIAA journal*, *36*(12), 2242–2249.

Williams, B., Santner, T., & Notz, W. (2000). Sequential design of computer experiments to minimize integrated response functions. *Statistica Sinica*, *10*(4), 1133–1152.

Wu, C. (1978). Some algorithmic aspects of the theory of optimal designs. *The Annals of Statistics*, (pp. 1286–1301).

Youn, B., & Wang, P. (2008). Bayesian reliability-based design optimization using eigenvector dimension reduction (EDR) method. *Structural and Multidisciplinary Optimization*, *36*(2), 107–123.

BIOGRAPHICAL SKETCH

Victor Picheny was born in Paris, France in 1983. After two years of preparatory classes at the *lycee Eugene Livet* in Nantes, he joined the *Ecole des Mines de Saint Etienne* for his graduate education. He received in September 2005 an engineering diploma and a master of science in applied mathematics. He pursued his education by a joint program between the *Ecole des Mines de Saint Etienne* and the University of Florida to work toward a Ph.D in aerospace engineering and applied mathematics, under the tutelage of Prof. Raphael Haftka and Prof. Nam-Ho Kim. During his Ph.D study, he did an internship at the Applied Computing Institute of the University of Maracaibo in Venezuela. His research interests include design and optimization methods, reliability analysis, surrogate modeling, and design of experiments.

École Nationale Supérieure des Mines
de Saint-Étienne

N° d'ordre : 537 MA

Victor PICHENY

IMPROVING ACCURACY AND COMPENSATING FOR UNCERTAINTY IN SURROGATE MODELING

Speciality : Applied Mathematics

Keywords : Metamodels, Conservative estimation, Reliability, Design of Experiments

Abstract :

This dissertation addresses the issue of dealing with uncertainties when surrogate models are used to approximate costly numerical simulators. First, we propose alternatives to compensate for the surrogate model errors in order to obtain safe predictions with minimal impact on the accuracy (conservative strategies). The efficiency of the different methods are analyzed with the help of engineering problems, and are applied to the optimization of a laminate composite under reliability constraints. We also propose two contributions to the field of design of experiments (DoE) in order to minimize the uncertainty of surrogate models. Firstly, we developed a sequential method to build DoEs that minimize the error in a target region of the design space. Secondly, we proposed optimal sampling strategies when simulators with noisy responses are considered.

École Nationale Supérieure des Mines
de Saint-Étienne

N° d’ordre : 537 MA

Victor PICHENY

AMELIORATION DE LA PRECISION ET COMPENSATION DES INCERTITUDES DES METAMODELES POUR L'APPROXIMATION DE SIMULATEURS NUMERIQUES

Spécialité: Mathématiques Appliquées

Mots clefs : Métamodèles, Estimations conservatives, fiabilité, Plans d’expériences

Résumé :

Cette thèse est consacrée à la planification et l'exploitation d'expériences numériques à l'aide de modèles de remplacement (métamodèles), et plus particulièrement à la prise en compte des incertitudes induites par l'utilisation de ces métamodèles. Dans un premier temps, différentes méthodes sont proposées pour compenser ces incertitudes en biaisant les modèles afin de limiter le risque d’erreur ‘défavorable’ (méthodes conservatives). Cette étude s’appuie sur des applications en mécanique des structures, et en particulier, l’optimisation d’un système soumis a des contraintes de fiabilité. Cette thèse propose également deux contributions au domaine de la planification d’expériences numériques. D’une part, une méthode a été développée pour construire des plans permettant de minimiser l’erreur du modèle dans une région cible de l’espace de conception. Enfin, nous avons proposé des résultats pour la planification optimale des calculs dans le cas de simulateurs à réponse bruitées.